Advances in bifunctional electrocatalysts towards high- performing Li-air batteries

Shadeepa Karunarathne [a], Chamali K. Malaarachchi [b,c], Amr M. Abdelkader [a*], Ali Reza Kamali [d,e*]

[a] Faculty of Science and Technology, Bournemouth University, Talbot Campus, Fern Barrow, Poole, BH12 5BB, UK

[b] Department of Materials Science and Engineering, University of Moratuwa, Moratuwa, Sri Lanka

[c] School of Sciences, RMIT University, Victoria, 3000, Australia

[d] School of Metallurgy, Northeastern University, Shenyang, 110819, China

[e] Department of Materials Science and Metallurgy, University of Cambridge, Cambridge CB3 0FS, UK

Abstract

The development of high-performance Li-air batteries (LABs) is an important quest for effectively utilizing high-energy density electric systems. One possible way to achieve this goal can be by introducing novel bifunctional electrocatalysts at the battery cathode, enhancing the cycle life and the discharge capacity of the LABs via promoting oxygen reaction kinetics. Understanding bifunctional catalysts' function and evolution is essential to developing a better-functioning LAB. In this review, we discuss the fundamentals, mechanisms, and key concepts related to LAB technology. We then provide thorough and critical discussions on recent advances in bifunctional catalysts used in LAB cathodes through material characterization, electrochemical analysis, battery performance, in-situ and ex-situ discharge product analysis, DFT calculations, and theoretical concepts to provide the most up-to-date, thorough, and broader discussion on the subject. These include the general and modified catalysts of carbon nanostructures, noble metals, transition metal oxides, nitrides, sulfides, and phosphides. Furthermore, special attention is given to techniques designed to enhance the catalytic activity

of Li-O_2 batteries through the modulation of electronic structures. Various facet engineering and e_g electron engineering approaches are explored, including heteroatom doping, alloying, hybridization, stoichiometric optimization, and selective facet growth. Finally, we suggest potential prospective pathways for future research.

Keywords:lithium air batteries; electrocatalyst; bifunctionality; transition metal compounds; orbital occupancy modulations

1. Introduction

Fossil fuels have met the majority of energy requirements over the last century, significantly elevating human living standards. However, the ongoing reliance on fossil fuels must be curtailed, not only due to resource depletion but primarily because of the environmental harm it inflicts through global warming, air pollution, and other factors. Consequently, there is an urgent call for scientific and technological advancements to develop advanced energy storage systems with high efficiencies and minimal or zero carbon emissions. This is crucial for maximizing the utilization of energy generated from renewable sources [1,2].

Lithium-ion batteries (LIBs) currently stand as the most widely used energy storage devices, already serving as an essential component of daily human life by powering numerous consumer electronics and communication devices. Furthermore, LIBs can be recognized as the most successful electrochemical energy storage technology in history. Despite their historical success, LIBs are currently facing challenges in meeting the necessary energy storage demands to achieve the ambitious goal of electrifying transportation. This entails replacing gasoline engines in automobiles with packs of secondary batteries. The limited gravimetric energy density in commercial LIBs (≈200 Wh kg^{-1}) hinders their effective use for long-range drives in

medium to heavy vehicles [3,4]. The current bottleneck resides in the cathode, where the commonly used graphite anode has a capacity of 372 mAh g^{-1}, while the most advanced nickel-rich layered NMC ($LiNi_xCo_yMn_zO_2$, $x \geq 0.8$) cathodes can only achieve capacities up to 240 mA h g^{-1} [5]. Other developments in LIBs such as Li-rich or Mn-rich NMC cathodes, Si-coated graphite anodes, and Li metal chips as anodes report suffering from respective issues related to electrolyte instability, unstable SEI formation, and safety concerns[6,7]. Consequently, significant advancements in LIB technology in terms of capacity are challenging to anticipate in the near future. These factors, coupled with the projected increase in energy demand [8–10], exert substantial pressure on battery researchers to advance battery technology beyond LIBs.

With concerns about potential shortages in lithium resources, the exploration of other metal-ion battery technologies has gained momentum in recent times, with sodium-ion batteries, in particular, making substantial progress [11]. Alongside metallic anodes, oxygen, and sulfur cathodes have demonstrated the capability to deliver higher energy densities within a broader operational window compared to metal-ion batteries [12,13]. Metal-sulfur batteries represent an intriguing field of research, with lithium-sulfur (Li-S) battery technology identified as the most matured beyond LIBs [14,15]. However, despite their promising progress, challenges related to polysulfide shuttling currently hinder the commercialization of Li-S batteries. A comprehensive review on Li-S batteries can be found elsewhere [16]. In this context, it is anticipated that metal-air batteries (MABs) have the potential to emerge as pivotal contenders, demonstrating significant promise as a battery technology poised to achieve substantially higher theoretical energy densities ranging from 500 to 3500 Wh kg^{-1} [17]. This positions MABs in proximity to the energy density levels of fossil fuels (13,000 Wh kg^{-1}) [18], signifying their potential to approach comparable performance.

A MAB, which can be considered as a hybrid architecture developed including the features of both metal-ion batteries and fuel cells, consists of a metallic anode, a porous cathode that breathes air/oxygen, and an electrolyte that operates similarly to conventional redox cells. As such, MABs can be categorized into four main types depending on their electrolyte: aqueous, non-aqueous (aprotic), solid-state, and hybrid. Among them, the application of anodes such as Zn [19], Al [20], Fe [21], and Mg [22] with aqueous electrolytes has frequently been studied since the early days of the 19th century Amongst, commercial Zn-air battery manufacturing was reported in the 1930s [23], while Al-air [24] and Mg-air [25] batteries were invented in the 1960s', before the recent excitements. However, the common drawback with aqueous MABs is that the batteries mostly operate as primary cells due to difficulties in electrochemical charging.

In contrast, air batteries based on alkali metals such as Li [26], Na [27], and K [28] primarily operate under an aprotic electrolyte mainly due to their high reactivity, where the metal could easily be oxidized in contact with water, and interestingly high reversibility is also reported [29,30]. Table 1 summarizes the performances of available MAB technologies.

Currently, most studies are focusing on developing an efficient Li-air battery (LAB) system mainly due to its very high theoretical energy density of 3500 W h kg^{-1} during discharge and 11 600 W h kg^{-1} during charging [31] which is an order of magnitude higher than the current delivery of existing LIB technology. Therefore, the LAB technology is predicted to be the main energy source for future electronic devices, electric vehicles, and grid storage [32]. However, despite these promising features, LABs are not commercially available, mainly due to technical issues related to their short cycle life and discharge capacity, owing to poor oxygen kinetics at the battery cathode and fast degradation of cathode and electrolytes as exposed to reactive species generated during the charging and the discharging steps.

Table 1: Electrochemical performances of typical MAB technologies.

Batteries	Theoretical Voltage (V)	Theoretical specific capacity (A h kg^{-1})	Theoretical energy density (kW h kg^{-1})	Practical operating voltage (V)
Zn–air [15]	1.65	658	1.35	0.5–1.6
Mg–air [30]	1.81	920	6.81	0.5–2.5
Na-air [31]	2.27/2.33	487/687	2.65	1.5- 4.5
K-air [32]	2.48	377	1.70	1.5- 3.0
Fe-air [33]	1.3	300	1.13	0.3- 1.6
Al–air [16]	1.2	1030	8.1	0.5–1.6
Li–air [34]	2.91	1170	11.6	2.4- 4.3

A LAB mainly consists of a lithium anode, an electrolyte, and a porous cathode. Its working mechanism is based on the successive lithium oxidation and reduction at the anode, accompanied by the oxygen reduction reaction (ORR) and oxygen evolution reaction (OER) at the cathode during the discharge and charge processes, respectively unless redox mediators are involved [33]. Figure 1 illustrates this schematic outlook of the Li-air battery and its mechanism.

As mentioned, the sluggish oxygen kinetics (ORR and OER) at the cathode is one of the main causes of the poor performances of LABs [34]. Aditionally, the decomposition of the cathode and electrolyte as exposed to various reactive oxygen species such as superoxide radicals, singlet oxygen radicals, and other protonated radicals is another cause for the fast decay in LAB performances [35,36]. Therefore, the selection of both the electrolyte and cathode material, along with the architectureof the latter, is crucial in defining the underlying reaction

mechanism for battery operation. While properties of electrolytes, such as ionic conductivity, donor number (DN), stability, and electrochemical window, are important factors in determining cell performance, the characteristics of cathodes, including their conductivity, surface area, pore size/volume, and, more importantly, the affinity of the cathode surface for oxygen and reduced oxygen species, are also critical in determining LAB performance and governing mechanisms.

Despite the substantial volume of research articles published in recent years on the synthesis and performance of catalysts in LABs, the availability of review articles summarizing such research remains limited. The avaialble reviews on electrocatalysts offer insights into metal-air battery technology [37–39], the impact of graphene [40] and carbon composties [41], single-atom catalysts [42], transition metal oxides [43,44], perovskite oxides [45], the significance of electrolyte properties [46–48]. These reviews, although insightful, tend to have limited coverage of the synthesis and performance of a diverse range of catalysts reported to date. Other recently published reviews related to Li-air/ Li-O_2 batteries includes light discussions on heterogeneous solid catalysts [49], considerations of parasitic reactions and contaminants [50,51], exploration of reaction mechanisms [52–54], investigations into the utilization of redox mediators in relation to Li-air/Li-O_2 batteries [55], application specific discussions [56], and the overall Li-air battery technology with limited attention to heterogeneous catalysts [57,58]. Consequently, recent advancements in various solid catalytic structures and associated novel insights, such as facet engineering and orbital energy modulation relevant to LABs, have yet to be comprehensively reviewed, with emphasis on identifying key challenges and outlining future perspectives. Therefore, the primary focus of this review article is to share insights and accumulated knowledge concerning innovative developments in cathode material architectures. Here, solid bifunctional catalysts take center stage in facilitating reaction kinetics and governing the morphologies and crystallinity of discharge products.

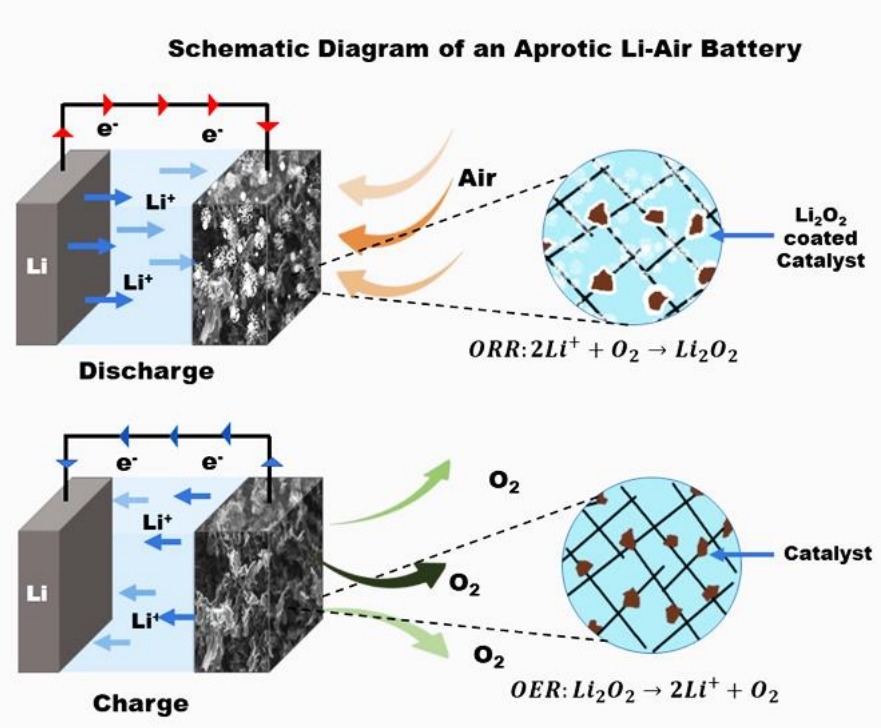

Figure 1: Schematic diagram of a typical Li-Air Battery.

2. Prospective of the current review

This review article provides a critical review of recent progress on utilizing potential bifunctional cathode catalysts in LABs. As the core component of our article, we systematically review the performances and the underlying mechanisms of bifunctional catalyst materials reported in recent publications. Key catalytic materials that are discussed in the article include; carbon nanostructures, single-doped and multi-doped carbon nanostructures, noble metals and oxides, transition metal oxides, transition metal nitrides, transition metal sulfides, transition metal phosphides, and solution-based redox mediator. Further, the effect of the morphology of the cathode, charge carrier/electron density, catalyst, and defect density, the affinity of the

reactive centers towards O_2 and discharge products (LiO_2/Li_2O_2) towards the output performance of the cell (charging overpotential, discharge capacity, cycling stability) are discussed with relevant theoretical facts and reaction mechanisms as available. Here, special effort is made to review the latest techniques employed to enhance the catalytic properties of the relevant catalysts through various methods, including edge engineering, stoichemetric optimization, facet engineering, and explanations were provided through DFT calculations discussing the associated modifications in the electronic properties of the materials promoting the reaction kinetics and certain reaction pathways. In addition to the active materials, our review also discusses aspects of engineering porous cathode networks, where carbon-based, metal-based, and binder-free/self-standing architectures are used to address the existing issues found in LAB research. Further, a statistical analysis was carried out to compare the performances of different catalysts and to evaluate the validity of the theoretical concepts discussed in the article. Such analysis hasn't been conducted before reviewing LAB performances statistically. As mentioned, only very few review articles were published recently focusing on the advances of LABs. For example, the recently published article by Tao Liu et al. [26] reviewed the current challenges related to LAB technology, where an extended discussion can be found related to LAB chemistry, issues encountered, and possible mitigation pathways. However, only a small part of the article is devoted to the developments in bifunctional catalysts. Likewise, most of the review articles published recently related to LAB technology [57,59–63] are not focused on synthesis strategies and efficiencies of different types of catalysts, and only little attention was given to the recent advancements in transition metal sulfide, phosphide, nitride, and hybrid catalysts, and new quantum engineering techniques which is fulfilled with our article, with more comprehensive, critique, and up to date content with new insights on the topic. Figure S1 provides a perspective of various bifunctional electrocatalysts discussed in this article.

3. Li-air Battery Configurations

A LAB cell combines a set of lithium anode, air cathode, membrane separator, and electrolyte [64]. These compartments and the main advantages and challenges regarding their utilization in an LAB are briefly discussed in this section.

3.1.Electrolyte and separator

The electrolyte is a key component in Li-air/Li-O_2 technology, determining the operational window and the associated reaction mechanisms involved in energy storage and release. In LABs, four different types of electrolytes have been tried out: aqueous, non-aqueous (aprotic organic solvents or ionic liquids), hybrid of aqueous and non-aqueous engineered configuration, and all-solid-state electrolytes [65]. An ideal electrolyte is expected to have all the required features, including high ionic conductivity with suitable viscosity and polarity, allowing ions to move without much hassle and enabling a sufficient amount of salts to dissolve in the solvent. Other desirable characteristics include appropriate stability against reactive species in the system, without any side reactions occurring, stability in the electrolyte for the full operational window of the electrochemical system, allowing all the necessary reactions to take place, and low volatility, high purity, and flame retardancy, ensuring safe operation [66,67].

The experimental and theoretical studies conducted to date favour aprotic electrolytes, in which the presence of a Li salt in combinations with other additives satisfy most of the mentioned criteria, where in contrast, fast corrosion of the Li anodes remain as major drawbacks against aqueous LABs raising concerns against the stability and the safety of the batteries [68]. The hybrid systems aim to protect the Li anode by placing an additional solid-state, or aprotic electrolyte next to the Li anode and utilizing an aqueous electrolyte towards the cathode

terminal. Despite numerous efforts, with several polymer and ceramic conductive membranes [69] and hybrid electrolyte architectures [70], none of the techniques have yet reached the expected success. In addition, there has been great enthusiasm in the last few years toward solid-state electrolytes in the overall battery community, including LABs [71,72]. However, in addition to several challenges associated with solid-state electrolyte conductivity, complexities related to reaction mechanisms, and storage of Li_2O_2 in Li-air/Li-O_2 need to be addressed as the technology matures, since currently, the properties of electrolytes mostly define the reaction pathways. Furthermore, it's difficult to incorporate redox mediators into such systems, and in such a scenario, the discharge capacity and the reversibility of Li-air/Li-O_2 batteries will solely depend on the properties of the cathode. On a positive note, most of the currently known parasitic reactions can be disregarded, and the least damage to the electrolytes and Li anode can be expected from contaminants in the air [69]. Therefore, aprotic electrolytes may be considered as the most studied electrolytes to date.

It should be mentioned that Abraham et al. [73] invented the Li-O_2 batteries in 1996 as O_2 was accidentally pumped into a Li-graphite cell. It took another decade to unravel the basic electrochemistry of the Li-O_2 batteries, where J. Read, D. Foster, P.G. Bruce, and T. Ogasawara made substantial early contributions. [74,75] Early research on LABs used alkali carbonates-based aprotic electrolytes with the influence of the already developed LIB technology. However, the batteries failed to cycle over 100 cycles maintaining full coulombic efficiency, and the reported charging overpotentials were very high. The findings related to the instability of carbonates against the discharge products such as LiO_2 and Li_2O_2, subjecting the electrolytes to nucleophilic attack by the reduced oxygen species forming Li_2CO_3 as a non-reversible product, well explained the mentioned observations [76,77]. More recent studies favour organic ethers due to their stability toward highly reactive discharge products. Specially glyme-based electrolytes have shown increased stability in the presence of reduced oxygen species,

and greater resistance was exhibited against nucleophilic attacks. Based on this, tetraethylene glycol dimethyl ether (TEGDME) is the most common electrolyte used in Li-air systems [78,79], even though the recent in-situ infrared spectroscopy studies suggest that diglyme (DG) is more stable compared to TEGDME [80]. The involvement of the solvent, salt, and donor number of the electrolyte for the reaction mechanisms will be discussed in the section 3.4 along with the associated operational mechanisms and parasitic reactions. Even though new solvents and solvent mixtures such as 2,3-dimethyl-2,3-dimethoxybutane (DMDMB) and related compounds [81] ionic liquids [82], and molten salts [83] were introduced recently, we do not attempt to discuss the state-of-the-art electrolytes used in LABs in detail. Review articles covering the electrolytes used in LAB technology can be found elsewhere [65].

Additionally, separators are employed in battery technologies to electrically isolate the anode and the cathode, ensuring no short circuits in the cell. The separator should also facilitate the migration of Li ions with minimal ionic resistance. Furthermore, the wettability by the electrolyte, electrochemical stability, thickness, pore structure, and porosity of separators are critical parameters affecting the long-term stability and the maximum current density of the battery cell [84]. Typically, glass fiber [85], polyamide (PA) [86], polyethylene (PE) [86] and polypropylene (PP) [87] membrane filters are used in LABs as the separator. Some attempts to use advanced membranes like polyvinylidene difluoride hexafluoropropylene (PVDF-HFP) with engineered pore structures are reported to allow fast Li^+ ion migration [88]. Review articles concerning the characteristics of separators in LAB technologies can be found elsewhere [89,90], while the primary focus of the current work is to provide a comprehensive review of the bifunctional catalysts developed to improve the performance of such novel battery systems. To this end, the mechanisms governing the function of LABs are discussed in the following sections.

3.2. Lithium Anode

The typical choice for the anode material in a LAB is lithium, providing a very high theoretical capacity of 3860 mA h g^{-1}, lightweight, and a very low potential of -3.04V [91]. Such a low potential allows a larger operational window and fast kinetics, while the mentioned properties make Li extremely reactive, raising safety and efficiency concerns. Other challenges with Li anodes include the high impedance during cycling due to the instability of the solid-electrolyte-interface (SEI) layer [57,64], the accumulation of shuttled discharge products at the anode surface [57], the Li dendrite growth [92] and low coulombic efficiency of the cell due to irreversible consumption of the Li anode and the electrolyte. In that sense, strategies such as incorporating protective films that limit the crossover of O_2, ROC and other contaminants [93], utilizing lithiated Si, Al, and C anodes [94,95], and promoting the growth of protective layers, including artificial SEI [49, 50] have already delivered promising results, but still need further fine-tuning for a better-performing anode. One other outstanding problem associated with Li anode is the morphological roughness introduced due to the continuous stripping and plating processes, particularly charging at higher current densities [98]. Therefore, typically aprotic electrolytes are recommended for use with Li metal anodes which minimize the damage to the anode material [92]. However, if other requirements are satisfied, using a solid electrolyte may be more protective for Li anodes in the future, since it limits most of the unwanted interactions with the Li metallic anode. Similar to electrolytes, advances in Li anode are only briefly discussed here, and in detailed review can be found in the recent reviews presented by Chen et al. and Wang et al. [99,100].

3.3.Li-Air battery cathode

The oxygen evolution reaction (OER), and the oxygen reduction reaction (ORR) are two sets of key reactions occurring at the cathode of a LAB. The oxygen is supplied from the

atmospheric air, and generally, an electrocatalyst is required to support such reactions. The cathode covers functions as a current collector, a catalyst layer, and a diffusion layer during the operation as three main responsibilities. The current section briefly discusses the features in the materialistic and structural composition of the cathode needed to fulfil the above requirements.

The cathodic structure should support the electron transport outward and inward from the cathode, acting as a current collector, which could be either a metallic or non-metallic material [100]. Porous metal foams of either Ni [101], Cu [102], Al [103] or metallic composites [104] are frequently being used as metallic current collectors. On the other hand, carbon-based materials [105] have been reported as the non-metallic current collecting layers. More recently, metal/carbon hybrid current collectors have gained attention, among which hybrids such as copper-coated carbon fibers [106], graphene-coated 3D porous Cu [77,78], and graphene-like conductive carbon coated Al [107] have shown excellent performance as current collectors. It is believed that the enhanced performance of non-metallic current collectors is due to inhibiting the corrosion that occurs in metallic current collectors and decreasing the interfacial energy barriers.

Cathode in an LAB should act as a gas diffusion layer (GDL) also providing multiple functionalities of (a) supporting the catalyst layer; (b) providing sufficient oxygen via diffusion channels, and (c) preventing the liquid leak out of the cell. Therefore, a large body of theoretical and experimental studies have targeted optimizing the porosity, pore structure, and the surface of the gas diffusion layer. A model developed by Read and Ren [83] presents a clear correlation between the LAB's discharge capacity and the cathode's pore volume, where mesopores have the highest contribution to carbon-based cathodes, and the micropores with smaller pore volumes were found to be less effective at storing discharge products, where the pores were

observed to be easily flooded with small amount of discharge products during the cell discharge.

Sahapatsombut and his team [108] developed another model by studying the dynamics of the porous cathode using a micro-macro homogeneous mathematical model. The model predicted that the discharge capacity of the battery depends on the cathode porosity and structure, kinetic parameters, and oxygen solubility in the electrolyte [108]. Further, the porosity of the electrode was found to decrease with the cycle number [109]. Therefore, controlling the pore distribution within the gas diffusion is suggested to be an effective technique to enhance the discharge capacity of the cathode. A 2D transient model developed by Faghri [110]suggested that a linear pore distribution with an average porosity of 0.75 could yield a higher specific capacity than a cathode of uniform pore distribution. The results also revealed that the electrode with a higher porosity at the air side had the highest specific capacity [110]. A recent article by Li and co-workers [111] further investigated the effects of linear pore distribution on the oxygen supply, porosity, Li_2O_2 volume fraction, and oxygen diffusion coefficient at various discharged stages using a cathode prepared with three layers of cathode material mixing CNT and carbon black in a way to have average pore sizes of 100 nm, 300 nm, and 500 nm respectively increasing towards the air side. As the article identified, the porosity of the electrode plays a critical role in the oxygen transfer, thus the specific capacity of the cell, as presented in Figure S2(a) [111].

To fulfil the requirements identified by the theoretical studies, the diffusion layer should ideally be made out of a lightweight porous material with a pore gradient where larger pores should be positioned toward the air side. Different carbon allotropes have been tested in practical scenarios. Deyang Qu and co-workers [112] developed a hierarchal structure in which larger pores can accommodate Li oxides without blocking the mass transferring pathways. Most micropores and mesopores can be blocked at the initial stages of oxygen reduction, reducing

the overall surface available for the reactions. However, the work proved a near-linear relationship between the average pore diameter and the cathode capacity [112]. Another study by the same group found a way to considerably increase the discharge capacity by delaying the cathode's passivation via long-chain hydrophobic molecules attached carbon black-based modified gas diffusion layer [113]. An article by Wang and co-workers [114] could achieve a discharge capacity of 6587 mA h g^{-1}_{carbon} at the rate of 0.15 mA cm^{-2} by using polytetrafluoroethylene (PTFE) attached to carbon paper as the GDL. The synergy between the large pores and partly wetted catalysts is believed to be responsible for the performance enhancements [114]. Following the suggestions made by previously conducted theoretical studies, a group led by Zhao[115] prepared a cathode with a stepwise gradient pore distribution with a selected pore distribution from 100 to 500 nm. The results indicated that the discharge capacity increased by 19.2% and 82.3% compared to uniform porous cathodes when 100 nm and 500 nm average pore size cathode was used, as illustrated in Figure S2(b). The enhanced capacity was attributed to improved oxygen diffusion pathways and sufficient pore volumes to accommodate the discharge product [115]. In summary, most recent studies suggest that cathodes of LABs containing mesopores with pore sizes around 20-30 nm are capable of accommodating Li_2O_2. On the other hand, micropores can easily get blocked by the discharge product and the embedded catalyst, reducing the effective surface area considerably [88].

In the cathode compartment of a typical LAB, the catalytic Layer is of specific importance. Even though the theoretical overpotential of Li_2O_2 is around 0.2 V, it can be as high as 1.5 V, as reported in several empirical studies[116,117]. Many factors, including poor reaction kinetics, the formation of large crystals of insulating Li_2O_2, and poor interfacial properties, contribute to the high overpotential. Therefore, the bi-functional catalysts have been efficiently used to improve the reaction kinetics in LABs [118]. While the OER and ORR kinetics are naturally slow, a catalyst layer can significantly enhance the kinetics of reactions. The catalysts

supporting OER, and ORR reactions are called “bi-functional” catalysts. The focus of the current article is to discuss and review the performances of different types of bifunctional catalysts for LAB electrodes in recent years and to highlight the ones with standout performances among them.

3.4.Working Mechanisms

As discussed, the basic aprotic cells consist of the Li anode, electrolyte, separator, and cathode. The cathode and the electrolyte involve the main chemical reactions occurring in an LAB cell, and an ideal cathode should provide favorable conditions for fast reaction kinetics and long-lasting performances [119]. Typical, LAB cells identified as batteries consist of Li metallic anode, aprotic electrolyte, and lightweight carbon [120,121] or metallic [57,122] conductive porous cathode unless mentioned otherwise, and the reaction mechanisms discussed under is associated with such a system.

3.4.1. Mechanisms on discharge

As the LAB discharges, O_2 molecules diffuse into the battery through the porous cathodic network and undergo a single electron reduction forming superoxide radical as indicated in equation 1, which was followed by Li ion coupling as shown in equation 2.

$$O_2 + e \rightleftharpoons O_2^- \quad (1)$$

$$O_2^- + Li^+ \rightleftharpoons LiO_2 \quad (2)$$

Current understanding is the initial one-electron reduction of the oxygen molecule doesn’t go through a chemisorption [123], but the fate of the produced superoxide radical ($O_2^{-\cdot}$) is determined by the properties of the cathode surface and the electrolyte. It’s hard to determine which effect the other, since most studies conducted, neglect the effect of the other while reporting.

From the perspective of the electrolyte, the stability of the superoxide in the electrolyte depends on the counteraction [124]. As observed in K-O_2 batteries, since K_2O_2 is not highly stable, long-life stability can be found with the superoxide (KO_2) [125]. In contrast, peroxides with smaller cations are more stable. Hence, the intermediate product of lithium superoxide has a shorter lifetime in the electrolyte before converting into lithium peroxide (Li_2O_2) via disproportionation as indicated in equation 3.

$$2LiO_{2(sol)} \rightleftharpoons Li_2O_{2\ (s)} + O_{2(g)} \qquad (3)$$

The produced Li_2O_2 is an insoluble solid product, and it's known to assemble as large toroid-like particles at the pores of the cathode, providing decent discharge capacity. The mentioned mechanism is well established as the "solution mechanism". A sizeable quantity of LiO_2 needs to be dissolved at the electrolyte to favour the solution mechanism, and the donor number (DN) of the solvent needs to be high to facilitate such a mechanism. Alternatively, solvents with low DN promote the superoxide to stay attached to the surface of the cathode till it subsequently reduces to the solid deposit of lithium peroxide. The overall process is called the "surface mechanism", and in addition to the DN of the electrolyte, the availability of the surface defects and the energy of the facet also contributed to governing superoxide reduction pathways at the cathode surface.

Hence, surface adsorbed LiO_2 can undergo the following reaction pathways, (1) disproportionate into Li_2O_2 as indicated in equation 3, (2) electrochemically reduce into Li_2O_2 by obtaining another electron as presented in equation 4, (3) stabilized on the surface as LiO_2 without further reduction. The third mechanism is yet to be fully accepted across the wide battery community, but it was reported that defect sites presented at the cathode surface could stabilize the superoxide [126].

$$Li^+ + LiO_{2(ads)} + e \rightarrow Li_2O_{2(ads)} \qquad (4)$$

Most of the pioneers in Li-air/Li-O_2 battery research, who are now interested in solution-based redox mediators, are recommending avoiding the surface-mediated process, which is known to deposit Li_2O_2 on the surface of the electrode as a film-like layer [127]. Despite, the arguments that the growth of a film-like layer could passivate the electrode surface, ineffectiveness in solid catalysts, and limit the discharge capacity, many researchers have published their findings, acknowledging decent LAB performance owing to surface-grown Li_2O_2 layers [128]. Figure 2 summarises the above discussion through graphical illustrations explaining different oxygen reduction pathways that could occur during the battery discharge.

The above reaction mechanisms are mostly valid for the Li-O_2 batteries under room temperature operation. The reaction mechanisms could be drifted towards either way with the varying temperature. As the temperature lowers, reaction kinetics as well as the solubility in the electrolyte also lowers promoting a more surface-mediated mechanism. While operating the Li-O_2 batteries at high temperatures benefiting from faster reaction kinetics [129], low-temperature operation helps suppress the side reactions [129]. The battery operation becomes more complicated in Li-air batteries, as the different components in the air could make a large number of non-reversible side reactions consuming Li, as well as blocking the pores in the cathode unless molecules find a way to shuttle towards the Li anode. Even though, moisture and CO_2, and NO_x are known as culprits, forming non-reversible parasite products such as Li_2CO_3 and $LiNO_3$. recent studies suggested that small quantities of moisture could benefit the performance of Li-O_2/Li-air batteries [130]. For example, it was mentioned that the presence of small percentages of water in electrolytes could act as an AN (acceptor number) additive, improving the solubility of LiO_2 and helping to form larger Li_2O_2 toroids, increasing the discharge capacity [130]. Recent findings by Clare P. Grey's group also support the existence of water/ moisture in LABs in the presence of solid or redox catalysts, where the successful reversibility of LiOH was demonstrated [131,132].

3.4.2. Mechanisms for Charging

. During the charging step, the solid discharge product decomposes, releasing O_2 into the air, known as the Oxygen Evolution Reaction (OER) [133]. The overall response can be written as reaction 5, for which the open-circuit voltage can be calculated as 2.96 V vs Li/Li^+ [91].

$$2\,Li_{(s)} + O_{2\,(g)} \rightleftharpoons Li_2O_{2\,(s)} \quad (E_{OCV} = 2.96\,V\ vs\ Li/Li^+) \qquad (5)$$

In a practical scenario, the specific discharge capacity varies from the theoretical value of 3500 W h kg^{-1}, and a charging overpotential ∼of 1 V is typically observed. It is believed that the discharge mechanism and the nature of the discharge product, including its morphology, crystallinity, and affinity to the cathode surface, are critical to determining the charging overpotential and the discharge capacity of the cell [92].

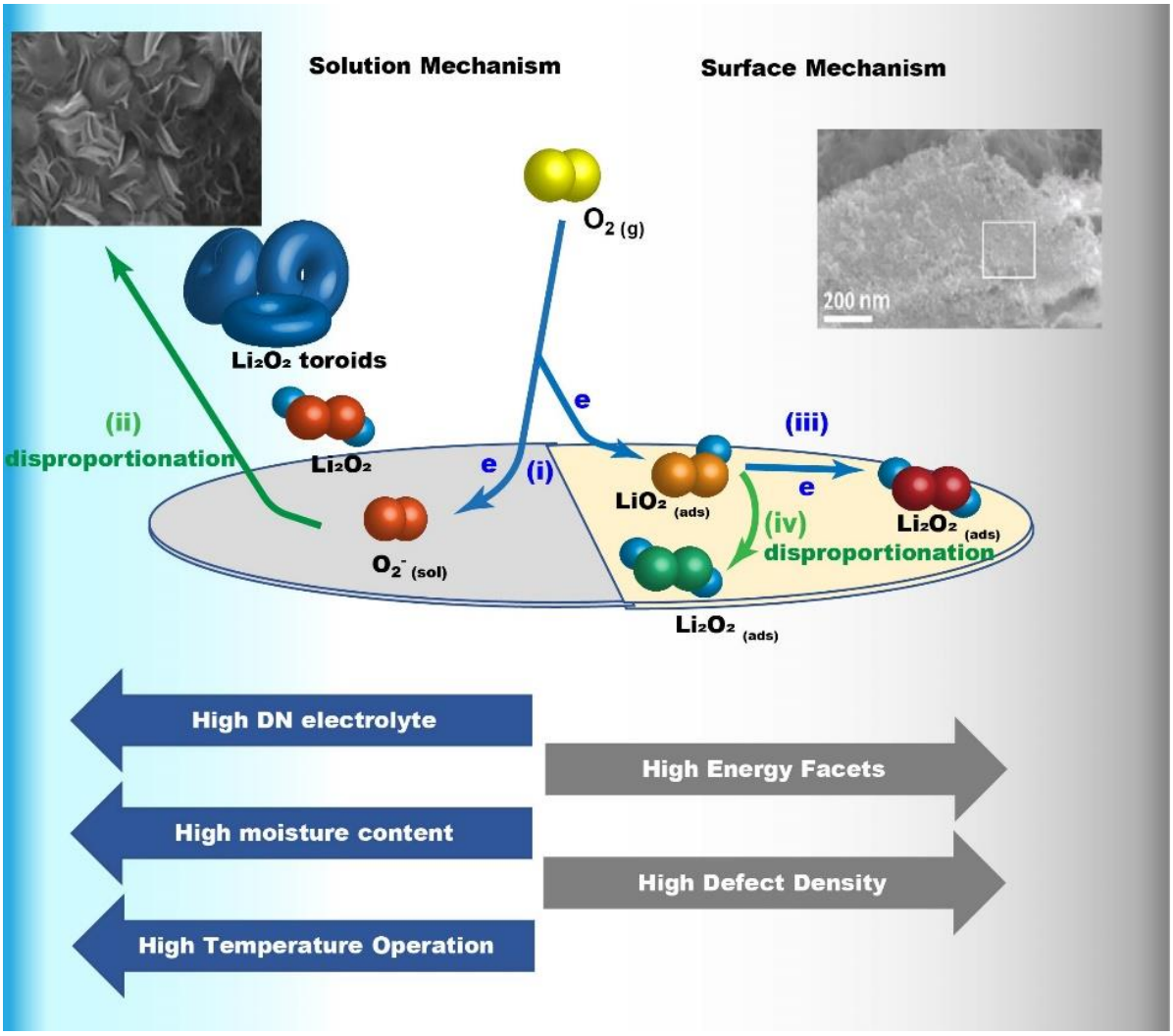

Figure 2: Surface- and solution-based mechanism involved in reactions taking place at the cathode of LABs. Reaction pathways illustration of the formation of toroid-like structures with a SEM image of a formed toroidal-shaped Li_2O_2 at the surface of the cathode after discharge [134], and an illustration of the formation of layered structure covering the cathode surface with a SEM of such a foamed Li_2O_2 thin film at the surface of LAB cathode after discharging [135]. Reprinted with permission from ref [133]. Copyright 2017 John Wiley and Sons.

The current understanding is that the LiO_2, surface-grown Li_2O_2, or the Li_2O_2 with an amorphous nature can easily be decomposable with lower charging overpotentials, and the generalized oxygen evolution reaction can be found in equation 6.

$$Li_{(2-x)}O_{2_{(S)}} \quad \rightarrow \quad xLi^+ + x\,e + O_2 \qquad (6)$$

Since the discharged product ($Li_{2-x}O_2$) is in good contact with the cathode surface, the interface resistance is reported to be low. With that, the cell's ability to be fully recovered without high charging overpotentials will keep the electrolyte and the carbonaceous components of the cathode safe without being decomposed, which are known to be susceptible to high potentials, ensuring a longer lifespan for the battery.

In contrast, the bulk Li_2O_2 toroid need a higher charging potential to get decomposed, showing a greater hysteresis in between discharging and charging voltage profiles. The weaker bonding between the active cathode material and the discharged product is the main reason for higher overpotentials upon charging, as the interfacial resistance is much higher in such instances [136]. Under the mentioned scenario, in some cases, the recovery of Li ions can only be partially possible after a full charge.

Generally, in a practical scenario, the charging profile contains both domains explained earlier at varying proportions, expanding the charging profile from 3.0V to 4.5V. However fast decomposition can be expected if the discharging mechanism is dominated by the surface-mediated route. Currently, there is a dispute about whether the defect density or the facet energy of the solid catalyst surface is more important for the reliable LAB operation, in addition to the conductivity, stability, stability of the electrolyte in the presence of the catalyst, and the scarcity and commercial viability of using the catalytic material. Before discussing individual domains of the solid catalyst and their performances, it's important to be aware of the possible

parasitic reaction pathways limiting battery performances, and eventually ending the life span of the LAB cell.

3.4.3. Parasitic Reactions and Degradation Mechanisms

Reduced oxygen species (ROC), lithiated oxygen species (Li_xO_2), protonated oxygen radicals, singlet oxygen ($^1O_2$), and some catalysts are now identified as the main culprits in promoting parasitic reactions in Li-air/Li-O_2 batteries.

Early studies on LAB degradation suggest that LiO_2 is the main source of parasitic reactions due to its high reactivity. The C and H atoms next to heteroatoms in organic electrolytes were found to be susceptible to nucleophilic attacks by O^{2-}, LiO_2, and Li_2O_2, but recent studies have identified singlet oxygen ($^1O_2$) is most responsible for the battery degradation through parasitic reactions, which is currently known to be produced during the chemical disproportionation of superoxide radicals, and the oxidation of Li_2O_2 [137]. Even though the thermodynamics and the kinetics of the mentioned singlet oxygen-generating reaction pathways are still under discussion [138], the increased singlet oxygen generation during the high overpotentials during the oxidation of the peroxides is believed to be the reason for fast battery degradation as battery charges over 3.8V [137]. Currently, further research is progressing toward understanding reaction pathways and reliable detection of singlet oxygen [139] and quenching the generated singlet oxygen via physical quenchers [140]. The carbon electrode materials and binders were found to be reacting with the mentioned ROC and singlet oxygen primarily forming Li_2CO_3, which needs potentials above 3.8V to decompose [141]. The degradation is reported to be intensified in the presence of moisture, which helps form more reactive protonated reduced oxygen compounds that could lead to chain reactions via H atom or H^+ abstraction [141,142]. Studies on the degradation mechanisms of non-carbonaceous cathode materials and their contribution to degradation mechanisms are yet to make significant progress. But we cannot

rule out the possibility of catalysts becoming inactive in contact with the mentioned radicals, and also the potential ability of catalysts like transition metal phosphides to promote the singlet oxygen generation by oxidating protonated/ non-protonated reduced oxygen radicals as reported elsewhere[143], which needed a careful study to be conducted soon.

4. Bifunctional Electrocatalysts for LABs

Various top-down and bottom-up approaches been used to synthesize the electrocatalysts used in LABs. As the section progresses, it will eventually realize that the chemical vapour deposition techniques, exfoliation techniques, and the pyrolysis of biochar and polymers were commonly used to synthesize the carbonaceous and doped-carbon catalysts. The noble metals are commonly derived from reducing the metal salts while the calcination of hydrothermal, sol-gel, or electro-spin prepared hydroxide precursor was used to prepared TMOs frequently. The sulfurization, phosphorization, and nitridation of the precursor catalysts are common approaches of synthesizing the TMS, TMP, and TMN catalysts respectively through the respective exposure to H_2S, PH_3, and NH_3 gases under elevated temperature environments. In addition, hydrothermal, co-precipitation, MOF-based approaches, and exfoliation from the natural transition metal dichalcogenides were also successful approaches used in literature in preparing effective catalysts.

Typically, once a catalyst was synthesized, numerous material characterization studies were conducted to realize the physicochemical and morphological properties of the catalyst materials as electrical conductivity, surface area and pore characteristics, and chemical phases of the material and details on analysis is provided in later sections. Once, a Li-air battery is assembled using the synthesized catalyst-based cathode, the performance of the catalyst is primarily been measured using its discharge capacity (commonly gravimetric), cycle performance (number of galvanostatic discharge-charge cycles before degradation), discharging and charging

overpotentials, and coulombic and faradaic efficiencies, while the peak positions in cyclic voltametric analysis, and OER and ORR Nyquist and Tafel plots can also be used to further understanding of the catalytic activities. Further, the morphological, chemical, and crystallographic properties of the discharged and recharged products are using to understand the reaction mechanisms and battery degradation mechanisms in experimental studies. Our expert discussions on electrocatalytic properties of the materials and the performances of LABs are mostly based on the mentioned parameters.

In addition to experimental studies, theoretical studies conducted through DFT calculations were also helpful in determining the catalytic properties of the materials and predicting the reaction mechanisms. Amongst, analyzing the projected density of states (PDOS) of molecular orbitals is useful in determining the band gap of the materials which can be used effectively to determine the electrical conductivity as well as the catalytic activity of the materials [144]. The high population of DOS around the fermi level is known to be beneficial towards promoting the reaction kinetics [145], and Fig S3 (a, b) presents the comparison of PDOS of two materials, and the catalyst present in Fig S3 (b) with high DOS near the fermi level was found to be a better catalyst over the other. In addition, ΔG-U phase diagrams and free energy diagrams can be effectively used to identify the favourable ORR and OER reaction pathways, and the materials with lower reaction overpotentials can be identified as the superior electrocatalysts as an example presented in the Fig S3 (c, d), where the NiCoFeO found to be a superior electrocatalyst over NiCoO with lower ORR and OER overpotentials [146]. Furthermore, the calculated adsorption energy for O_2 and reaction intermediates will reveal the catalytic performances of different crystal facets, and DFT calculations predicts the surface-mediated pathway will governs the reactions if the reaction intermediates are strongly adsorbed to the catalyst surfaces [147].

Noble metals like platinum, silver, and palladium are known to catalyze the chemical reactions including the ones taking place at the air cathode of LABs. These catalysts, however, have limited practicality due to their high cost, susceptibility to gas poisoning, and poor durability. Therefore, an intensive research effort is being taken to develop bifunctional catalysts based on less expensive materials with matching or better cell efficiency and durability. This section discusses the significance and the success of non-noble metal bifunctional catalysts. Particularly, we would focus on carbon allotropes, doped carbon nanostructures, transition metal derivatives, and hybrid structures utilized in the literature as electrocatalysts for LABs.

4.1. Metal-free Carbon-based Electrocatalysts

Carbon, a non-metallic tetravalent element with several allotropes, is one of the most abundant elements in the universe with a wide range of applications in energy-related sectors. This family of materials includes fullerene, carbon nanotubes (CNTs), graphene, and graphite, with structures varying from zero- to three dimensions. As electrocatalysts, carbon materials offer excellent choices due to their many favourable characteristics, such as high conductivity and durability and light weight [148,149]. Carbon nanomaterials can have high electrical conductivities, adjustable molecular structures, and stability in acidic/alkaline solvents with reduced environmental impact. Therefore, the use of carbon materials has been receiving a great deal of attention in the context of metal-free electrocatalysts.

The carbon-based electrocatalysts are often composed of porous network structures with a high surface area that increases the density of active catalytic centres. Such structures can promote electrochemical reactions by enhancing the efficient transport of electrons and increasing the interface with electrolytes. Many techniques have been investigated to improve the performance of carbon-based electrocatalysts, including doping the carbon materials lattice,

functionalizing the surface, and hybridizing with other non-carbonaceous materials. The next sections review the current situation of the progress toward the use of carbon-based cathode materials in LABs, where a lot of disputes are still on whether the facet energies or the vacancies/dopant sites in the carbon structures are providing prominent catalytic activity

4.1.1. Carbon Structures

The lightweight, high conductive, low-cost flexible carbon structures with high porosity and high surface match most of the requirements needed for a LAB cathode. Early studies used non-fully crystalline types of carbon black as Super P, Ketjen Black, and Vulcan XC-72, with limited success [150,151]. In comparison, more crystalline carbon as carbon nanotubes (CNT), reduced graphene oxide (rGO), graphene nanoplatelets (GNP), and hierarchical 3D graphitic structures were more successful as cathodes, allowing a larger Li_2O_2 accumulation and longer life span [152]. The paper-like cathode prepared by Kim et. Al. By mixing GNP and graphene oxide (GO) with a sulfonic acid stabilizer can be identified as one of the finest carbon cathodes reported in recent years, which delivered a discharge capacity of 9760 mA h g^{-1} at 100 mA g^{-1} current rate [153]. In addition, a successful attempt was reported by hybridizing two graphene structures via hydrothermal activation of glucose and GO by Xin et al., and a large discharge capacity (9760 mA h g^{-1}) and an extended cycle life (170 cycles) were reported during the study [154]. Many of the above-mentioned studies focused on achieving the optimized pore structure with a superior inter-connected network of mesopores and macropores, where better support towards Li^+/O_2 diffusion and storing large amounts of discharge products was expected. Further, the presented defect sites at the graphitic surfaces are expected to provide a greater catalytic activity lowering the charging overpotential.

Belova et al. provided further insight into the mechanisms involving carbon cathodes in Li-O_2 batteries, through a series of cyclic voltametric and X-ray absorption near edge structure

(XANES) analyses, determining the reaction pathways involving LiO_2 are strongly affected surface properties of the cathode electrodes even in the systems with high DN electrolytes as DMSO [123]. As illustrates in Fig S4 (a), the study further reveals that the pure graphitic basal plane supports the electrochemical reduction of the lithium superoxide as previously presented in equation 4, and the defective carbon structures as glassy carbon or the edge planes of the pyrolytic carbon are promoting the solution-mediated process. The study further warns against engineering materials with high defect concentrations, revealing that deformations could lead to surface stabilization of LiO_2, and it could result in reacting with carbon substrate forming the parasitic product of Li_2CO_3. With the results from the above study, a reasonable explanation can be provided for the high performances in the graphitic carbon allotropes as CNT, GNP, and rGO, over the carbon black-like amorphous structures, where the supportive crystal facet is important at supporting the reactions with higher binding energies. Heteroatom doping on carbon is an interesting approach to modulating the electronic structure, which could be used to enhance the electrokinetic performances of the LAB cathodes.

4.1.2. Mono atom doped Carbon Structures

Various approaches have been used in the literature to replace the atoms in a carbon skeleton with foreign atoms of different sizes and electronegativity. This replacement is known as doping, and when the dopant is of a single type of heteroatom, it is called mono-atom-doping. The heteroatom doping helps to enhance the catalytic activity of the carbon structure by introducing alterations to existing energy states. Verifying the concept through theoretical means via density function theory (DFT) calculations, Novcic et al. found that doped- -graphene provides better support for oxygen kinetics as doped-graphene surfaces favor fast adsorption of oxygen, intermediates, and discharge products [155].

Even though several atoms like N [156], B [157,158], and S [159] can be used for doping purposes, nitrogen dominates among them as the most frequently reported dopant [160–162]. Due to the comparable atomic size (155 pm for nitrogen and 170 pm for carbon), nitrogen can easily be incorporated into the basal plane of carbon materials. With five electron valances, nitrogen can tune the physical and chemical properties of the carbon materials, leading to enhanced electro-catalytic performance. Upon doping, the lone pair electrons in nitrogen (with higher electron negativity) render the adjacent carbon atoms more attractive to negatively charged particles since the electron density of carbon is lower than nitrogen [163]. This phenomenon increases the catalytic activity of the doped carbon. Moreover, N-doping further increases the electrical conductivity of carbon materials, with a profound impact on the electrochemical performance of nanoparticles such as N-doped CNT and N-doped graphene, as discussed in a review article by Peng et al. [160]. In addition, Shin and his group [164] identified that the higher number of defects that occurred in nitrogen-doped CNT could provide additional support for ion and electrolyte diffusion. Moreover, Wang and his co-workers [165] discovered that the oxygen reduction reaction (ORR) takes place more effectively at the edges of graphitic structures than in the basal plane due to the high level of defects on the edges, not quite agreeing with the previously introduced concepts.

Graphene and CNTs doped with nitrogen are commonly used in the literature as cathodes for LABs. Exposing to plasma environments is one of the frequently used method to modify the surface functionality in carbonaceous structures [166], and chemical vapor deposition (CVD) and plasma enhanced chemical vapor deposition (PECVD) are commonly techniques reported in literature for bottom-up synthesis of heteroatom-doped CNT/ graphene [161]. For example, Li et al. [161] have used a floating-catalyst CVD method employing imidazole as the carbon/nitrogen source and ferrocene as the catalyst precursor to produce N-doped CNT. Despite the interesting approach, the LAB failed to provide a meaningful storage capacity or

reversibility. It will be interesting to see the performances of the reconstructed cell, replacing the parasitic reaction-prone carbonate electrolyte with a more stable glyme-based electrolyte. A vertically-grown parallel porous array of N-doped CNT-based integrated air cathode was reported by Li et al. as shown in Figure S4 (b), where the catalyst was, synthesized via these-impregnated CVD method. Ferrocene dissolved in ethylenediamine, and xylene were used as the carbon and nitrogen source, respectively, and doping level was determined by controlling the N/C feed ratios. Also, very limited cycle stability was reported, most possibly accounting for the weak OER activity provided by the derived pyridinic carbon structure [167].

Graphene has been one of the most commonly used carbon allotropes at the air cathode in LABs in the past few years. Its ultimate lightweight planer morphology, electrical conductivity, chemical and electrochemical inertness, and favourable basal plane make graphene an ideal candidate for LAB's cathode [168–170]. As theoretical studies suggested, doping with nitrogen enhances many of the graphene properties and more importantly, decreases the adsorption energy barrier for the reduced oxygen species favouring the fast kinetics in LABs. Thermal treatment processes with nitrogen-containing gases are frequently used to dope graphene. In this regard, Li et al. [171] used high-purity ammonia mixed with Ar at 900 °C to produce N-doped graphene. Even though the researchers were able to achieve an initial discharge capacity of 11,660 mA h g^{-1}, at a current density of 75 mA g^{-1} for the N-doped graphene nanosheets, which is about 40% higher than undoped graphene nanosheets (8530 mA h g^{-1}), there also a reasonable cycle stability was not achieved.

Apart from graphene and CNT, Su et al. [172] developed N-doped onion-like carbon (OLC) structures that can be very efficiently used as bi-functional electrocatalysts in LABs. In this case, promising results were obtained, including a very high specific capacity (~12180 mA h g^{-1}_{carbon}), lower overpotential (0.88V), and reasonably good round-trip efficiency of 70.0% even

after 194 cycles [172]. In this work, OLC structures were produced by the thermal annealing of nanodiamonds at 1200 ^{0}C for 4 h under an argon environment, followed by another annealing process at 550 ^{0}C for 4 h under ammonia to produce N-doped OLC; see Figure S4(c). Mesoporous morphology, high specific surface area, and a high degree of graphitization were common features of the prepared OLC and N-OLC. Effective nitrogen doping (mostly with pyridinic and pyrrolic nitrogen) and structural defects in the graphene basal plane were the highlighted modifications in the N-OLC over OLC, as revealed by the XPS and Raman studies. These modifications can be considered responsible for the superior catalytic activity exhibited by N-OLC.

Another common engineering approach for heteroatom-doped 3D carbon networks is by pyrolyzing/annealing the selected polymer or biochar structures[168]. By this, more control over the pore structure and the defect density can be achieved. For example, dopamine has been used as a nitrogen source to prepare many N-doped carbon nanostructures for many applications, including LABs, where the large number of ammine groups presented in the structure allows for the achievement of high doping concentration [173]. Also, dopamine is very easily polymerizable into polydopamine (PDA) in mild alkaline media [173]. In separate studies, Kim et al. used PDA coated on graphitic carbon as illustrated in Figure S4 (d) [174] and polyester fibers [175] to produce N-doped hollow tubular carbon structures by annealing the PDA-coated material at higher temperatures under an Ar environment. The polyester fiber-based graphitized structure was used as the self-standing cathode exhibited reasonably good discharge capacity (~ 6000 mA h g^{-1}) even though the cyclability is still limited. Even though the researchers were light on the discovery of 12% of Li_2CO_3 on the discharged product, it could be the limiting factor for fast-degrading battery performance. Further efforts were conducted to yield higher catalytic activity by optimizing the parameters involving the N-doping [176,177]. Nitrogen could be inserted into the graphitic basal plane by four main

configurations namely: pyrrolic nitrogen, pyridinic nitrogen, graphitic nitrogen, and pyridinic-N-oxide [174]. In pyridinic nitrogen and graphitic nitrogen, the sp^2 hybridization of carbon can be observed. In contrast, carbon hybridization is mainly sp^3 in pyrrolic nitrogen. The pyridinic nitrogen contributes to the pi-electron system with one electron, while the pyrrolic nitrogen contributes with 2 electrons. Graphitic nitrogen forms when a carbon atom is replaced with nitrogen. A recently concluded study by Yi et al. shred light into the N-doping configuration on the growth mechanism of Li_2O_2 through molecular dynamics and DFT calculation [178]. The study reveals pyridinic N has a smaller binding energy for Li_2O_2 allowing a highly adsorbed localized growth of Li_2O_2, compared to branched growth of Li_2O_2 in graphitic N, making it difficult to decompose upon charging. High defect density and the preference for nucleophilic reactions in the presence of pyridinic nitrogen are due to its electronic structure, which may make it favourable for the OER [179,180]. It was also discovered that the type of N doping in carbon structures could be varied depending on the starting material and the annealing temperature [174]. Typically, at lower annealing temperatures (~600- 700 ^{0}C), the formation of pyrrolic and pyridinic types of N is more favourable. As the temperature increases, the pyrrolic and pyridinic N tend to convert to graphitic N. Hence, the catalytic activity will also depend on the annealing/pyrolyzing temperature, and several experimental studies verified that pyridinic N is most suited to catalyzing oxygen kinetics in Li-O_2 batteries [174,180].

In addition to N, other heteroatoms were also used for doping graphitic structure, and doping with B has also yielded successful results owing to the electron-deficient nature of B-doped carbon as theoretically and experimental studies verified [181,182]. Xiao et al. find a large amount of B doping can be achieved in defect-rich carbon structures, where a 6.7% B doping was achieved on holey carbon, which is produced by thermal annealing GO. High adsorption of O_2 at the partially positively charged B sites, due to electronegativity differences between B and C, is identified as the main supporting mechanism for the improved ORR activity. Hence,

impressive Li-O_2 battery performance with a discharge capacity of 19698 mA h g^{-1} and cycle stability up to 120 cycles were achieved [183]. Meng et al. further reveal the possible support that could be provided by electron-deficient B towards the fast Li^+ diffusion and electrolyte immersion, facilitating enhanced oxygen kinetics, and further theoretical and experimental studies are needed to verify the introduced hypothesis [181].

The synergy of two or more heteroatoms doped at once, could yield better performance in carbon cathodes, providing enhanced catalytic support promoting ORR and OER kinetics at LABs.

4.1.3. Dual-doped Carbon Structures

Co-doping of carbon with more than one element can further increase the catalytic activity of the carbon-based cathodes used in LABs. Dual, or multi-doping with heteroatoms is mostly reported using sulfur [184], phosphorous [185], iodine [186] and boron [187] along with nitrogen. Commonly, the dopants have approximately similar sizes as carbon. However, if the dopant atom size is larger than the carbon atom, there would be a higher possibility of generating structural defects in carbon [185]. Different heteroatom doping affects the catalytic properties differently depending on their physical and electronic structural properties. Moreover, a synergistic effect can be expected when two or multiple doping atoms are simultaneously applied [188,189].

With the high electronegativity of nitrogen and comparably the larger atomic size of sulfur, the induction of structural distortions, modification of charge, and spin densities in the carbon structure are commonly observed in N and S-doped Carbon [190]. Kim et al.[191], Jang et al.[192] and Wang et al.[193] have conducted experimental work on synthesizing a carbon cathode doped with nitrogen and sulfur as heteroatoms, using thiourea as the source of both sulfur and nitrogen.

Kim et al. [194] used a cathode composed of mesoporous carbon and graphene nanosheets co-doped with nitrogen and sulfur. The catalyst was prepared via a two-step process by the high-temperature activation of hydrothermally produced hydrochar on graphene oxide sheets as illustrates in Figure 3 (a). The doping of N and S was achieved through the decomposition of thiourea into NH_3 and H_2S gases, forming C-S and C-N bonds, in the same environment where the hydrochar is forming. Growing mesoporous carbon on graphene nanosheets prevented the restacking of graphene sheets and accommodated the insoluble ORR product, and TEM and XPS studies have proven the incorporation of sulfur and nitrogen (graphitic, pyridinic, and pyrrolic) into the carbon network. High cathodic current density (10.4 Ag^{-1}) and peak power density (26.4 W g^{-1}) directly represent the efficiency of O_2 converting into Li_2O_2 in the aprotic medium (ORR), while the reported low charging overpotential with doped graphene nanosheets indicates OER enhancement [194].

Jang et al. [195] and Wang et al. [196] have undertaken a slightly different approach for synthesizing nitrogen and sulfur co-doped graphene. They replaced the hydrothermal step with a sonochemical process due to some evidence of partial dopant loss during the prolonged hydrothermal treatment [197]. In both works, the catalyst was prepared by mixing GO with thiourea in ethanol using ultrasonication, followed by an annealing step at 600°C, 700°C, 800°C, 900°C or 1000°C. Thiourea can reduce the GO below its decomposition temperature at 200°C. After 200°C, the reduction occurs due to the thermal annealing. The defect sites left by the removal of oxygen from the GO surface during the reduction bind with the decomposition products of thiourea [196]. Overall, the cathode material annealed at 700°C (NSG700) showed excellent ORR catalytic activity in terms of cathodic onset potential, peak potential, and highest current density. Authors suggest that optimized composition and the effective heteroatom binding configuration at this temperature are responsible for the excellent performances of NSG 700.

In a similar study, Jang et al. [195] suggested annealing at 900°C (NSG900) is forming the best cathode structure which could reach the discharge capacity of, 11252 mA h g^{-1} at 200 mA g^{-1} current density. NSG900-based cathode comparatively has a high content of graphitic/pyridinic nitrogen and thiophene sulfur and enhanced the electronic conductivity and the facet energy of the graphitic plane by providing electron pairs as illustrates in Figure 3 (b), by graphitic and pyridinic types of nitrogen may provide the ultimate support the electrochemical performance [198]. Further, the higher content of thiophene favours the ORR activity as it is the ORR active form while SO_x is the ORR inactive form. Even though the synergy of N and S has undoubtedly helped to enhance the initial discharge capacity of the assembled LABs with high electrical conductivity, high spin and charge density, and active sites, a solid mechanism for OER support is yet to be introduced. Further disputes can be recognized with the conditions for material activation, where the researchers are yet to find the best balance between the optimized conditions for doping and the most suited pore structure, and future studies should consider both critically while optimizing the catalyst synthesizing process.

Wang et al. [187] prepared graphene co-doped with nitrogen and boron using ammonia and boric acid as the precursors by annealing the precursor and the GO mixture at 1000°C in a quartz tube furnace. The study synthesized three different boron and nitrogen-doped graphene types by varying the annealing temperature, and the $B_{12}C_{77}N_{11}H_{26}$ structure showed the best ORR activity with the highest onset potential and electron transfer number (3.8). The density functional calculations (DFT) by Lipeng Zhang and Zhenhai Xia [199,200] also confirmed the high carbon-content composition ($B_{12}C_{77}N_{11}H_{26}$) has the best ORR activities suggesting the randomly distributed B and N atoms and the small B-N clusters in $B_{12}C_{77}N_{11}H_{26}$ with the higher spin and charge densities may significantly contributed to the catalytic activities.

Aiming Wu et al. reported I and N co-doped bifunctional carbon catalysts for Li-O_2 batteries [186]. Iodine was selected because of its ability to create free hole carriers within the carbon material that improve the density of free charge carriers, accelerating the electron transport. Iodine also formed I_3^- and I_5^- species which act as catalytic sites to promote the formation and decomposition of the discharge products. With nitrogen and iodine doped at the carbon skeleton, the researchers reported improved catalytic activity promoting surface adsorption and reduction of O_2 and higher electron and mass transport properties, as shown in Figure 3 (c).

Longjun Li and Arumugam Manthiram observed similar enhancement in their work on hybrid LABs developed with O and N-doped carbon nanowebs-based catalysts [201]. The N and O co-doped graphene was synthesized via a three-step process. Initially, monodispersed polystyrene spheres were added to pre-prepared GO dispersion, and the mixture was autoclaved for 16 hours at 180°C with added ammonium hydroxide as the source of N. The resulting product was heated to 80°C with I_2 in a sealed container to achieve the iodine doping, then followed sintered at 900°C under N_2 environment. The fabricated cells with iodine and nitrogen-doped porous graphene (INPG) based cathodes performed well with a specific reversible capacity of 14017 mA h g^{-1} at 200 mA g^{-1} and with outstanding cycling stability of over 225 cycles at a current density of 500 mA g^{-1} for a limited capacity of 1000 mA h g^{-1}. As identified during the study, I hierarchical mesoporous network of the catalyst, the uniform distribution of the dopants (identified with SEM, XPS, and TEM analysis), and the high amount of surface/edge distortions (high I_D/I_G ratio) present in the INPG led to better ORR and OER reaction kinetics by providing electron and oxygen transportation pathways and providing enough reaction sites and space to accommodate the discharge products as Li_2O_2 [202].

In summary, the studies conducted up to date produced enough theoretical and experimental proof to verify the effectiveness in carbonous structures with many advantages as the cathode

material for Li-air/Li-O_2 batteries with a suitable pore structure and oxygen reduction support. The oxygen adsorption capabilities at the graphitic surface are found to be pivotal in providing superior catalytic support towards oxygen reduction, and the derivation of more favourable surface properties via heteroatom doping was also found to be effective at promoting oxygen kinetics. Even though a solid mechanism favouring the OER kinetics is yet to be introduced with carbon cathodes, the discharged product could be easily decomposed on occasions where it is well attached to the cathode surface avoiding the branched growth. Irrespective of the obtained initial capacity, the lifetime of the battery is limited to a small number of cycles in many studies as summarized in Table 2, and the occurrence of side reactions could be the main cause of premature death. In particular, the instability of C in contact with Li_2O_2, producing a layer of Li_2CO_3 in between the cathode and Li_2O_2, as observed by Gallant et al. [203] , is the main obstacle facing carbon cathodes against succeeding. Despite the support at initial discharge capacity, the presence of defects and deformations could worsen the degradation by retaining the more reactive lithium superoxide at the cathode surface. The mentioned vulnerability of carbon cathode against parasitic reactions forced the researchers to search for more stable alternatives, which as reviewed below.

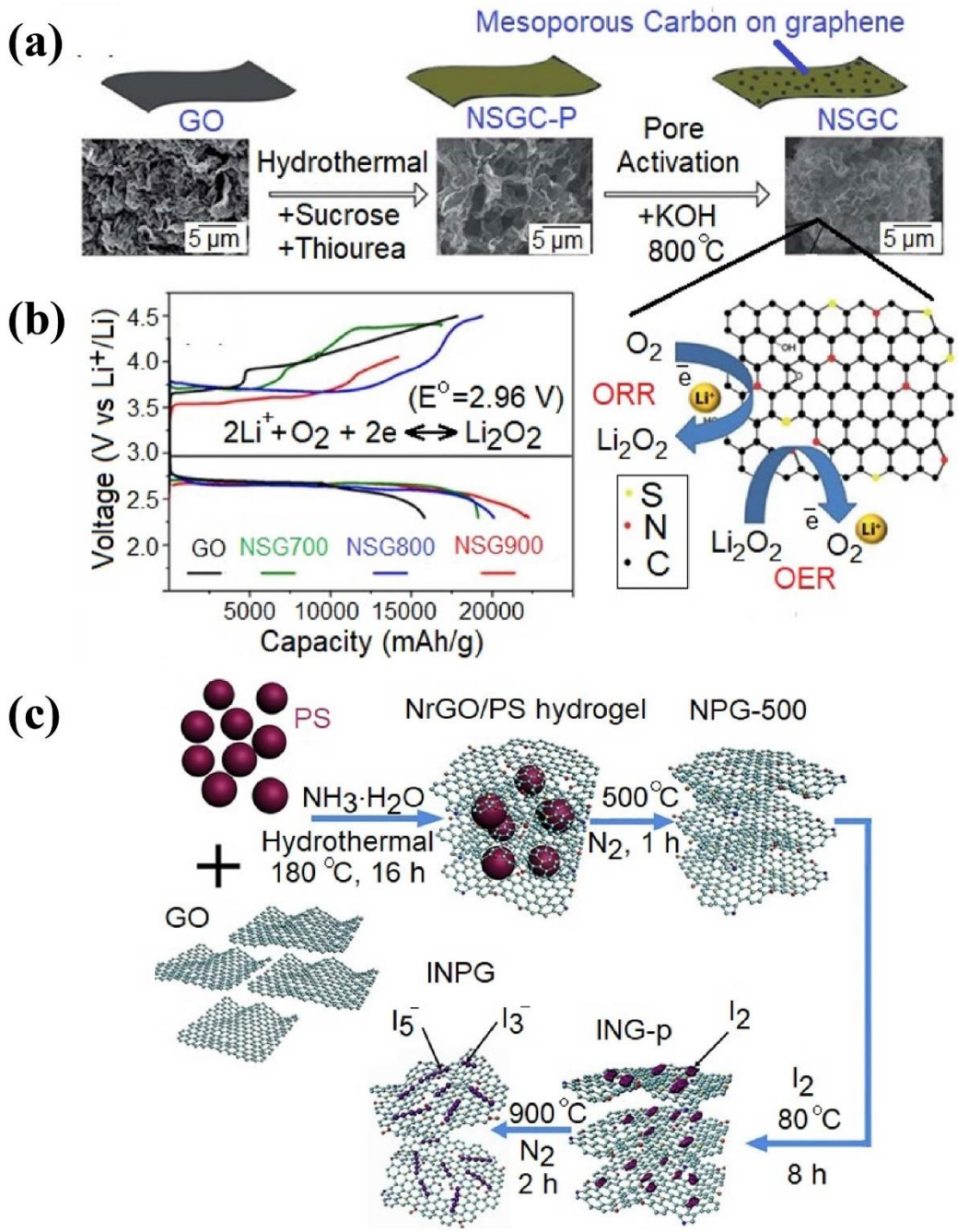

Figure 3: Dual-doped Carbon Cathodes for LABs (a) N, S-doped Graphene synthesized using hydrothermal and carbonization techniques [188], (b) Initial galvanostatic discharge/charge profiles of N, S -doped cathodes carbonized at different temperatures [150], and (c) Schematic diagram of the process of developing N, I-doped Graphene cathode through hydrothermal reaction and heat treatment [180]. Reprinted with permission from ref 188 and 189. Copyright 2015 The Royal Society of Chemistry and 2019 Elsevier.

Table 2: Summary of design parameters and output properties of LABs made using doped-carbon cathodes.

Type	Catalyst	Shape	Substrate	Method	Surface area ($m^2 g^{-1}$)	Pore Size (nm)	Discharge Capacity (mA $h g^{-1}$)	Rate (mA g^{-1})	Cycle Number	Rate/ Limit	Over Potential (V)	Li_2O_2 shape	Ref
Mono Doped Carbon	N-doped CNT	Bamboo-like	CNT	CVD	40.92		866	75			1.7		[161]
“	N-doped CNT	Parallel-array	CB/ Carbon Paper	CVD			2203	60	5	60	1.81		[167]
“	N-doped Graphene	NS	Celgard 3500 GDL	Annealing			11,660	75				Particle	[171]
“	N-doped GNP/ N-doped CB	Porous 3D	Ni foam	Annealing	900	11.86	1687.3						[204]
“	N-doped Onion-like Carbon	shells	carbon paper	Annealing	406.4	20	12180	25	196	50	0.88	film-like	[172]

Dual doped carbon	N and S co-doped graphene nanosheets	NS	35BC GDL	Hydrothermal/ Annealing	1730	4	11431	100	38	100	1.3	Film-like	[194]
	N and S co-doped graphene nanosheets	NS	Sigracet GDL 10 BC	Annealing	310	10-25	22252	200	20	200	0.88	-	[195]
	N and I co-doped graphene	3D porous	Carbon paper	Hydrothermal / Annealing	417	2-10	14017	200	225	500	0.76	Toroidal	[175]

4.2.Noble Metal/Metal Oxide-Based Catalysts

Over the years, noble metals have been used to catalyze various electrochemical reactions. The limited performance, electrolyte decomposition, and the high cost of using the catalyst were found to be the main obstacles to using them in LABs on a commercial scale. But the recent development of nanotechnology and the novel synthesis routes of developing noble metal structures with desired physicochemical properties at low cost again turns noble metals and noble metal derivatives attractive among Li-air application researchers [66,205–208]. The successful utilization of noble metal nanoparticles in related applications encouraged further studies on LABs using noble metal-based bifunctional electrocatalysts [207,209,210]. Further, the recent understanding in surface modulations to reach high O_2 adsorption, and to tailor the size, shape, nucleation. and the growth routes of Li_2O_2 via high energy metallic facets and optimizing the e_g orbital occupancy via alloying are promising techniques for improving LAB performances.

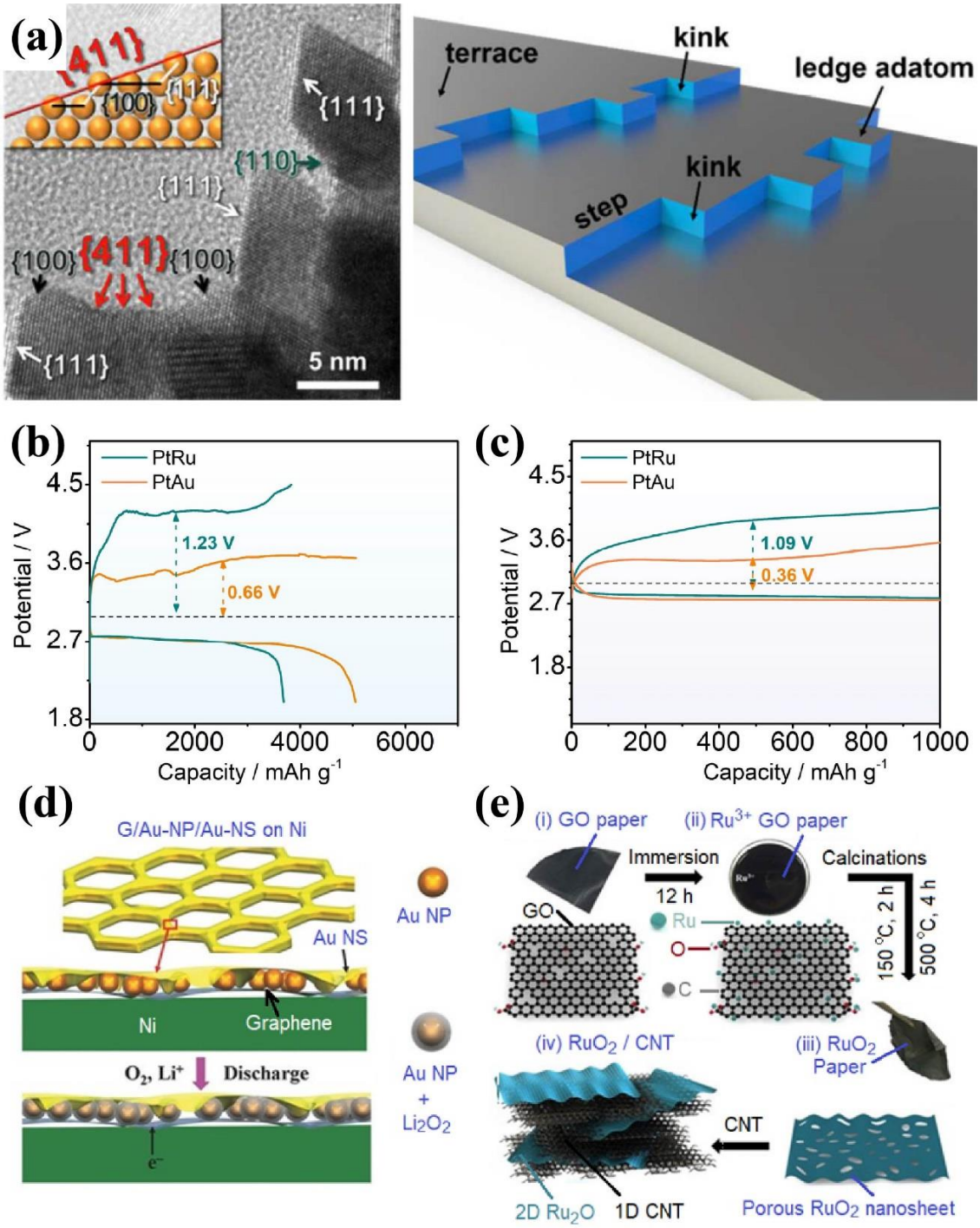

Figure 4: Noble metal-based cathodes for LABs, (a) Pt catalysts with anisotropic structures exposing high-indexed (411) facets [205], (b) The full discharge–charge profiles and (c) galvanostatic curves of the PtAu and PtRu catalysts at a current density of 0.1 A g^{-1} [210], (d) Graphical illustration of discharge product coated around the Au nanoparticle catalyst which sandwiched in-between graphene and Au sheets [207] and (e) schematic illustration of the synthesis of RuO_2/CNT catalyst [216]. Reprinted with permission from ref [205, 207]. Copyright 2018 ACS publishers and 2017 John Wiley and Sons

Pt is the most exploded noble metal in energy applications. Feng Wu et al.[211] reported platinum-coated hollow graphene nanocages as the cathode material in lithium-air batteries. The synthesis method is composed of the combustion of magnesium metal with dry ice to produce cubic MgO nanoparticles covered with a few layers of carbon, followed by the removal of MgO with dilute HCl to obtain hollow graphene cages. Then the material was functionalized with OH groups using concentrated nitric acid and subsequently coated with Pt nanoparticles via PVD technique. The nanocage hierarchical network with adequate active sites exhibited cycling stability of up to 54 cycles at 100 mA g^{-1} was observed while forming easily decomposable discharged product with roughly 200 nm diameter toroidal-shaped Li_2O_2. However, the study has reported major drawbacks, including the complete consumption of the lithium anode and the decomposition of the electrolyte-generated side products, significantly reducing the cyclability.

A more in-depth analysis conducted by Song et al. [212]. has found the catalytic activity of Pt is dependent on its structure, where Pt catalysts with anisotropic structures exposing high-indexed (411) facets are found to be significantly reactive than low-indexed facets. Anisotropic (411) faceted catalyst was synthesized by a polyol-mediated process at 200°C for 2h, and the exposed atomic steps as step-edge, kink, and ledge sites in the facet as presents in Fig 4 (a) were found to have high surface energies and strong bindings with O, supporting enhanced OER and ORR activity. The Li-O_2 battery exhibited a stable catalytic performance with a large discharge capacity (12,985 mA h g_{carbon}^{-1}) and the growth of Li_2O_2 as sub-micron-sized pellets allow easy decomposition with the low charge overpotential and the cycle retention for 70 cycles.

Other than Pt, Bing Sun et al. reported using Ru nanocrystals as the cathode material in LABs. Using a surfactant-assisted method, the Ru nanocrystals were supported on carbon black (CB).[206] TEM images and other spectroscopic analyses revealed 2.3 nm averaged sized Ru nanoparticles (34% by weight) uniformly anchored on the CB surface, helping to obtain a strong catalytic activity with 9800 mA h g^{-1} initial discharge capacity at 200 mA g^{-1}. A small charge plateau was observed for the Ru-CB electrode indicating the improved OER activity, which also helped at lasting 150 cycles. Researchers verified the complete decomposition of Li_2O_2 and LiOH upon charging, further verifying the high bifunctional catalytic activity in Ru.

The fine catalytic activity of Ru was confirmed by Yo Sub Jeong et al. [196] by systematically studying the catalytic performance of various rGO composites with Pt, Pd, and Ru metal nanoparticles, with a focus on OER. The composites were prepared by distressing GO in ethylene glycol together with the noble metal salts (H_2PtCl_6, Na_2PdCl_4, or $RuCl_3$), and reducing the mixture with sodium borohydride to form the final catalysts. Among the tested composites, Ru-rGO showed the best catalytic performance for ORR and OER activity by forming film-like discharge products However, the cycle life was limited in all the samples, and detecting HCOOLi in the discharged product was identified as the reason for the fast deterioration of the cells. Even though the authors describe HCOOLi as a result of a reaction between Li and residual HCOO groups on the rGO due to the poor reduction, this study is another example of the vulnerability of carbon structures/carbon scaffolds in the presence of Li_2O_2.

The study below proves Ni foam is a better scaffolding/conductive gas diffusion layer, where an excellent bifunctional catalytic activity provided by Ru nanoparticles decorated on vertically grown graphene nanosheets on Ni foam (VGNS@Ni) helped to yield an inspiring electrochemical performance on the assembled LAB, which used the novel structure as the free-standing cathode. The specific discharge capacity was reported as 23864 mA h g^{-1} at a

current density of 200 mA g^{-1}, and interestingly, the full cycle discharge capacity was only reduced up to 18887 mA h g^{-1} even after 50 cycles of deep discharge, and the charging overpotential was only high as 0.43V. The cells could be cycled over 200 cycles under a discharge depth limit of 1000 mA h g^{-1} and at the rate of 200 mA g^{-1}. According to researchers, the enhanced performance of the catalysis was referred to the abundance of nanoparticles on the surface, the large surface area of the vertically aligned graphene sheets, and the voids provided by the Ni foam. [213]. The electrochemical stability of Ni foam against parasitic reactions may also play a critical role in the extended stability of the cell.

Au nanoparticles also exhibited a decent catalytic activity promoting oxygen kinetic on Li-O_2 batteries as they sandwiched in between CVD-grown graphene layers, used as a binder-free cathode for Li-O_2 batteries by Wang et al. [202,214] using a solution impregnation technique; see Figure 4(d). The battery was reported as it survived over 300 cycles and it was able to deliver 3347 mA h g^{-1} initial discharge capacity at 400 mA g^{-1}. However, the fast covering of the active surface with a thin layer of Li_2O_2 discharge product was believed to be responsible for limited discharge capacity and also for the extended cycle life [214].

In addition to scrunty and the expenses regarding noble metals as catalysts, the main other issues regarding noble metal catalysts are that they promote the degradation of the electrolyte, carbon cathode, and the binder by promoting the nucleophilic attack by O^{2-} and singlets oxygen as identified by McCloskey et al. [215] and Samojlov et al. [216] Recently, it was identified that the catalytic activity of noble metals can be controlled by alloying them with another metal.

4.2.1. Bimetallic/Alloyed catalysts

Several research groups experimented with bimetallic noble metal nanostructures to optimize the catalytic activity. One possible way of enhancing the OER activity of a catalyst is by improving the adsorption energy with an intermediate of LiO_2, and altering the e_g occupancy in

transition metals can be used to tune the adsorption properties [217]. Pt has a high e_g occupancy, causing a weak OER performance as well as a high charging overpotential. But since Pt (generally transition metals) has a tuneable d-orbital structure, it was realized that the e_g occupancy can be altered by alloying Pt with other metals to obtain an improved catalytic activity.

Zhou et al. recently reported e_g engineered Pt as an efficient catalyst promoting oxygen kinetics at Li-O_2 batteries, by modifying e_g occupancy of Pt by alloying with Ru and Au. It was found that alloying with Au is more fruitful, where the electronegativity of Au helped to attract electrons from Pt, lowering the electron occupancy in e_g, which allows having a higher binding energy with LiO_2 intermediate, as proven by XPS and DFT studies. The effect of alloying with Au helped to have high discharge capacity with lower the charging overpotential as demonstrates in Fig 4 (b, c) and to have a decent cycle performance with 220 cycle stability in the assembled batteries.

Up to date, the conducted limited studies with bimetallic structures delivered mixed results, where the PtAu core-shell nanoparticle incorporated LAB cathode derived by Cheng Chao Li only helped to survive 30 cycles [218], while the LAB constructed on Pt_2Ru/Vulcan XC-72 on Ni foam cathode by Yao Yang et al. [219] barely lasted 10 cycles indicating the necessity of optimizing the alloying/e_g engineering process with suitable materials at correct ratios to obtain more maturity and reliability over the technique.

4.2.2. Noble Metal oxide

Other than the pure metal itself, noble metal oxides, especially RuO_2, were also effective as bifunctional catalysts. Several composites were tested, including SWCNT/RuO_2 composite [220], CNTs decorated by RuO_2[221], Ketajan Black/RuO_2 composite [222], $RuO_2.nH_2O$

clusters anchored on carbon nanofibers [223], and porous RuO_2 nanosheets anchored on carbon fibers [135].

Among the mentioned works, the study conducted by Jiaqiang et al. [135] demonstrated extraordinary cycle ability where the LAB cells survived for 200 cycles at a very high current rate of 1000 mA g^{-1}. The discharge product was in the form of a thin film, which, together with the low charging overpotential (0.71V), contributed to the long-stable behavior. The catalyst was synthesized by annealing the Ru^{3+} ions immersed GO sheets, as illustrated in Figure 4(e). The study conducted by Liyuan et al. [223] with $RuO_2.nH_2O$ clusters anchored on electro-spun carbon nanofibers (CNFs) also yielded promising results. Excellent OER activity was observed with the decomposition of Li_2O_2 and Li_2CO_3 to a greater extent, and this is one of the very few incidents where successful decomposition of Li_2CO_3 was recorded. The assembled LAB could run up to 300 cycles at a 200 mA g^{-1} rate after replacing the anode after 200 cycles.

Theoretical calculations have provided insights into parameters involving in the performance of RuO_2-based electrocatalysts. It should be mentioned that the adsorption energy influences the rate at which the LiO_2 intermediate forms and reacts on the electrode surface. A catalyst with an appropriate adsorption energy can facilitate the adsorption of intermediate species and subsequently promote their decomposition, enhancing the overall reaction kinetics. On the other hand, the stability of the LiO_2 intermediate on the electrode surface is also affected by its adsorption energy. If the adsorption energy is too low, the intermediate may desorb from the catalyst surface before completing the reaction, leading to poor stability and efficiency of the battery. Conversely, if the adsorption energy is too high, it may hinder the release of reaction products, affecting the reversibility of the battery [224–227]. A recent study using DFT calculations [224] reveals that the adsorption of LiO_2 intermediate on the RuO_2 electrocatalyst involves an enhanced adsorption energy (ΔE_{ads}) of −4.26 eV, comparing to that of Co

(−2.17 eV) in Co-N-C. In RuO_2/Co-N-C hybrid structure, the LiO_2 intermediate is associated with active atoms at the heterointerfaces, presenting a moderate ΔE_{ads} of −3.13 eV due to the cooperative interaction between RuO_2 and Co-N-C [225], thereby accelerating the ORR process. In this case, RuO_2/Co-N-C exhibits an increased adsorption energy for intermediates compared to Co-N-C, but a reduced value than RuO_2, which is beneficial to the desorption of LiO_2 [226]. Therefore, an appropriate intermediate adsorption energy is an important parameter to consider, diminishing the impedance by the RuO_2-based cathodes throughout the charging process [227].

Table 3 provides a summary of key material properties, synthesis conditions, and design parameters used for the cell assembly, as well as the main electrochemical performances of the LABs, which discussed various noble metal and noble metal oxide-based LABs. Even though the doped carbon structures mostly supported the ORR activity, noble metals., especially e_g engineered bimetallic structures and oxides like RuO_2 evidenced to provide better support towards OER performances. Hence, noble metals and their derivatives provide better overall bifunctional activity over the previously discussed non-metallic catalysts, as summarised in Table 3.

We next review the first block transition metal oxides and other derivatives as bifunctional catalysts for Li-O_2/Li-air batteries, which have a considerable interest over the last few years as a more affordable and abundant alternative for noble metals, and the engineered processes conducted at enhancing the catalytic activity of noble metals are also valid for first-block transition metals as well.

4.3. Transition Metal Compounds

Transition metal-based bifunctional catalysts were introduced at LABs as a cost-effective replacement for noble metals. But in recent years, some transition derivatives and their hybrids

started to overperform the noble metal catalysts. The following section will discuss the key developments in different transition metal-based catalytic structures towards efficient bifunctional catalytic activity. The progress of transition metal oxides, sulfides, nitrides, phosphides, and their hybrids as bifunctional catalysts for LABs will be discussed in the following sections.

Table 2: Summary of design parameters and output properties of LABs made using noble metal-based cathodes.

Type	Catalyst	Shape	Substrate	Method	Surface area ($m^2 g^{-1}$)	Pore Size (nm)	Discharge Capacity (mA h g^{-1})	Rate (mA g^{-1})	Cycle Number	Rate/ Limit	Over Potential (V)	Li_2O_2 shape	Ref
Single noble metal	Ru	NP	Carbon black	Soft template / heat treatment			9800	200	150	200	0.37	Toroidal	[211]
	Pt / Graphene	NP/ hollow nanocages	Carbon Paper	Combustion / PVD	374	1.5-10	5600	100	54	100	1.45	Toroidal	[205]
	Ru/ rGO	NP		Hydrothermal	124.0		10000	500	30	200	1.15	Film-like	[206]
	Ru/ graphene	NP/ NS	Ni foam	Chemical Reduction/ CVD	448.2		23864	200	200	200	0.43	Toroidal	[213]
	Au/ Graphene	NP/NS	Ni foam	Solution impregnation/ CVD	-	-	3347	400	300	400	-	Film-like	[214]
	Ru/ Mesoporous	Nanoparticle/ nanocube	Glass Fiber	Chemical reduction/ Hard	492.3	50-100	26100	200	120	400	0.28	Toroidal	[228]

	Carbon			Template									
	Ru/ ordered Porous C	Nanoparticle/ Ordered Pores	Ni foam	Chemical reduction/ Hard Template	451	250, 6.6-18.5	37523	500	120	1000	0.63	Nanosheets	[229]
Noble metal oxide	RuO_2/ CNF	Clusters of NP	Carbon paper	Chemical reduction/ Electrospinning			4680	100	300	200	1.3	Toroidal	[223]
	RuO_2	Ordered Porous	Al foil	Hard Template	116.9	16	555.5	100	70	100	1.1	Toroidal	[230]
	RuO_2/ CNT	Layered/ Nanotubes	Ni foam	Chemical oxidation/ Annealing/ Ultrasonication	226	30			224	1000	0.71	Film-like	[135]

4.3.1. Transition Metal Oxides and Derivatives

Several transition metal oxides (TMO) structures have been tested as bifunctional catalysts for LABs and related energy applications, including metal oxides [231], ferrites [232], binary spinel structures [233], perovskites [234] and their hybrids. MnO_2 and Co_3O_4 are two examples of TMO that are repeatedly reported for their better catalytic activity, low cost, and natural abundance[220–223].

The low electrical conductivity of most TMOs is the major concern since it leads to fast capacity degradation [235]. One strategy introduced in the literature to overcome some of the TMO-based cathode problems is to develop conductive binder-free electrodes. In-situ hybridization techniques can be adapted to typical TMO synthesis techniques such as hydrothermal [236,237] and electrochemical synthesis [238] to minimize the charge transfer resistance and the production of undesired side products during the Lab operation.

For example, a free-standing Co_3O_4 nanofiber-based electrode produced by Lee and Park using electrospinning has shown promising results [239]. Further, to minimize the effect of low conductivity, C.J. Park and co-workers made several attempts to hybridize MnO_2 with Co_3O_4 [240,241]. One of their latest studies reported impressive performances with hydrothermally produced MnO_2 and Co_3O_4 co-catalyst anchors on Ni foam [241]. The optimum result of 9690 mA h g^{-1} initial discharge capacity and 66 cycles at a high rate of 400mAg^{-1} was observed with a flower-like catalyst structure. High anodic and cathodic current peaks also further verify the developed catalyst's enhanced bi-functional catalytic activity [241]. Iron oxide binary oxides, especially in the form of ferrite crystal structures, showed reasonably good results as a bifunctional catalyst for LABs.

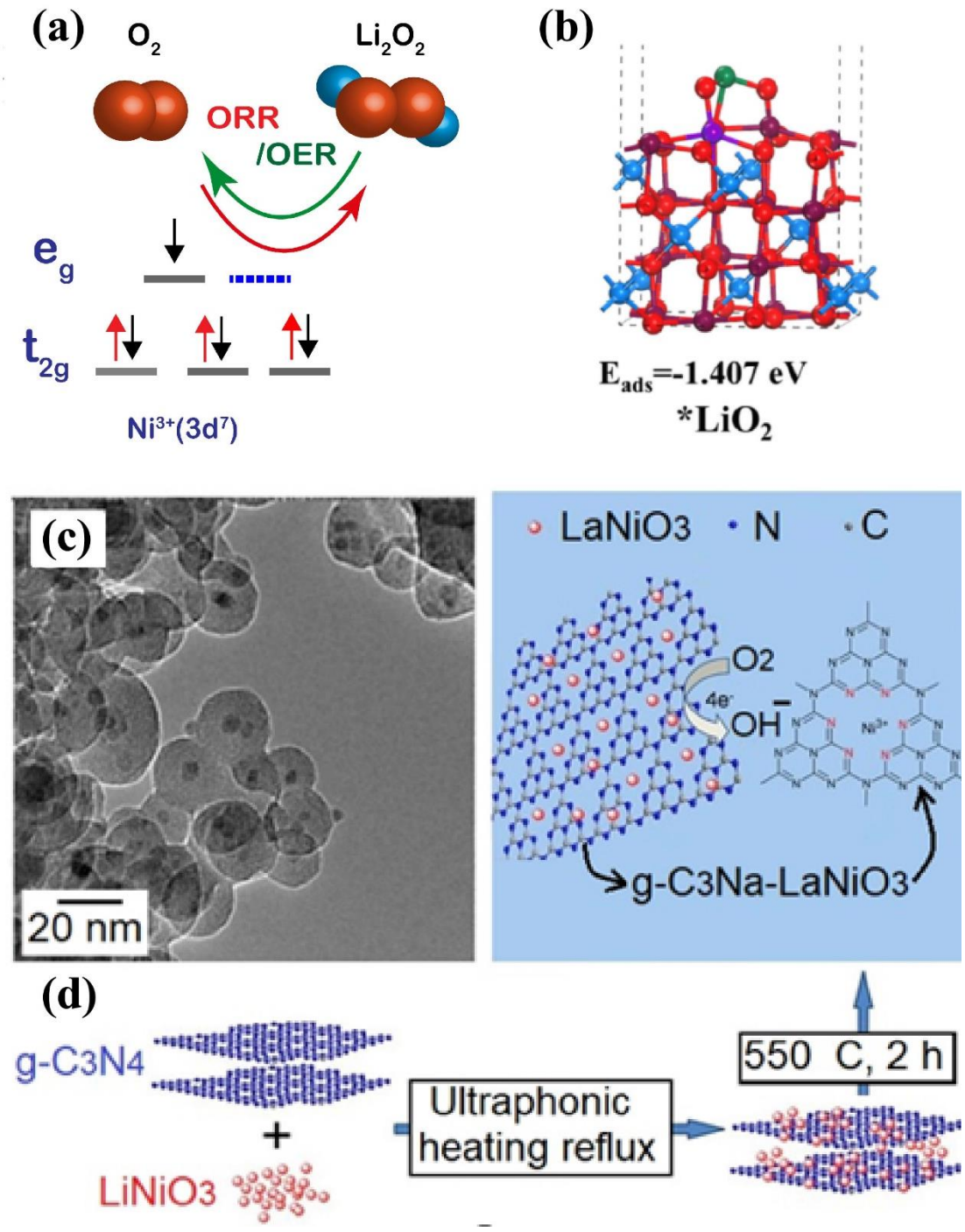

Figure 5: (a) ORR and OER catalytic support in semi filled e_g orbitals in transition metals [242], (b) high adsorption of LiO_2 at the surface of NiCoFeO catalyst [147], (c) TEM image of silica-coated $ZnFe_2O_4$ catalyst with a shell thickness of 11 nm [232], and (d) schematic of the synthesis steps of the CNL composite and its ORR mechanism [243]. Reprints with the permission from ref [243]. Copyrights 2022 Elsevier.

Compared to unary transition metal oxides, the presence of metallic cations in multiple valances and a large number of unsaturated coordination sites makes binary oxides more attractive as solid catalysts in Li-O_2 batteries [244]. The study conducted by Metin and co-workers reported the initial discharge capacity of 7510 mA h g^{-1} for $CoFe_2O_4$ nanoparticles anchored on Vulcan XC-72 cathode and the binary oxide was prepared by thermally decomposing cobalt (II) acetylacetonate and iron (III) acetylacetonate as Co and Fe sources [245]. Using a mesoporous hard silica template (KT-6), Yang et al. developed a 3D-ordered mesoporous $NiFe_2O_4$ catalyst with a controlled pore structure having an average pore size of 25.1 nm [88] The catalyst-coated cathode performed well compared to the bare Ketjen black cathode in terms of initial capacity (10830 mA h g^{-1}) and capacity retention over cycling (100 cycles at 0.1 mA cm^{-2} current rating), indicating the enhanced ORR and OER activity [88].

As in alloyed noble metals, electron structure modulation was found to be an attractive strategy for enhancing the catalytic activity and the electronic properties in the binary oxides. DFT calculations provide evidence on σ-bond formed through strong overlapping between 3d e_g orbitals of transition metals and 2p orbitals in oxygen is having a significant impact on the electronic structure of the intermediate discharged products associated with the ORR and the OER processes, compared to the π-bond occurs in between the 3d t_{2g}- 2p orbitals in transition metals and oxygen respectively [246]. Further, the theoretical calculations suggest semi-filled e_g orbitals are benefited, leaving room for oxygen to get adsorbed at the valent sites [247] as schematically illustrates in Figure 5a. Karunarathne et al. used a simple strategy of optimizing the stoichiometry of Ni and Co oxides to obtain a semi-filled e_g orbital occupancy in the hydrothermally derived microstructures. The high Ni^{3+} presence at the cathode surface obtained through substitutional disorders with crystal imperfections were reported to support a high adsorption to the reduced oxygen compounds and the assembled LABs reported to demonstrate an exceptional lifespan, operating for 3460 hours and completing 173 cycles while

achieving the highest discharge capacity of 13 759 mA h g^{-1} and low charging overpotentials [242]. Further, the research on ternary structures prepared by Pd-impregnation on $NiCo_2O_4$ [248] and Fe-doping on Ni-Co oxides [147] modifying the e_g orbital occupancy were also yielded improved outcomes. Ren and co-workers observed the near-unity e_g occupancy in the Fe-doped $NiCo_2O_4$ (NiCoFeO), which was prepared through respective hydrothermal and calcination steps [147]. As the authors describe, Fe^{3+} replaces some of the Co^{3+} at octahedral sites, and as an effect, the surface Ni^{3+}/Ni^{2+} ratio increases while the Co^{3+}/Co^{2+} ratio decreases, allowing high occupancy of Ni^{3+} ($t_{2g}^6e_g^1$) at the surface making sure a strong covalent metal-oxygen bond occurs, facilitating a high electrochemical activity in the material. The large carrier concentration and the high intrinsic conductivity with electronic states concentrates near the fermi level leads to fast oxygen transport in NiCoFeO. Furthermore, the increased adsorption capacity of oxygen in NiCoFeO (E_{ad} = -1.189 eV) compared to that of -0.547 eV of NiCoO demonstrated the contribution in Fe doping to enhance the oxygen adsorption, while strong adsorption of LiO_2 (E_{ad} = -1.407 eV) to the surface of the NiCoFeO catalyst as illustrated in Figure 5 b was found to be favouring the surface mediated mechanism as discussed in section 3.

The assembled Li-O_2 by using the engineered material as the self-standing cathode yielded an initial discharge capacity of 14, 978 mA h g^{-1} and cycle performances over 790 hours at the current rate of 500 mAg^{-1}, with low charging overpotentials, showcasing the effective use of controlled e_g orbital occupation as presented in Figure 5 (a).

Following the successful attempts with using protective alumina [249] and silica [250] coating on LIB cathodes enabling high-capacity retention and protection against HF, an attempt to enhance the catalytic activity of the $ZnFe_2O_4$-based catalyst by adding a coating silica layer was reported by Metin et al. [232]. During the study, $ZnFe_2O_4$ nanoparticles were prepared via

forming micelles using oleic acid with diameters around 6 nm. The silica coating thickness varied from 9 to 13 nm by varying the added TEOS amount from 0.5 ml to 1.5 ml in the emulsifying mixture. The TEM image in Figure 5(c) verified the successful formation of silica coating over ferrite nanoparticles. The discharge capacity and cyclic stability varied with the coating thickness and the optimum results were obtained with an 11nm coating thickness.

In recent years, highly improved photovoltaic performances have been shown by perovskites. Perovskites, ABO_3-like metal oxide structures were found to be similarly effective as electrocatalysts to promote ORR and OER reactions, especially when an early transitional metal occupies the B site. The transition metal enhances the electrical conductivity by altering the electronic structure and providing numerous reaction sites for enhanced catalytic activity [251,252]. Zhang. Y et al. developed a hybrid catalyst by mixing graphitic carbon nitride (g-C_3N_4) with $LaNiO_3$ [243]. g-C_3N_4 is a layered structure where every C atom is bonded with three N atoms, either as graphitic or pyridinic nitrogen. The lone-pair electrons in the pyridinic structure are ideal for bonding with oxide ions, and they also help to alter the electronic structure [253]. Further, it was understood that the presence of Ni^{3+} at the B site of the $LaNiO_3$ perovskite enhanced both ORR and OER by introducing favourable binding energies with semi-filled e_g orbit, verifying the effectiveness in the concept discussed related to ternary oxides. During the study, the researchers were able to enhance the bifunctional catalytic activity of $LaNiO_3$ by elevating the Ni^{3+}/Ni^{2+} ratio as it composites with g-C_3N_4 and producing the composite catalyst called CNL. The g-C_3N_4 was produced by pyrolyzing melamine at 550 ^{0}C and $LaNiO_3$ nanoparticles were produced by calcining the previously produced metal citrate gel via a sol-gel method. The final composite was prepared by heating the ultrasonicated g-C_3N_4 and $LaNiO_3$ dispersion at 550 ^{0}C for 2 hours in an N_2 atmosphere as shown in the schematic diagram in Figure 5(d). The composite with 10% g-C_3N_4 loading delivered the best outcome with lower ORR and OER polarization potentials, discharge capacity over 5000 mA

h $g^{-1,}$ and cycling stability over 65 charge/ discharge cycles at a high current of 250 mA g^{-1}. The XPS analysis verified the higher Ni^{3+}/Ni^{2+} ratio in the composite using the Ni $2p^{3/2}$ spectrum and it also identified that stronger Ni-O bond in the composite, promoting ORR and OER kinetics for better catalytic activity.

Table 3: Summary of input parameters and resultant outputs in LABs made using TMO-based cathodes

Type	Catalyst	Shape	Substrate	Method	Surface Area ($m^2 g^{-1}$)	Pore Size (Nm)	Discharge Capacity (mAh g^{-1})	Rate (mA g^{-1})	Cycle Number	Rate/ Limit	Over Potential (V)	Li_2o_2 Shape	Ref
Transition Metal Oxides/ Derivatives	Mn/Co Oxide	Spherical Flower-Like	Ni Foam	Hydrothermal/Annealing	105.71	12.55	9690	200	66	400	1.04	Semi-Circular	[241]
	$CoFe_2O_4$/ Vulcan C	Spherical	Copper Foil	Chemical Conversion/ Self-Assembly			7510	100	4	100	1.0	-	[245]
	Silica Coated $ZnFe_2O_4$	Nanoparticles	Carbon Paper	Cmc / Reverse Microemulsion	-	-	6200	100	45	1000	0.85	Toroidal	[232]
	$NiFe_2O_4$	Spinel-Structured	Ketjen Black	Hydrothermal/ Calcination	105.2	25.1	10830	50	100	50	0.85	Toroidal	
	G-C_3n_4-$LaNiO_3$	Layered	Carbon Paper	Pyrolysis/ Calcination	-	-	5000	250	65	250	1.2	-	[243]

	Fe_3O_4/ CoO	Core-Shell Nanostructure	Nickel Foam	Hydrothermal/ Calcination	-	200	5100	100	50	100	0.45	Toroidal	[254]
	$La_{0.9}Mn_{0.6}Ni_{0.4}O_{3-\delta}$	Nanofibers	Carbon Paper	Sol-Gel / Electrospinning	29	35	9959	100	100	300	1.11	Film-Like	[128]
	$La_{0.6}Sr_{0.4}Co_{0.2}Fe_{0.8}O_3$	Spherical	Nickel Foam	Sol-Gel /Calcination	10.69		13979	200	20	200	0.89	Leaf-Like	[255]
	$LaCo_{0.6}Ni_{0.4}O_3$/ Co_3O_4	Nanofibers	Toray Carbon Paper	Electrospinning/ Hydrothermal	30.7	50	11288	1000	116	1000	0.97	Sheet-Like	[256]

In a more recent development, the catalytic reaction kinetics of the perovskite structures has been enhanced by replacing the B site with two transitional metals. The cathode produced with wrinkled $La_{0.9}Mn_{0.6}Ni_{0.4}O_{3-\delta}$ nanofibers demonstrated excellent rate capability and could withstand 100 cycles under 300 mAg^{-1} current density. Doping the B sits with different valence ions has improved the conductivities and introduced numerous active sites that promote the oxygen reaction kinetics [128]. A similar study was conducted by Cheng et al. with $La_{0.6}Sr_{0.4}Co_{0.2}Fe_{0.8}O_3$ nanoparticle-based cathode. Even though an impressive discharge capacity of 13,979 mA h g^{-1} was recorded, the battery could not survive more than 20 charge/ discharge cycles[255]. Further, an outstanding synergy in betweenCo_3O_4 nanoparticles and $LaCo_{0.6}Ni_{0.}4O_3$ nanofibers was reported by Sun et al. towards providing improved electrocatalytic activity [256]. During the study, ultrafine Co_3O_4 nanoparticles were anchored on electrospun $LaCo_{0.6}Ni_{0.}4O_3$ nanofibers via a hydrothermal process, as illustrated in the schematic diagram in Figure S5(a). Figures S5(b, c) provide SEM and TEM micrographs of the synthesized catalyst. A low charge voltage plateau around 3.7 V and a high specific

discharge capacity of 11,288 mA h g^{-1} were observed at the first charge. Outstanding stability with 116 cycles at 1000 mA g^{-1} current density further verified the excellent catalytic activity of the $Co_3O_4/LaCo_{0.6}Ni_{0.}4O_3$ catalyst towards OER and ORR kinetics. The researchers urged that the sheet-like morphology of the produced Li_2O_2; shown in Figure S5(d), was the key to the low charging overpotential and the better cycling stability, which facilitates the dissolution of the peroxide during the battery charges. The article also stressed that the uniformly distributed Co_3O_4 nanoparticles at the surface of $LaCo_{0.6}Ni_{0.}4O_3$ may help to form such a 2D-structured Li_2O_2. As graphically illustrated in Figure S5(e), a higher number of surface catalytic sites in the developed catalyst helped to increase the chemisorbed of oxygen. As a result, the discharge products formed uniformly along the surface of the cathode in a thin sheets-like rather than spherical morphology. This study is one key example advocating the surface-mediated mechanism over the solution-mediated mechanism, even though it's not very clear whether a thicker layer exceeding 9 nm was formed during the study to achieve such a high discharge capacity.

Surprisingly fairly limited facet engineering studies were conducted up to date on metal oxides, and we believe it's very important to identify the high-performing crystal facets and engineer the cathode structure in a way of maximizes the exposure of oxygen and discharged products Cr2O3at the identified high-energy facets, to achieve enhanced oxygen kinetics in Li-O_2 batteries. Lai et al. provided useful insight in this regard through the analysis of OER activity of different facets of Cr_2O_3, and they found high OER activity in Li-O_2 batteries can be achieved by inhibiting the growth of low-energy facets of Cr_2O_3 [136]. Researchers were able to inhibit the growth of (012) low-energy facet by adding anatase TiO_2 into the synthesis mixture and achieved impressive OER activity during the battery charging (0.12 V lower than Ru/C) owing to strong interactions between uncoordinated sites on the high-energy facets (ex.

116 and 110) and the intermediates as $Li_{2-x}O_2$. We believe it's worth investigating the strategy further with better-performing catalysts as MnO_2, and Co_3O_4 and their complex structures.

Table 4 summarises the different design parameters discussed related to TMO-based catalysts with the corresponding reported performance. High resistance is one of the critical drawbacks repeatedly reported in the literature. In general, binary oxides and perovskites with mixed valances provided improved catalytic activity. Even though the techniques were yet to mature, the novel design strategies focusing on the surface energy of metal oxides e_g orbital occupation modulation via inhibiting the low energy facet growth, and heteroatom doping started to be proven as vital approaches in addressing the shortcomings in TMOs. As synthesis approaches, the hydrothermal technique was more frequently used to synthesize binary and ternary metal oxides, and perovskites were mostly synthesized through carbonizing the electrospun nanofibers.

4.3.2. Transition Metal Sulfides and Selenides

Transition metal Sulfides (TMSs), selenide (TMSes), and TMOs have similar physicochemical properties due to the similarity in their electronic structure [257]. However, TMSs have the advantage of high electrical and lower tuneable optical bandgap. Many TMSs and TMSes, such as CdSe and SnS_2, are ideal semiconductors for applications like solar cells, photocatalytic processes, and energy storage applications [257–260]. Therefore, TMSs can overcome the previously mentioned shortcomings observed with TMOs associated with their poor electrical conductivity. Moreover, loosely stacked structures and 2D structures of TMSs such as 2D MoS_2 can provide enough spacing to accommodate discharge products such as Li_2O_2 with low volume expansion. They can also act as the cathode, eliminating electrochemically unstable carbonous electrodes and binders [261]. Furthermore, the verification of the support of TMSs

towards ORR kinetics in fuel cell applications [262,263] and OER kinetics in water splitting applications [264–266] are a few other facts that favour the applications of TMSs in LABs.

***Nickel and Cobalt Sulfide*:** The first study with a metal sulfide catalyst in aprotic LABs was reported in 2015 by Zhang, Z. et al. [267]. They synthesized flower-like (f-NiS) and rod-like (r-NiS) nickel sulfide electrocatalysts via a hydrothermal method. During this initial study, f-NiS performed with better OER and ORR activities over r-NiS, showing a higher discharge capacity and cycling stability with 6733 mA h g^{-1} and 30 cycles, respectively, at 75 mA g^{-1}. The later studies conducted on Ni_3S_2 [268] were able to provide superior performances through enhanced catalytic performances and controlling the morphological properties of the discharged product, achieving stability over 100 cycles. Among various cobalt sulfide catalysts experimented [269], CoS_2 nanocage catalysts reported synthesized using a zeolitic imidazolate framework (ZIF-67) as a precursor [270] yielded superior conductive network. Nevertheless, the battery performances were limited. We believe, the identified parasitic products as $LiCO_3$ and HCO_2Li are believed to be responsible for the early decay in performances. However, the study doesn't conclude the possible mechanisms of parasitic reactions, where an in-depth analysis would help determine the factors affecting the forced decay in battery performances. In comparison, DFT calculations conducted by Lin et al [271] reveals Co_9S_8 is having high adsorption to O2 and intermediate discharged products over cobalt oxides as CoO. The experimental evidence seems to be reflecting the theoretical observations where closely arranged distribution of small hydrangea-like Li_2O_2 particles were observed in very large quantities deposited along the edge sites of the Co_9S_8 on the discharged cathode.

***Molybdenum Sulfide*:** Following the excellent catalytic activity provided by MnO_2, the efficiency of MoS_2 as a cathode catalyst material was also investigated for Li-O_2/Li-air batteries, and particularly its 2D allotrope can be useful in LABs because it could allow for

easy oxygen diffusion[272]. In previous reports, MoS_2 provided a superior catalytic activity towards ORR and HER reactions at its edge sites [273,274]. However, as in many other TMSs, MoS_2 has low intrinsic electrical conductivity [275]. MoS_2 mainly was anchored on a conductive carbon skeleton, such as the work reported by Angun Hu et al.[268] to improve the conductivity. MoS_2 nanosheets were in-situ grown on hollow carbon spheres (HCS) using a hydrothermal reaction (at 200 °C for 24 h.) using thiourea and $(NH_4)_6Mo_7O_{24}\cdot 4H_2O$ as sulfur and molybdenum precursors, respectively as illustrates in Figure 6(a). The cathode with 4–9 layers thick MoS2 sheets on HCS performed well in the assembled LAB with a good discharge capacity of 4010 mA h g^{-1} and long cycling stability of 105 cycles.

Asadi et al. experimented with using the naturally occurring 2D transition metal dichalcogenides as Li-O_2 battery cathode by using the exfoliated MoS_2 [261]. The battery cathode was prepared by homogenously depositing 1–3-layer thick MoS_2 nanosheets on a Toray carbon paper which was used as the GDL. The prepared electrode combined with an ionic liquid (1-ethyl-3-methylimidazolium tetrafluoroborate (EMIM-BF4)) was reported as a fine system catalyzing ORR and OER kinetics. As identified via DFT calculations, in the MoS_2/ IL co-catalyst system, $EMIM^+$ ions cover the Mo atoms present at the edge, making the Mo atoms isolated. However, the cycling ability of the assembled LAB cell is only limited to 25 cycles with relatively poor discharge capacity with 1450 mA h g^{-1}. Better conducting layered dichalcogenides could provide improved performances with improved interfacial properties.

***Manganese Sulfide*:** Even though MnO_2 has been identified as a very good catalyst to promote oxygen kinetics at the cathode of the Li-O_2 battery [85], it was only very recently the electrocatalytic activity of MnS was evaluated. MnS is known as a p-type semiconductor and is known to have three different phases called α, β, and γ. Among these phases, α-MnS is a green-colored rock salt-like stable structure, and the pink colour γ-MnS is only stable at low

temperatures [276]. Shuling Li et al. synthesized γ-MnS using a solvothermal technique, and α-MnS was also produced by heating γ-MnS at 450 ^{0}C for 10 hours under an argon environment as shown in the schematic presented in Figure 6(b) [277]. The LAB cathode fabricated by spraying the ethanol-dissolved mixture of γ-MnS catalyst onto a nickel foam exhibited strong bi-functional catalytic activity showing only 0.693V potential differences in-between OER and ORR peak potentials during the CV study, which is one of the lowest polarization potentials reported. An outstanding discharge capacity (14017 mA h g^{-1} at 100 mA g^{-1} current rate) and stable cycle performance (87 cycles at 400 mA g^{-1} current rate for a discharge depth of 900 mA h g^{-1}) further verified the strong bifunctional catalytic activity of α-MnS. The researchers suggested; that (a) the unique cross-linked cashew-like and spherical pellets-like morphologies of the discharged product (Li_2O_2) and (b) the high conductivity of large lattice volume accounted for the improved performance.

***Binary sulfides*:** In addition to monometallic transition metal sulfides, few studies reported binary sulfides, such as $NiCo_2S_4$ [278], $CoNi_2S_4$ nanorods [279], $ZnCo_2S_4$ nanosheets [280], and $MnCo_2S_4$ nanosheets [281] as suitable cathode materials for Li-O_2/Li-air batteries. Compared with TMOs and monometallic TMS, binary sulfides have high electric conductivities and a larger number of redox catalyst sites, which could enhance the catalytic performance [282].

The LAB cathode prepared by growing $MnCo_2S_4$ nanosheets (MCS NSs) on carbon paper (MCS/CP) showed a discharge capacity of 10760 mA h g^{-1} and excellent cycle stability with the cell sustained over 96 cycles at 200 mA g^{-1} current rate for a discharge depth of 500 mA h g^{-1} [281]. The binder-free electrodes were prepared by vulcanizing the electrochemically deposited Mn-Co-sulfate NSs on the carbon paper as illustrated in Figure S6(a). It was reported that Mn-Co-sulfate NSs were modified as mesoporous structures of MCS under given

conditions (Teflon-lined stainless-steel autoclave at 180 ^{0}C for 10 h). The mesoporous structure, superior electrical conductivity, larger surface area, and high affinity toward LiO_2 in MCS/CP are responsible for the superior catalytic performance over the similarly prepared ternary oxide (MCO/CP) electrode.

In another important study conducted by Anjun Hu et al. [279], the remarkable cycling stability of 588 cycles (at 500 mA g^{-1} current rate for a limited capacity of 1000 mA h g^{-1}) was achieved by anchoring 3D mesoporous $CoNi_2S_4$ nanorods on a carbon textile (CNS-RAs/CT) as the cathode of LAB. The CNS-RAs/CT cathode was prepared by directly growing the CNS nanorods on the CT through a two-step hydrothermal procedure. Co/Ni nanorod arrays were grown on CT in the first step. Then, the Co/Ni nanorods were converted into CNS structures by reacting with Na_2S in an autoclave at 160 ^{0}C for 6 hours where the schematic of the process is shown in Figure S6(b). The authors observed a full coverage of the CT with the CNS nanorods. The CNS-RAs/CT showed very good electrical conductivity and open spaces in the cathodic structure, which contributed to the superior stability of the cell. In addition to the long cycle stability, the cell also exhibited a reasonable discharge capacity (5438 mA h g^{-1}) and lower ORR (0.36V) and OER (1.19V) overpotentials.

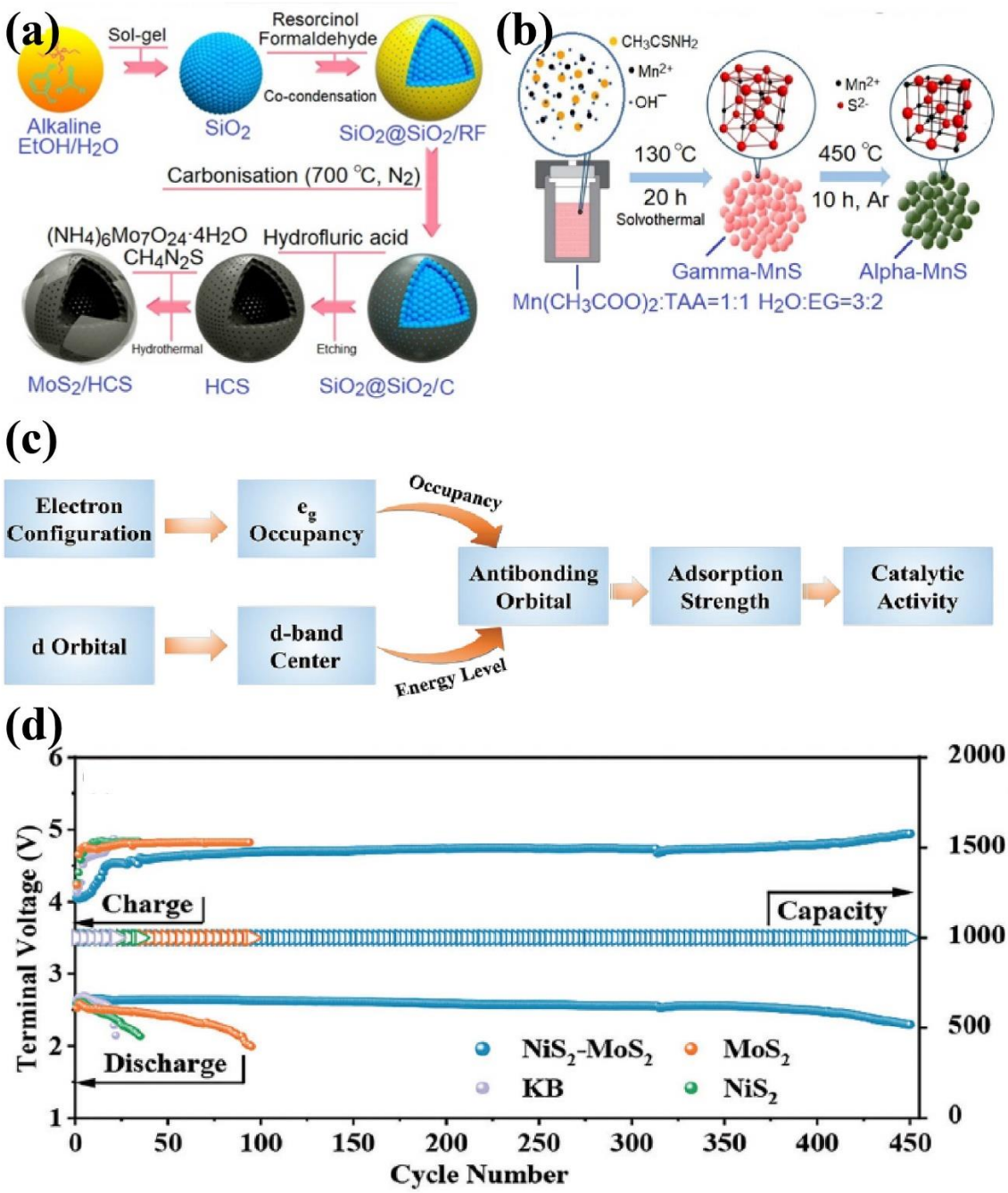

Figure 6: Binary Sulfides used at LAB cathodes (a) In-situ growth of MoS_2 nanosheets on hollow carbon spheres (HCS) using a hydrothermal reaction [254], (b) Schematic diagram for solvothermal synthesis of γ-MnS and the production of α-MnS via heat treatment of γ-MnS at 450 ^{0}C under argon environment [277], (c) illustration of d-band electron configuration modulation for higher catalytic activity using DFT calculations, and (d) its effect on Li-O_2 battery cycle performance at 1000 mAg^{-1} [272]. Reprints with permission from ref [254]. Copyright 2019 American Chemical Society

***TMS on doped carbon nanostructures*:** The hybrid cathode prepared by P. Ramakrishnan et al. by wrapping FeS nanoparticles with N and S doped 3D nanofoam (FeS-C) delivered a high discharge capacity of 14 777.5 mA h g^{-1} at 0.1 mA cm^{-2} current rate [283] The cell survived for 100 cycles when cycled at a limited discharge depth of 500 mA h g^{-1} at 0.1 mA cm^{-2} with a relatively lower polarization gap of 0.73V. The hybrid was prepared by carbonizing the MOF using iron sulfate heptahydrate, citric acid, glycine, and DI water at 1200 ^{0}C for 5 hours. In this hybrid, the uniformly distributed FeS nanoparticles promote the OER reaction by oxidizing Li_2O_2 while the 3D carbon provides the necessary support for gas diffusion, electron transfer, and accommodating Li_2O_2. The dopant sites promote ORR reaction by adsorbing Li^+, as discussed in many other articles. It is worth mentioning here that the hybrid catalyst has a very low percentage of carbon (< 5%). As was understood by reviewing the previous reports, it could help to minimize the number of side products produced during the discharge, which leads to deuterating the Li-O_2 battery performance and cycle life.

In another study, Yuan Cao et al. prepared a cathode based on Co_9S_8 nanoparticles encapsulated by S and N dual-doped graphitic shells (Co_9S_8@G/NS-PCNF) as indicates in the provided schematic diagram; see Fig S6(c) [284]. The prepared cathode showed a high of 8269 mA h g^{-1} at a current density of 100 mA g−1 and a small polarization gap (1.52 V). The LAB with the Co_9S_8@G/NS-PCNF cathode could be cycled for over 60 cycles at 200 mA g^{-1} with a fixed capacity of 1000 mA h g^{-1}. Suyeon Hyun et al. prepared $NiCo_2S_4$ nanoparticles anchored on S-doped porous carbon nanostructure [285] and used them as the active materials for the cathode of the LAB. A high discharge capacity of 14173 mA hg^{-1} at 150 mAg^{-1} and considerably high cyclability over 100 cycles for 1704 h were achieved. The improved electrocatalytic activities were attributed to the low ohmic resistance and the mesopore structure with 20-30 nm pore diameters.

It was noteworthy to mention that, during the studies by Anjun Hu et al. [279] and Yuan Cao et al. [284], the researchers were careful about exposing the least amount of carbon materials to the discharged and intermediate products, and it seems to work in favour of the researchers. This could be another strategy that could be experimented with in future studies not limited to TMS.

In previous sections, different strategies were used to improve the battery performance by enhancing the catalytic activity via reducing the occupancy in the high energy sub-state (e_g) of the d-orbitals, allowing strong adsorption on catalytic sites, and the diagram in Figure 6(c) is further illustrating the concept. Zhou et al. were successfully able to enhance the Li-O_2 battery performances by modulating the e_g occupancy of NiS by forming a hierarchical heterostructure with MoS_2 [146]. As DFT calculations suggests, as the heterostructure forms, the relatively high electronegativity of Ni atoms was able to withdraw electrons from the Mn atoms, leaving unsaturated eg orbitals as its occupancy was lowered. The conducted density of the state (DOS) calculations reveals the formation of an internal electrical field promoting migration of charges through the formed interface as the common facets of MoS_2 (002) and NiS_2 (210) are having different work functions, where the MoS_2 and NiS_2 phases are having characteristic semiconductor and metallic properties respectively. The formed semiconductor-metallic interface was proven to support the adsorption of reaction intermediates, while the delocalized electrons in MoS_2 was also understood to promote the reaction kinetics and the overall battery performances. The heterostructure cathode material helped achieve high cyclability with 450 cycles as illustrates in Figure 6 (d) and a large discharge capacity of 16528 mA h g^{-1} exceeding the performance of many other TMS-based cathodes used in Li-O_2/Li-air batteries.

The performances of discussed different binary, ternary, and hybrid TMS catalysts are summarised in Table 5. Among them, manganese-based catalysts produced better catalytic

activity, but the performances were fairly limited. In contrast, the ternary and hybrid catalyst-based batteries exhibited much-improved performances. The relatively higher conductivity of such compounds may reduce the interfacial resistance between the electrolyte and the current collector, allowing the cell to operate at a relatively lower potential window, which minimizes the decomposition of the electrolyte and the supportive carbon network. But the long-term stability of the catalyst doesn't report to be as strong as the oxides. A distinguishable improvement in electrocatalytic performances was observed as a minimum portion of the carbon scaffold is exposed, and also through the e_g orbital occupation modulation, further research in the mentioned topics is essential to uncover the successful pathways of designing advanced LAB technology.

4.3.3. Transition Metal Phosphides

Despite continued improvements, the cathodes based on TMOs and TMSs and their hybrids still have many challenges to overcome related to cyclability and charging overpotential mainly due to the relatively low conductivities. As an alternative, Transition Metal Nitrides (TMNs) and Transition Metal Phosphides (TMPs) were started to be utilized as LAB cathodes since they are known for higher electrical conductivity and better stability elsewhere related to anticorrosive studies and water-splitting applications. As a fact, TMPs and TMNs have shown promising results in water-splitting studies as bifunctional catalysts for HER and OER reactions in the last couple of years. Ni_3N produced by calcining Ni foam with thiourea [286], Co_4N produced by N_2 plasma treatment of Co_3O_4 nanowires [287], and Co-doped Co_4N prepared via hydrothermal process [288] are some examples of the TMN used for water splitting applications. With regard to TMPs, the most common methods to prepare the catalysts are the thermal treatment with PH_3 gas, the thermal decomposition of NaH_2PO_2 [283,286,287,289] or the treatment with red phosphorous[288,290].

***Monometallic Phosphides*:** Nanoflakes of MoP was one of the first TMPs tested in LAB functionality. During the study conducted by Minghui Wei et al., hydrothermally produced MoO_3 was converted into MoO_2 and MoP nanoflakes by thermal phosphodising using NaH_2PO_2. The free-standing cathode prepared with in-situ deposited MoP nanoflakes on carbon cloth could deliver a discharge capacity of 4.15 mA h at a current of 0.1 mA and a long cycle life of 400 cycles. The cell also exhibited higher anodic current density, lower overpotential between cathodic and anodic onset potentials (0.81V), higher cyclic efficiency (95%), and full decomposition of discharge product (Li_2O_2) [291]. The same group also developed an LAB cathode based on MoP quantum dots. Instead of carbon cloth, MoP quantum dots were anchored on N, P co-doped hollow carbon fibers (MoP QD@HCF) via hydrothermal and subsequent heat treatment step at 800 ^{0}C for 3 hours [292]. The synthesis of MoP QD@HCF was confirmed by XRD, SEM, TEM, and EDX analysis, as shown in Figures 7(e-f).

The hollow fiber structure provided reasonable support for gas diffusion, numerous catalytic sites, and a large contact area between the electrolyte and the cathode. The assembled Li-O_2 cell could deliver a relatively high discharge capacity (6.75 mA h cm^{-2}) and lower overpotential. However, the cell struggled with low cycle stability (30 cycles), raising questions about the practicality and stability of MoP QDs as bifunctional catalysts. In another example, Zhang et al. prepared CoP microspheres via a hydrothermal process using CTAB as the soft template and $Co(NO_3)_3.6H_2O$, and $NaH_2PO_4.2H_2O$ as Co and P sources, respectively, exhibited in Figures 7(a, b). The cathode fabricated using these CoP microspheres delivered encouraging results with good round trip efficiency (>90%), reasonable discharge capacity (2994 mA h g^{-1} at 100mA g^{-1}), and cycle stability (up to 80 cycles at 500mA g^{-1} current rate) [293].

Table 4: Summary of input parameters and resultant outputs in LABs made using TMS-based cathodes

Type	Catalyst	Shape	Substrate	Method	Surface area ($m^2 g^{-1}$)	Pore Size (nm)	Discharge Capacity (mA h g^{-1})	Rate (mA g^{-1})	Cycle Number	Rate/ Limit	Over Potential (V)	Li_2O_2 shape	Ref
Transition metal sulfides	NiS	Flower-like	Carbon paper	Hydrothermal	-	-	6733	75	30	75	1.38	toroidal	[267]
	Ni_3S_2	Porous Foam	Ni foam	Hydrothermal	171.1	10.3	7478	300	100	300	1.36	Laminar-2D	[268]
	Co_3S_4	nanosheets	Ni Mesh	Hydrothermal	23.21	15-24	6990	200	25	100	0.92	-	[269]
	CoS_2 / CNT	nanocages	Celgard 3500 GDL	Hydrothermal	-	-	2400	188.5	52	188.5	1.05	Film-like	[270]
	Co_9S_8	Flower-like	Porous carbon film	Hydrothermal	14.5	-	6875	50	105	100	0.57	hydrangea-like	[271]
	MoS_2/ hollow carbon spheres	nanosheets	Carbon paper	Hydrothermal	244.98	7.66	4010	200	105	200	1.44	Film-like	[294]
	MoS_2	nanosheet	Carbon Paper	Exfoliation	-	-	1450	222	50	222	0.8	Film-like	[261]
	α-MnS	Rock salt-like	Nickel	Solvothermal	17.93	-	14017	100	87	400	0.693	Pellets-like	[277]

			Foam										
	$MnCo_2S_4$	nanosheet	Carbon paper	Hydrothermal	55.4	14.36	10760	200	96	200	0.90	Film-like/ pellets-like	[281]
	$CoNi_2S_4$	nanorods	Carbon textile	Hydrothermal	19.93	6.21	5438	500	588	500	1.54	Film-like	[279]
	FeS	nanoparticles	N, S doped 3D carbon foam	MOF/ Carbonisation	88.5	18.3	14 777.5	0.1 mA cm^{-2}	100	0.3 mA cm^{-2}	0.73	Toroidal	[283]
	Co_9S_8	nanoparticles	N, S doped graphitic sheets	Electrospin/ Pyrolysis	204.71	6-12	8269	100	60	200	1.52	Film-like	[284]
	$NiCo_2S_4$	nanoflakes	S doped porous carbon	hydrothermal	461	2.9	14173	150	100	150	1.32	Toroidal	[285]

***Bimetallic Phosphides*:** Similar to bimetallic sulfides and oxides, binary phosphides could provide better OER activity over the monometallic due to the improved conductivities and abundance of the active sites. Bimetallic Co and Fe were amongst the first TMPs to be investigated [295,296]. Kailing Sun et al. developed a LAB cathode using CoFeP nanodots as the active catalytic layer [297]. A three-step process prepared the catalyst: pyrolysis and phosphorization, followed by a freeze-drying step. The egg white was used as the nitrogen-rich carbon source, and the NaCl was used as the template and washed away before the

phosphorization step as illustrated in Figure 7(c). The LAB assembled with the CoFeP nanodots as the active material sustained up to 141 cycles and delivered a maximum specific discharge capacity of 11969 mA h g^{-1} at 100 mA g^{-1} displaying better cycle stability. We believe the capacity could be further improved by increasing the percentage of mesopores in the catalyst structure since the morphology indicates the micropores are dominant.

During the study conducted by Huagen Liang at el., a Li-O_2 battery was assembled using a self-standing cathode prepared using NiFeP nanoparticles deposited on a 3D biochar network, shown in Figure 7(d) [298] The cathode was prepared via the phosphodisation of pre-synthesized NiFe-Prussian blue analogs (PBA)/biomass precursors using red phosphorous at 900 °C for 4 h under an Ar environment. The synthesis of NiFe-PBA)/biomass precursor was carried out by following one of their previous studies [299], and NiFe-PBA deposited pomelo peels were calcined at 1000 ^{0}C under an Ar environment to prepare the NiFe-PBA/Biomass precursor. The XRD, HRTEM, and XPS analysis indicated that NiFeP nanoparticles had the composition of Fe-doped Ni_2P, and the surface of the catalyst was also oxidized. The Li-O_2 battery assembled with the NiFe-PBA-based catalyst performed better than the TMP-free P-doped Biochar catalyst. The battery with NiFe-PBA-based catalyst survived over 90 charge-discharge cycles and provided a specific discharge capacity of 10.9 mA h $g^{-1}_{cathode}$ at a current density of 0.05 mA cm^{-2}.

With limited literature, it's difficult yet to provide an in-depth review of the performances of TMPs as LAB cathodes. But it's great to observe the results presenting in more meaningful means as capacity/cm^2 or as capacity/weight of the cathode. With that information only, one could have a real impression of the capacity of the assembled battery. As per previous sections, the results summarised in Table 6, and overall, of TMPs provide impressive outcomes, and

better-performing TMPs could expected to be reported sooner if the previously discussed catalytic activity boosting strategies could effectively tune the properties of TMPs.

4.3.4. Transition Metal Nitrides

To overcome the barriers of forming irreversible Li_2O_2, side products, and low electrical conductivity of the air cathode, transition metal nitrides (TMNs) have also been utilized as a potential alternative bifunctional catalyst as TMPs in recent years. TMNs such as nickel nitride [300], cobalt nitride [301] and bimetallic nitrides as cobalt-molybdenum nitrides [302] were successfully utilized in various energy storage applications.

Among various TMPs, Co_4N is reported to be an efficient bifunctional catalyst due to its metallic nature, good stability, and better catalytic activities[298,299]. Ki Ro Yoon et al. reported that long-cycle stability (177 cycles at 200 mA h g^{-1} current rate with the restricted capacity of 1000 mA h g^{-1}) was achieved as brush-like Co_4N catalyst anchored on N-doped carbon nanofiber (CNF) used as the free-standing cathode. The brush-like Co (OH)F nanoparticles were grown on the electrospun CNF via a hydrothermal process, where $CoNO_3.6H_2O$, urea, and NH_4F were used as the key ingredients. The self-standing cathode (Co_4N/CNF) was prepared through a nitridation step at 550 ^0C for 2 hours under an NH_3 gas environment. The Co_4N particles were found to be coated with a thin layer of cobalt oxide, giving additional support for the adsorption of LiO_2. It also facilitated the deposition of film-like Li_2O_2 on the cathode surface, which is known to be easy to decompose in the charging over the toroidal Li_2O_2 crystal and could form through the solvation-mediated pathway.

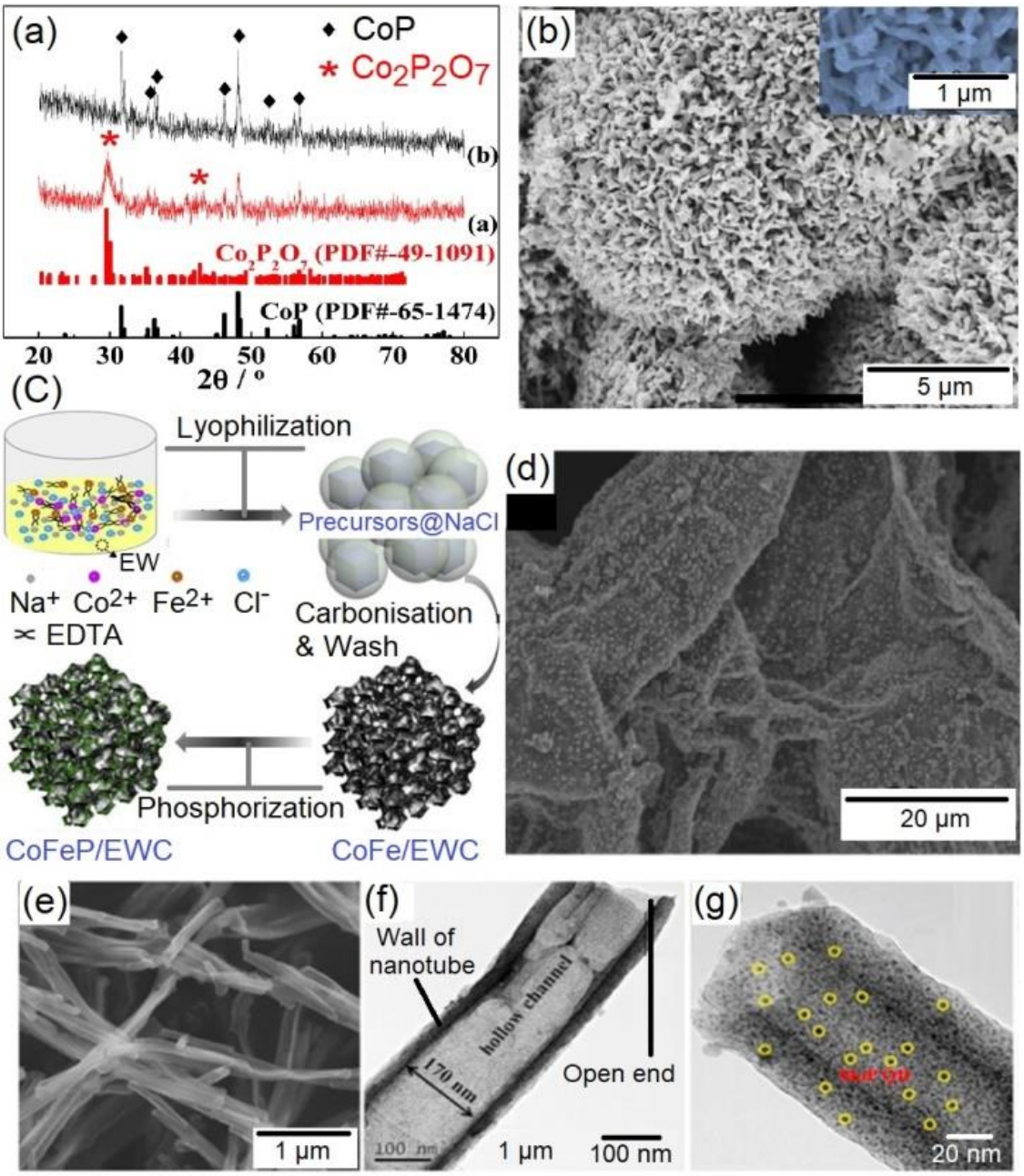

Figure 7: (a)XRD (b)SEM of hydrothermally synthesized CoP microspheres [280], (c) synthesizing procedure of CoFeP bimetallic phosphide [284], (d)SEM image of NiFeP nanoparticles deposited on 3D biochar network [285], (e- g) SEM and HRTEM images of MoP quantum dots on N, P doped carbon fiber [279]. Reprints with permissions from ref [279, 280, 285, 286]. Copyrights 2019 Elsevier, 2018 Elsevier, and 2020 Elsevier.

Table 5: Summary of input parameters and resultant outputs in LABs made using TMP and TMN-based cathodes.

Type	Catalyst	Shape	Substrate	Method	Surface area ($m^2 g^{-1}$)	Pore Size (nm)	Discharge Capacity (mA h g^{-1})	Rate (mA g^{-1})	Cycle Number	Rate/Limit	Over Potential (V)	Li_2O_2 shape	Ref
TMPs	MoP	nanoflakes	Carbon Cloth	Hydrothermal/ in-situ phosphating			5187.5	125	400	125 (	0.81	Toroidal	[291]
	MoP	Quantum dots	N, P doped hollow carbon fibers	Hydrothermal/ in-situ phosphating			6.75 mA h cm^{-2}	0.1 mA h cm^{-2}	30	0.5 mA h cm^{-2}	1.05	Film-like	[292]
	CoP	microspheres	Carbon paper	Hydrothermal			2994	100	80	100	1.43		[293]
	CoFeP	nanodots	N doped porous carbon	Lyophilization/ Phosphating	420.6	30	11969	100	141	100	1.35	Flake-like	[297]
	NiFeP	nanoparticles	3D biochar	MOF/ Phosphating			10.9 mA h cm^{-2}	0.05 mA h cm^{-2}	91	0.05 mA h cm^{-2}	1.25	Flake-like	[298]
TMNs	Co_4N	Brush-like	N-doped Carbon fiber	Hydrothermal/ Ammonia Annealing			11.9 mA h cm^{-2}	0.05 mA h cm^{-2}	177	200	1.23	Film-like	

	MoN / Graphene Nanosheets	nanoparticles	Stainless steel	Hydrothermal/ Ammonia Annealing			1490	0.04 mA h cm^{-2}	7	0.08 mA h cm^{-2}	1.55	Toroidal	[303]
	MoN / N-doped Carbon	nanospheres	Stainless Steel	Hydrothermal/ Ammonia Annealing	93	2-20	1410	62.5	30	400	1.38	nanosheets	[304]
	TiN/ Vulcan C	nanoparticles	Carbon Paper	MOF/ Ammonia Annealing	172		6407	50	20	50	1.45	-	[305]
	Co_3Mo_3N	nanoparticles	Stainless Steel	Ammonia Annealing	16	10-30	1850	62.5	16	62.5	1.55	nanosheets	[306]

In addition to Co_4N, molybdenum nitrate was also tested as the air cathode of LABs. The study by Shanmu Dong et al. was not very successful, with the assembled cell surviving only for 7 cycles and the specific discharge capacity limited to 1490 mA h g^{-1}. The catalyst was synthesized by annealing hydrothermally produced MoO_2 under NH_3 gaseous environment at 800 ^{0}C. The electrolyte decomposition (ethylene carbonate (EC) and dimethyl carbonate (DMC)) might have caused the early deterioration of the battery performance. [303] Cycle life was improved up to 30 cycles when a TEGDME-based electrolyte was used with a similarly produced MoN catalyst-based cathode [304].

In another attempt, Fujun Li et al. used TiN nanoparticles anchored on Vulcan XC-72 as a bifunctional catalyst for Li-O_2 batteries [305]. The selection of TiN as the active material was based on the success of its nanowires allotrope attached to carbon black in fuel cell experiments

[307]. The catalyst was prepared through a template-based method to obtain better contact between the carbon skeleton and the metal nitride nanoparticles. The TiN catalyst exhibited high bifunctional catalytic activity due to high electrical conductivity and the electrochemical stability of TiN. The reported discharge capacity was 6407 mA h $g_{carbon}^{-1,}$ and the cycle performance (20 cycles) was not among the recent best results. As discussed by the authors, the gradual oxidation of TiN into TiO_2 (especially at higher potential) might rapidly depreciate the battery performance.

The improved catalytic performance of bimetallic oxides, sulfides, and phosphides over their monometallic counterparts encouraged several research groups to try bimetallic nitrides. Kejun Zhang et al. developed Co_3Mo_3N as an effective bifunctional catalyst at LABs [306] The catalyst selection was strongly based on previous success in the selected binary nitride in catalyzing hydrogen evolution [308] and ammonia synthesis [309] The prepared mesoporous catalyst was homogeneously distributed on a stainless-steel current collector. The desired electrochemical performances were not achieved, where the specific discharge capacity was limited below 1850 mA h g^{-1} at a current density of 0.1 mA cm^{-2}. Further, the LAB could only be cycled for 16 cycles. Improving the interface between the catalyst and the stainless-steel skeleton may improve the battery performance by reducing the impedance. Also, better engineering of the electrode might help reduce the corrosion observed in the current system during the discharging of the cell.

As summarized in Table 7, the TMNs were commonly produced by annealing the intermediate product under an ammonia environment. In most cases, the catalytic performances of these materials are found to be not as good as other types of previously discussed catalysts. The reported discharge capacities and cycle stability were considerably low as compared with TMOs, TMPs, and noble metal derivatives. Since a relatively small number of studies carried

out up to date using TMNs at LAB cathodes, improved results can be expected in future studies, employing TMNs as standalone catalysts, and as a component of hybrid catalysts.

4.4. Hybrid Catalysts

In recent years, various hybrid bifunctional catalysts were tested at the cathode of LABs expecting better functionality over individual catalyst materials. In addition to the hybridization of the active materials with carbon skeleton, which has been discussed in previous sections, there are attempts to use more than one catalytically active material per cathode.

Lulu Huang et al. reported a hybrid bifunctional catalyst suitable for LABs produced by in-situ synthesizing yucca-like CoN- CoO nanoarrays on top of a pre-treated carbon paper. The catalyst was produced by partial nitriding the hydrothermally synthesized Co(OH)F nanoarray precursor. The assembled Li-O_2 cell sustained 200 cycles at 100 mA g^{-1} with a limited capacity of 500 mA h g^{-1} and delivered a discharge capacity of 5423 mA h g^{-1} at 50 mA g^{-1}. The authors highlighted that partial nitridation is critical for enhanced cell performance. The additional oxygen vacancies and nitridation provided the required support to obtain enhanced OER and ORR performances. The 3D mesoporous morphology of the cathode provided enough space for gas diffusion and to accommodate the discharge products [310].

A better-performing hybrid cathode for LABs was reported by Zonghuai Zhang et al. The catalyst was produced by decorating the Ni_3S_2 layer on top of electrospun fibers of double perovskite $PrBa_{0.5}Sr_{0.5}Co_2O_{5-\delta}$ (PBSC) [311] As discussed in previous sections, perovskites' catalytic activity and pore structure yield a high specific discharge capacity of over 10, 000 mA h g^{-1} [251]- [256]. However, the full reversibility remained questionable, and many authors reported fast capacity fading [128,312]. The work by Zhang et al. addressed this issue by depositing a layer of Ni_3S_2 via the atomic layer deposition (ALD) technique. The novel cathode yielded high discharge capacity (12784 mA h g^{-1} at 100 mA g^{-1}), low overpotential (0.68 V),

and good cycle life (120 cycles with a limited capacity of 1000 mA h $g^{-1,}$ which discharged at a rate of 100 mA g^{-1}). The authors reported improved performance over the uncoated perovskite or the transition metal sulfide. The synergy of two catalysts and the high amount of surface oxygen vacancies (O_2^{2-} and O^-) generated as the sulfide was deposited were recognized to be responsible for the enhanced performances of the LAB.

Peng Wang et al. developed a hybrid cathode where the noble metal Ru and TMP (Co_2P) were anchored on N-doped CNT. The assembled cell outperformed previously reported cells with a TMP catalyst-based cathode with a discharge capacity of 18 048 mA h g^{-1} at 100 mA g^{-1} (12800 mA h $g^{-1)}$. The cell exhibited good cycle stability of 185 cycles at 100 mA g^{-1}. The low ORR/OER overpotential (0.75V) and high peak currents further verified the effectiveness of the synergy of Co_2P and Ru in promoting oxygen kinetics. Unlike the previously reported mechanisms of synthesizing TMPs, the researchers produced the hybrid catalyst by in-situ pyrolyzing all the precursor materials together at 900 ^{0}C under Ar flow [313].

Outstanding cyclic stability of more than 300 cycles (with 1000 mA h g^{-1} limited discharge depth at 200 mA h g^{-1}) was reported by Peng Wang et al. for a composite of NiO and $NiCo_2S_4$ [314]. NiO nanotubes were hydrothermally grown on $NiCo_2S_4$ nanoarrays, which were also synthesized hydrothermally on pre-treated carbon paper. The developed three-phase hybrid heterostructure was used as a binder-free self-standing air cathode. In addition to the long cycle stability, the NiO/$NiCo_2S_4$ cathode demonstrated a lower overpotential (0.88 V) and high specific discharge capacity (10 050 mA h g^{-1} at 200 mA g^{-1}), thanks to the synergy of NiO and $NiCo_2S_4$ towards promoting ORR and OER kinetics. The authors explained the reversibility and the low potential of the 2D nature of the Li_2O_2 product [128]. Interestingly the relatively large 3-5 µm length peasecod-like Li_2O_2 particles were successfully decomposed during the subsequent charging. This is one of the few instances

where large Li_2O_2 particles could be successfully recycled, including the previously discussed study of Xiaodong Lin et al. with hydrangea-like large Li_2O_2 deposits [271,315].

A few other articles can also be found that achieved a similar outcome by hybridizing two or few noble metal derivatives, transition metal compounds, and doped porous carbon structures. For example, stability of over 200 cycles could be achieved on a cathode fabricated with RuO_2 nanoparticles and NiO nanosheet catalyst [316]. In another example, a low overpotential (0.32V), outstanding discharge capacity (26 833 mA h g^{-1}), and remarkable cycling stability (200 cycles at 300 mA g^{-1}) were recorded for Sr and Fe co-doped $LaCoO_3$ perovskite-based cathode. [317] Overall, hybrid catalysts were shown to improve discharge capacity as well as cycle stability.

It's wonderful to observe some better-performing catalysts can be derived through hybridizing two or more individual catalysts. But also, it has been witnessed above that a hybrid catalyst does not guarantee an enhanced LAB performance, and the individual materials need to be selected carefully with a meaningful rationale. Further, it's essential to develop an in-depth and solid theoretical understanding of the role of solid catalysts on Li-O_2 battery cathode, and we believe associated concepts related to molecular orbit theory need to be studied to a depth to understand the possible combinations of catalysts that could work together. With such an understanding, the electronic structure of the hybrid structure can be modulated to obtain a useful e_g orbital occupancy, enabling enhanced interactions with oxygen and reduced oxygen compounds.

It's further important to adhere to the Sabatier principle in constructing catalyst heterostructures. It's a very popular concept related to HER catalysts [318], and it could align with Li-O_2 batteries with the meaning that the ideal ORR/OER catalyst should have balanced adsorption of the oxygenated intermediates neither too strong nor too weak to achieve a greater

balance between the adsorption and desorption of adsorbates. Tian et al. recently obtained a volcano-type correlation between the catalytic activity and the d-band centre, indicating the applicability of the Sabatier principle as a general guidance to develop high-performing catalysts for the Li-O2 battery applications [319].

Table 6: Summary of input parameters and resultant outputs in LABs made using hybrid cathodes

Type	Catalyst	Shape	Substrate	Method	Surface area ($m^2 g^{-1}$)	Pore Size (nm)	Discharge Capacity (mA h g^{-1})	Rate (mA g^{-1})	Cycle Number	Rate/ Limit	Over Potential (V)	Li_2O_2 shape	Ref
Hybrid	CoO/ CoN	nanoarrays	Carbon Paper	Hydrothermal/ Partial nitridation		1-30	5423	50	200	100	1.30	Film-like	[310]
	Ni_3S_2/ $PrBa_{0.5}Sr_{0.5}Co_2O_{5-\delta}$	Nanoparticles/ nanotubes	Carbon Paper	Electrospin/ ALD	10.79	1-20	12784	100	120	100	0.68	toroidal	[311]
	Ru/ Co_2P/ N-doped CNT	Nanoparticles/ nanotubes	Carbon Paper	pyrolyzing	105	4-30	18048	100	185	100	0.75	nanosheets	[313]
	NiO/ $NiCo_2S_4$	Nanotubes/ nanoarrays	Carbon Paper	Hydrothermal/ Annealing			10050	200	300	200	0.88	peascod - like	[314]
	α-MnO_2/ Co_3O_4	Nanorods/ nanosheets	Carbon paper	Hydrothermal / electrodeposition/ annealing	71.18		5940	51	55	103	0.95	Particles/ film-like	[315]
	RuO_2/ NiO	Nanoparticles/	Ni foam	Chemical conversi	5.92		3240	250	200	500	1.18	toroidal	[316]

		Nanosheets		on/ Heat treatment									
	Sr, Fe-doped $LaCoO_3$		Carbon cloth	Sol-gel/ annealing	49.6	24.16	26 8 33	50	200	300	0.32	large granule-like	[317]
	Fe3O4/ PtRu/ C	nanoparticles	Ni foam	Hydrothermal/ Chemical reduction	44.36	2-3	7996	200	32	200	1.16	Film-like	[320]
	Co/ N-doped CNF	Nanoparticle/ nanofiber	-	Electrospin/ Calcination	301.5	2-25	4583	100	40	100	1.22	Film-like	[321]
	Co/ N, S-doped CNF	Nanoparticle/ nanofiber	-	Electrospin/ Calcination	121.3	1.7 - 38.8	6995	100	34	200	0.97	Film-like	[322]

4.5.Redox Mediators

In addition to solid-state bifunctional electrocatalysts, solution phase catalysts as redox mediators (RM) have been used to improve the oxygen reaction kinetics and to protect the cathode from side reactions. Even though the scope of our article is limited to solid catalysts, we would like to acknowledge the recent developments in solution phase/homogeneous catalysts through a brief discussion of their recent progress.

We believe the initial thought behind developing homogeneous catalysts is to reduce the charging overpotential. The charging mediators were designed in a way that they oxidized at the electrode surface (RM to RM^+), and they promoted the oxidation of Li_2O_2 in the electrolyte, as they diffuse to the electrolyte. Chen et al. reported one of the early studies on oxidating RMs using tetrathiafulvalene (TTF) [323], demonstrating that OER kinetics can be greatly improved by using redox mediators. Passing generations, nitroxide-based mediators are

currently considered state-of-the-art technology, and 2,2,6,6-tetramethylpiperidinyloxyl (TEMPO) [324] gained much attention due to its superior performance.

Similarly, the ORR redox mediators were able to support the oxygen reduction process, supporting the formation of Li_2O_2 by acting as mediators. But the advanced ORR redox mediators like 2,5-ditert-butyl-1,4-benzoquinone (DBBQ) were able to catalyze the reaction, through an alternative reduction pathway skipping the production of highly reactive LiO_2 as reaction intermediates, with elevated reduction potentials compared to direct reduction [325].

As Gao et al initially demonstrated, the bi-functional redox mediators with the combination of TEMPO and DBBQ were able to demonstrate a substantial improvement in Li-O_2 battery performances observing a greater synergistic effect [326]. The ability to perform the reactions away from the electrode surface helped to minimize the parasitic reactions, helping the endurance of the battery significantly. Further, carbon-based porous cathode materials could be sustained in the mentioned systems where the electrodes are least affected during the operation.

The current challenges observed related to redox mediators are, shuttling pollutants towards the Li metal anode known as redox-shuttling, and their instability against ROC and singlet oxygen [327]. However, we believe the main challenge for redox mediators will arise in the future with the further developments in ionic liquids and solid-state electrolytes, and the current development in organic electrolyte-based redox mediators will become ineffective under such environments. In such scenarios, the solid-state catalysts are ones expected to provide the essential catalytic activity. Even though many such efforts have yet to be conducted, an interesting study was recently reported by a group of researchers from the Illinois Institute of Technology, led by the pioneers of the field, Larry A. Curtiss, and Mohammad Asadi [328]. The battery is made out of Li chip anode, composite polymer solid-state electrolyte with

$Li_{10}GeP_2S_{12}$ nanoparticles embedded in LiTFSl- polyethylene oxide (PEO) matrix, and Mo_3P nanoparticles-based cathode delivered extraordinary well performances with reaching 1000 cycles with only 0.43V overpotential mainlining a almost 100% coulombic efficiency throughout. Hence, we could assume that future directions in LAB will bench-mark the mentioned study.

5. Summary and Perspectives

In the article, we have reviewed recent advances in designing bifunctional catalysts for LAB cathode, emphasizing the relevant catalyzing and degradation mechanisms. The article was initiated by introducing state-of-the-art technology, identifying the challenges ahead for energy storage devices, and emphasizing the need of the hour for a viable LAB technology. While introducing the LAB technology, a brief introduction to unsolved challenges and an overview of the article were provided.

In the next section, we discussed the role of individual components of the battery, state-of-the-art technology, and the current concerns regarding it. Later in the section, we provided a rich discussion on the ORR and OER operation principles according to current understanding, where some concepts are still contradictory, and in which, we summarised the contribution of the properties in the cathode to determine the morphology of the Li_2O_2 and the stability of the intermediate lithiated-reduced oxygen components ($Li_{2-x}O_2$). The discussion was further extended towards providing an in-depth briefing on parasitic reactions and battery degradation mechanisms, which is one of the areas, where significant grounds were made in recent years.

We identified six main categories of solid-state bifunctional catalysts: carbon-based nanostructures, noble metals and oxides, transition metal oxides, transition metal nitrides, transition metal sulfides, and transition metal phosphides. In individual sections, the reaction mechanisms with pathways for parasitic reactions were discussed. Further, the advantages and

the challenges against the progress as individual catalysts were discussed, including the potential pathways to improve the catalytic activity by providing expert insight and relevant examples.

We discussed the progress in carbon and doped-carbon structures as metal-free catalysts. The studies we reviewed provided solid evidence of critical support by the graphitic basal plane towards oxygen reduction, while the defective structures could accelerate the degradation process through stabilizing highly reactive intermediate products on the cathode surface. Electron structure modulation through N, S, P, I, and B doping was found to help promote fast kinetics as individual or dual-doped structures. But irrespective of all the favouring facts as lightweight, high conductivity, suitable pore structure, and inherent oxygen reduction support, the major bottleneck against using carbon cathodes at Li-O_2/LABs is that their instability against Li_2O_2 and other reduced oxygen intermediates, where only possible use case scenario is with dual redox mediators, in which total oxygen chemistry is occurring away from the cathode surface.

As in many other related fields, we found excellent catalytic activity by noble metals in Li-O_2 batteries as well. While Pt, Pd, and RuO_2 provided excellent ORR and OER support. Studies revealed that electronic structure in noble metals can be tuned by alloying with other metals, where the occupation in the high energy e_g orbitals can be reduced by withdrawing the electrons out, facilitating a better-suited unsaturated environment for strong oxygen and intermediate product adsorption. Particularly, it's interesting to observe the surface electron modulation achieved for other reviewed catalysts yielding strong outputs. Anyway, the high cost and scarcity of resources are still serious concerns against using noble metals in batteries.

We review the progress in first-block transition metal-based catalysts with great excitement, where many studies were conducted on transition metal oxides. TMOs were able to provide

high OER catalytic support through adsorbing reaction intermediates, which enough evidence could not be found for carbons. In Li-air batteries, binary oxides, and perovskites provided greater catalytic support over unitary oxides, with the availability of multiple cations at different valances, and their tuneable nature. Similar to carbon doping and noble metal alloying, the e_g occupancy in TMOs was able to be optimized through several techniques. One key technique discussed during the study was doping the binary oxides with a third heteroatom or synthesizing the ternary oxides. The other approach we discussed with great interest was related to facet engineering, where high reaction kinetics were obtained through the selective growing of high-energy facets with suitable adsorption energy for reaction intermediates.

Newly developing catalysts of transition metal sulfides, nitrides, and phosphides were also found to progressing well, exceeding the performances of TMOs, where the semiconducting features in those found to overcome the conductivity barrier and the high charging overpotential observed in the TMO-based LABs. The studies proved that similar approaches could be used to further boost the catalytic activity in the sulfides and the phosphides. Further, we pointed out that hybrid catalysts don't always guarantee a better synergistic effect unless they are selected wisely with a reasonable rationale. Even though research on TMPs and hybrid catalysts is still in its initial stages, we believe, those materials could turn out into superior bifunctional catalysts delivering stable fast kinetics allowing Li-O_2 batteries to operate faster for long durations with high energy efficacy. Since phosphides and sulfides were already found with high energetic facets and edge sites respectively, we believe a hybrid structure of those could optimize the e_g orbital electron structure for better effect. We further emphasize closely following the Sabatier principle in constructing catalyst heterostructures, in which very limited efforts were taken to date related to Li-O_2/Li-air batteries.

Even though it's not the greatest interest in the review article, we briefly review the progress related to redox mediators acknowledging its decent growth in recent years. Simultaneously, we illustrate the greatest obstacle against its future, its incompatibility with solid-state electrolytes, demonstrating a recent publication from Asadi et al., where the synergy of solid-state electrolyte and Mo_3P-based cathode was used to drive LABs over 1000 cycles with near 100% efficiency and <0.5 V charging overpotential. We believe the parallel success in solid-state electrolytes will lead to an interesting future for LAB research even though many complexities are yet to unravel in understanding the stability of newly developed catalysts, the stability of the electrolytes in their presence, and so on.

Finally, we tried to build a possible correlation in-between the properties of the cathode materials, and its design parameters against the outcome of the study as presented in Figure 8, using the results available in the reviewed documents. But surprisingly, we couldn't generalize the relationships confidently. Rather than the unavailability of correlations, the issue could be related to the style of reporting, which makes it difficult to compare the outcomes of two similar studies. We propose reporting areal capacity or the capacity considering the whole cathodic weight could be a more consistent approach, which allows a more adequate and accurate comparison between studies, ultimately helping for the true evolvement of the field.

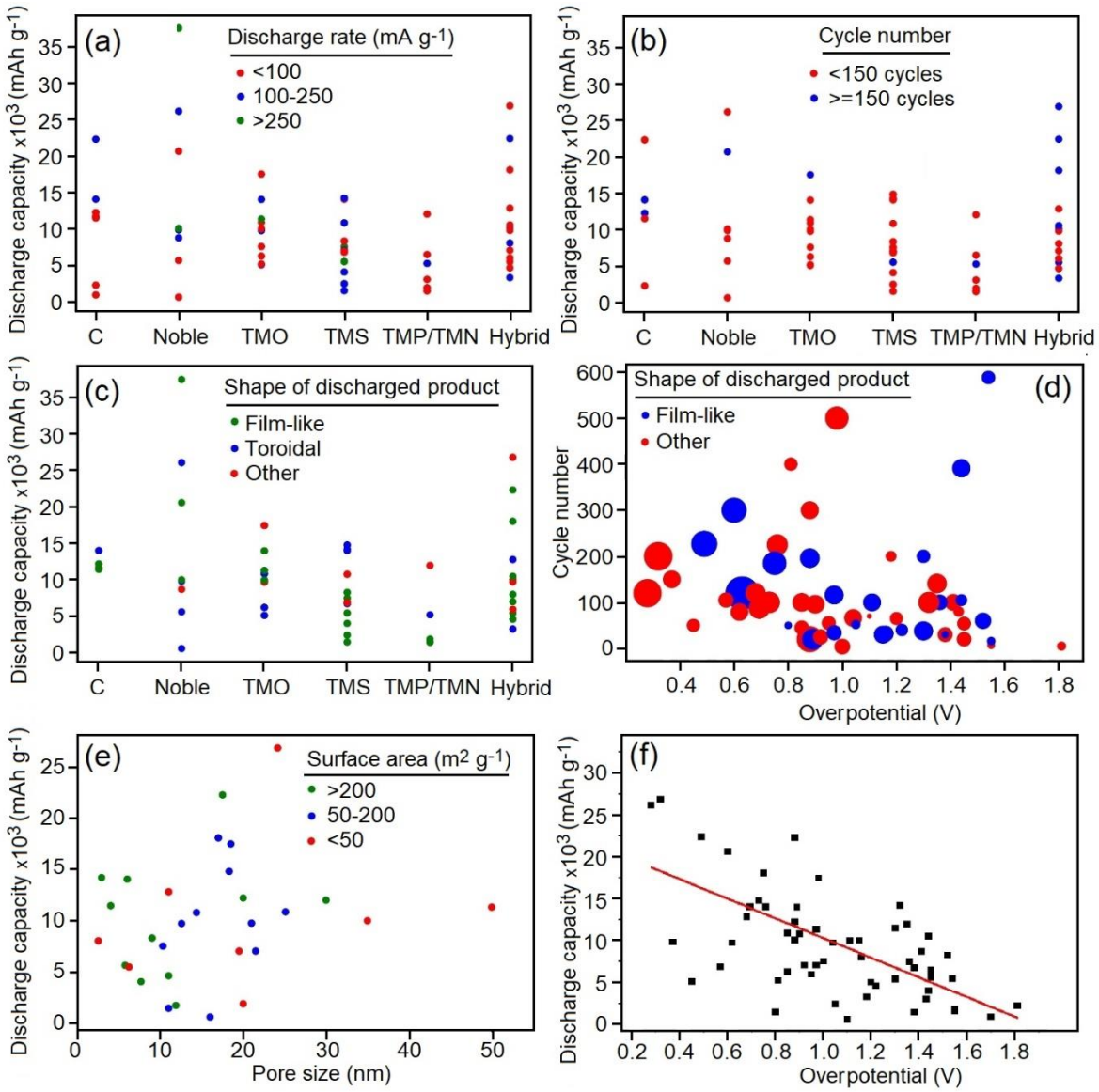

Figure 8: Summary of LAB performances, (a)-(c), (e), (f) Discharge capacity variation in different catalyst type and their co-relations with discharge current density, cycle number, shape of the discharge product, pore size, and overpotential respectively, (d) Cycle number and discharge capacity variation vs. overpotential.

Acknowledgment

The authors acknowledge and thank Ms. H.E.K Fernando, researcher in Artificial Intelligence, for the continuous support given during the statistical analysis section of the manuscript.

References

[1] J.F. Mercure, P. Salas, P. Vercoulen, G. Semieniuk, A. Lam, H. Pollitt, P.B. Holden, N. Vakilifard, U. Chewpreecha, N.R. Edwards, J.E. Vinuales, Reframing incentives for climate policy action, Nature Energy 2021 6:12 6 (2021) 1133–1143. https://doi.org/10.1038/s41560-021-00934-2.

[2] D. Welsby, J. Price, S. Pye, P. Ekins, Unextractable fossil fuels in a 1.5 °C world, Nature 2021 597:7875 597 (2021) 230–234. https://doi.org/10.1038/s41586-021-03821-8.

[3] A. Kamali, D.J. Fray, Tin-based materials as advanced anode materials for lithium ion batteries: A review, Reviews on Advanced Materials Science 27 (2011).

[4] L. Kong, Z. Li, W. Zhu, C.R. Ratwani, N. Fernando, S. Karunarathne, Amr.M. Abdelkader, A.R. Kamali, Z. Shi, Sustainable regeneration of high-performance LiCoO2 from completely failed lithium-ion batteries, J Colloid Interface Sci 640 (2023) 1080–1088. https://doi.org/https://doi.org/10.1016/j.jcis.2023.03.021.

[5] U.-H. Kim, L.-Y. Kuo, P. Kaghazchi, C. S. Yoon, Y.-K. Sun, Quaternary Layered Ni-Rich NCMA Cathode for Lithium-Ion Batteries, ACS Energy Lett 4 (2019) 576–582. https://doi.org/10.1021/acsenergylett.8b02499.

[6] A. Masias, J. Marcicki, W. A. Paxton, Opportunities and Challenges of Lithium Ion Batteries in Automotive Applications, ACS Energy Lett 6 (2021) 621–630. https://doi.org/10.1021/acsenergylett.0c02584.

[7] G.D.J. Harper, E. Kendrick, P.A. Anderson, W. Mrozik, P. Christensen, S. Lambert, D. Greenwood, P.K. Das, M. Ahmeid, Z. Milojevic, W. Du, D.J.L. Brett, P.R. Shearing, A. Rastegarpanah, R. Stolkin, R. Sommerville, A. Zorin, J.L. Durham, A.P. Abbott, D. Thompson, N.D. Browning, B.L. Mehdi, M. Bahri, F. Schanider-Tontini, D. Nicholls, C. Stallmeister, B. Friedrich, M. Sommerfeld, L.L. Driscoll, A. Jarvis, E.C. Giles, P.R. Slater, V. Echavarri-Bravo, G. Maddalena, L.E. Horsfall, L. Gaines, Q. Dai, S.J. Jethwa, A.L. Lipson, G.A. Leeke, T. Cowell, J.G. Farthing, G. Mariani, A. Smith, Z. Iqbal, R. Golmohammadzadeh, L. Sweeney, V. Goodship, Z. Li, J. Edge, L. Lander, V.T. Nguyen, R.J.R. Elliot, O. Heidrich, M. Slattery, D. Reed, J. Ahuja, A. Cavoski, R. Lee, E. Driscoll, J. Baker, P. Littlewood, I. Styles, S. Mahanty, F. Boons, Roadmap for a sustainable circular economy in lithium-ion and future battery technologies, Journal of Physics: Energy 5 (2023) 021501. https://doi.org/10.1088/2515-7655/acaa57.

[8] B.J. van Ruijven, E. De Cian, I. Sue Wing, Amplification of future energy demand growth due to climate change, Nature Communications 2019 10:1 10 (2019) 1–12. https://doi.org/10.1038/s41467-019-10399-3.

[9] T. Ahmad, D. Zhang, A critical review of comparative global historical energy consumption and future demand: The story told so far, Energy Reports 6 (2020) 1973–1991. https://doi.org/10.1016/J.EGYR.2020.07.020.

[10] A. El Kharbachi, O. Zavorotynska, M. Latroche, F. Cuevas, V. Yartys, M. Fichtner, Exploits, advances and challenges benefiting beyond Li-ion battery technologies, J Alloys Compd 817 (2020) 153261. https://doi.org/10.1016/J.JALLCOM.2019.153261.

[11] H. Zhao, A. Rezaei, A.R. Kamali, Electrolytic Conversion of Natural Graphite into Carbon Nanostructures with Enhanced Electrical Conductivity and Na-ion Storage Performance, J Electrochem Soc 169 (2022) 54512. https://doi.org/10.1149/1945-7111/ac6bc2.

[12] J. Ma, Y. Li, N.S. Grundish, J.B. Goodenough, Y. Chen, L. Guo, Z. Peng, X. Qi, F. Yang, L. Qie, C.-A. Wang, B. Huang, Z. Huang, L. Chen, D. Su, G. Wang, X. Peng, Z. Chen, J. Yang, S. He, X. Zhang, H. Yu, C. Fu, M. Jiang, W. Deng, C.-F. Sun, Q. Pan, Y. Tang, X. Li, X. Ji, F. Wan, Z. Niu, F. Lian, C. Wang, G.G. Wallace, M. Fan, Q. Meng, S. Xin, Y.-G. Guo, L.-J. Wan, The 2021 battery technology roadmap, J Phys D Appl Phys 54 (2021) 183001. https://doi.org/10.1088/1361-6463/abd353.

[13] X. Yu, A. Manthiram, A Progress Report on Metal–Sulfur Batteries, Adv Funct Mater 30 (2020) 2004084. https://doi.org/https://doi.org/10.1002/adfm.202004084.

[14] J. Ma, M. Wang, H. Zhang, Z. Shang, L. Fu, W. Zhang, B. Song, K. Lu, Toward the Advanced Next-Generation Solid-State Na-S Batteries: Progress and Prospects, Adv Funct Mater 33 (2023) 2214430. https://doi.org/https://doi.org/10.1002/adfm.202214430.

[15] J. Wang, S. Yi, J. Liu, S. Sun, Y. Liu, D. Yang, K. Xi, G. Gao, A. Abdelkader, W. Yan, S. Ding, R.V. Kumar, Suppressing the Shuttle Effect and Dendrite Growth in Lithium–Sulfur Batteries, ACS Nano 14 (2020) 9819–9831. https://doi.org/10.1021/acsnano.0c02241.

[16] J.B. Robinson, K. Xi, R.V. Kumar, A.C. Ferrari, H. Au, M.-M. Titirici, A. Parra-Puerto, A. Kucernak, S.D.S. Fitch, N. Garcia-Araez, Z.L. Brown, M. Pasta, L. Furness, A.J. Kibler, D.A. Walsh, L.R. Johnson, C. Holc, G.N. Newton, N.R. Champness, F. Markoulidis, C. Crean, R.C.T. Slade, E.I. Andritsos, Q. Cai, S. Babar, T. Zhang, C. Lekakou, N. Kulkarni, A.J.E. Rettie, R. Jervis, M. Cornish, M. Marinescu, G. Offer, Z. Li, L. Bird, C.P. Grey, M. Chhowalla, D. Di Lecce, R.E. Owen, T.S. Miller, D.J.L. Brett, S. Liatard, D. Ainsworth, P.R. Shearing, 2021 roadmap on lithium sulfur batteries, Journal of Physics: Energy 3 (2021) 031501. https://doi.org/10.1088/2515-7655/abdb9a.

[17] M. Salado, E. Lizundia, Advances, challenges, and environmental impacts in metal–air battery electrolytes, Mater Today Energy 28 (2022) 101064. https://doi.org/10.1016/J.MTENER.2022.101064.

[18] H. Weinrich, Y.E. Durmus, H. Tempel, H. Kungl, R.A. Eichel, Silicon and iron as resource-efficient anode materials for ambient-temperature metal-air batteries: A review, Materials 12 (2019). https://doi.org/10.3390/ma121321341-55.

[19] S. Chandrasekaran, R. Hu, L. Yao, L. Sui, Y. Liu, A. Abdelkader, Y. Li, X. Ren, L. Deng, Mutual Self-Regulation of d-Electrons of Single Atoms and Adjacent

Nanoparticles for Bifunctional Oxygen Electrocatalysis and Rechargeable Zinc-Air Batteries, Nanomicro Lett 15 (2023) 48. https://doi.org/10.1007/s40820-023-01022-8.

[20] A. Holland, R.D. Mckerracher, A. Cruden, R.G.A. Wills, An aluminium battery operating with an aqueous electrolyte, J Appl Electrochem 48 (2018) 243–250. https://doi.org/10.1007/S10800-018-1154-X/FIGURES/9.

[21] Y. Yu, M. Chen, S. Wang, al -, H. Liu, J. Zhang, D. Ahuja, K. Varshney, P.K. Varshney, Metal air battery: A sustainable and low cost material for energy storage You may also like Laser Sintering of Printed Anodes for Al-Air Batteries Synthesis of-MnO 2 /Reduced Graphene Oxide Hybrid In Situ and Application in Mg-Air Battery Metal air battery: A sustainable and low cost material for energy storage, (2021) 12065. https://doi.org/10.1088/1742-6596/1913/1/012065.

[22] L.D. Chen, J.K. Norskov, A.C. Luntz, Theoretical Limits to the Anode Potential in Aqueous Mg-Air Batteries, Journal of Physical Chemistry C 119 (2015) 19660–19667. https://doi.org/10.1021/ACS.JPCC.5B05677/SUPPL_FILE/JP5B05677_SI_001.PDF.

[23] J. Zhang, Q. Zhou, Y. Tang, L. Zhang, Y. Li, Zinc–air batteries: are they ready for prime time?, Chem Sci 10 (2019) 8924–8929. https://doi.org/10.1039/C9SC04221K.

[24] Y. Liu, Q. Sun, W. Li, K.R. Adair, J. Li, X. Sun, A comprehensive review on recent progress in aluminum–air batteries, Green Energy & Environment 2 (2017) 246–277. https://doi.org/https://doi.org/10.1016/j.gee.2017.06.006.

[25] T. Zhang, Z. Tao, J. Chen, Magnesium–air batteries: from principle to application, Mater Horiz 1 (2014) 196–206. https://doi.org/10.1039/C3MH00059A.

[26] T. Liu, J.P. Vivek, E.W. Zhao, J. Lei, N. Garcia-Araez, C.P. Grey, Current Challenges and Routes Forward for Nonaqueous Lithium-Air Batteries, Chem Rev 120 (2020) 6558–6625. https://doi.org/10.1021/ACS.CHEMREV.9B00545/ASSET/IMAGES/MEDIUM/CR9B00545_M040.GIF.

[27] Z. Khan, M. Vagin, X. Crispin, Z. Khan, M. Vagin, X. Crispin, Can Hybrid Na–Air Batteries Outperform Nonaqueous Na–O2 Batteries?, Advanced Science 7 (2020) 1902866. https://doi.org/10.1002/ADVS.201902866.

[28] G. Cong, W. Wang, N.C. Lai, Z. Liang, Y.C. Lu, A high-rate and long-life organic–oxygen battery, Nature Materials 2019 18:4 18 (2019) 390–396. https://doi.org/10.1038/s41563-019-0286-7.

[29] Md.A. Rahman, X. Wang, C. Wen, High Energy Density Metal-Air Batteries: A Review, J Electrochem Soc 160 (2013) A1759–A1771. https://doi.org/10.1149/2.062310JES/XML.

[30] Y. Liu, Q. Sun, W. Li, K.R. Adair, J. Li, X. Sun, A comprehensive review on recent progress in aluminum–air batteries, Green Energy and Environment 2 (2017) 246–277. https://doi.org/10.1016/j.gee.2017.06.006.

[31] Y.S. Jeong, J.B. Park, H.G. Jung, J. Kim, X. Luo, J. Lu, L. Curtiss, K. Amine, Y.K. Sun, B. Scrosati, Y.J. Lee, Study on the Catalytic Activity of Noble Metal Nanoparticles on Reduced Graphene Oxide for Oxygen Evolution Reactions in Lithium-Air Batteries, Nano Lett 15 (2015) 4261–4268. https://doi.org/10.1021/NL504425H/SUPPL_FILE/NL504425H_SI_001.PDF.

[32] X. Guo, G. Zhang, Q. Li, H. Xue, H. Pang, Non-noble metal-transition metal oxide materials for electrochemical energy storage, Energy Storage Mater 15 (2018). https://doi.org/10.1016/j.ensm.2018.04.002.

[33] L.N. Song, W. Zhang, Y. Wang, X. Ge, L.C. Zou, H.F. Wang, X.X. Wang, Q.C. Liu, F. Li, J.J. Xu, Tuning lithium-peroxide formation and decomposition routes with single-atom catalysts for lithium–oxygen batteries, Nature Communications 2020 11:1 11 (2020) 1–11. https://doi.org/10.1038/s41467-020-15712-z.

[34] C. Xia, C.Y. Kwok, L.F. Nazar, A high-energy-density lithium-oxygen battery based on a reversible four-electron conversion to lithium oxide, Science (1979) 361 (2018) 777–781. https://doi.org/10.1126/SCIENCE.AAS9343/SUPPL_FILE/AAS9343-XIA-SM.PDF.

[35] L.A. Archer, P.G. Bruce, E.J. Calvo, D. Dewar, J.H.J. Ellison, S.A. Freunberger, X. Gao, L.J. Hardwick, G. Horwitz, J. Janek, L.R. Johnson, J.W. Jordan, S. Matsuda, S. Menkin, S. Mondal, Q. Qiu, T. Samarakoon, I. Temprano, K. Uosaki, G. Vailaya, E.D. Wachsman, Y. Wu, S. Ye, Towards practical metal–oxygen batteries: general discussion, Faraday Discuss (2024). https://doi.org/10.1039/D3FD90062B.

[36] E. Mourad, Y.K. Petit, R. Spezia, A. Samojlov, F.F. Summa, C. Prehal, C. Leypold, N. Mahne, C. Slugovc, O. Fontaine, S. Brutti, S.A. Freunberger, Singlet oxygen from cation driven superoxide disproportionation and consequences for aprotic metal–O2 batteries, Energy Environ Sci 12 (2019) 2559–2568. https://doi.org/10.1039/C9EE01453E.

[37] D. Sharon, D. Hirshberg, M. Afri, A.A. Frimer, M. Noked, D. Aurbach, Aprotic metal-oxygen batteries: recent findings and insights, Journal of Solid State Electrochemistry 2017 21:7 21 (2017) 1861–1878. https://doi.org/10.1007/S10008-017-3590-7.

[38] Y.L. Zhang, K. Goh, L. Zhao, X.L. Sui, X.F. Gong, J.J. Cai, Q.Y. Zhou, H. Da Zhang, L. Li, F.R. Kong, D.M. Gu, Z.B. Wang, Advanced non-noble materials in bifunctional catalysts for ORR and OER toward aqueous metal–air batteries, Nanoscale 12 (2020) 21534–21559. https://doi.org/10.1039/D0NR05511E.

[39] E. V. Timofeeva, C.U. Segre, G.S. Pour, M. Vazquez, B.L. Patawah, Aqueous air cathodes and catalysts for metal–air batteries, Curr Opin Electrochem 38 (2023) 101246. https://doi.org/10.1016/J.COELEC.2023.101246.

[40] G. Gollavelli, G. Gedda, R. Mohan, Y.C. Ling, Status Quo on Graphene Electrode Catalysts for Improved Oxygen Reduction and Evolution Reactions in Li-Air Batteries, Molecules 2022, Vol. 27, Page 7851 27 (2022) 7851. https://doi.org/10.3390/MOLECULES27227851.

[41] Y.J. Wang, B. Fang, D. Zhang, A. Li, D.P. Wilkinson, A. Ignaszak, L. Zhang, J. Zhang, A Review of Carbon-Composited Materials as Air-Electrode Bifunctional Electrocatalysts for Metal–Air Batteries, Electrochemical Energy Reviews 1 (2018) 1–34. https://doi.org/10.1007/S41918-018-0002-3/TABLES/5.

[42] T. Bai, D. Li, S. Xiao, F. Ji, S. Zhang, C. Wang, J. Lu, Q. Gao, L. Ci, Recent progress on single-atom catalysts for lithium–air battery applications, Energy Environ Sci 16 (2023) 1431–1465. https://doi.org/10.1039/D2EE02949A.

[43] J. Pan, X.L. Tian, S. Zaman, Z. Dong, H. Liu, H.S. Park, B.Y. Xia, Recent Progress on Transition Metal Oxides as Bifunctional Catalysts for Lithium-Air and Zinc-Air Batteries, Batter Supercaps 2 (2019) 336–347. https://doi.org/10.1002/BATT.201800082.

[44] J. Zhao, R. Pathak, Z. Zhao, X. Chen, M.B. Saud, H. Li, F. Wu, Q. Qiao, J.W. Elam, X. Wang, Advanced nano-bifunctional electrocatalysts in Li–air batteries for high coulombic efficiency, Green Chemistry 25 (2023) 10182–10208. https://doi.org/10.1039/D3GC02151C.

[45] Y. Dai, J. Yu, C. Cheng, P. Tan, M. Ni, Mini-review of perovskite oxides as oxygen electrocatalysts for rechargeable zinc–air batteries, Chemical Engineering Journal 397 (2020) 125516. https://doi.org/10.1016/J.CEJ.2020.125516.

[46] Z. Gu, X. Xin, M. Men, Y. Zhou, J. Wu, Y. Sun, X. Yao, Advancements, Challenges, and Prospects in Rechargeable Solid-State Lithium-Air Batteries, Batter Supercaps 6 (2023) e202300267. https://doi.org/10.1002/BATT.202300267.

[47] Q. Zhu, J. Ma, S. Li, D. Mao, Solid-State Electrolyte for Lithium-Air Batteries: A Review, Polymers 2023, Vol. 15, Page 2469 15 (2023) 2469. https://doi.org/10.3390/POLYM15112469.

[48] J. Wang, J. Zheng, X. Liu, The key to improving the performance of Li–air batteries: recent progress and challenges of the catalysts, Physical Chemistry Chemical Physics 24 (2022) 17920–17940. https://doi.org/10.1039/D2CP02212E.

[49] W.-J. Kwak, D. Sharon, C. Xia, H. Kim, L. R. Johnson, P. G. Bruce, L. F. Nazar, Y.-K. Sun, A. A. Frimer, M. Noked, S. A. Freunberger, D. Aurbach, Lithium–Oxygen Batteries and Related Systems: Potential, Status, and Future, Chem Rev 120 (2020) 6626–6683. https://doi.org/10.1021/acs.chemrev.9b00609.

[50] L. Johnson, C. Li, Z. Liu, Y. Chen, S.A. Freunberger, P.C. Ashok, B.B. Praveen, K. Dholakia, J.M. Tarascon, P.G. Bruce, The role of LiO2 solubility in O2 reduction in aprotic solvents and its consequences for Li–O2 batteries, Nature Chemistry 2014 6:12 6 (2014) 1091–1099. https://doi.org/10.1038/nchem.2101.

[51] Y. Liu, L. Wang, L. Cao, C. Shang, Z. Wang, H. Wang, L. He, J. Yang, H. Cheng, J. Li, Z. Lu, Understanding and suppressing side reactions in Li–air batteries, Mater Chem Front 1 (2017) 2495–2510. https://doi.org/10.1039/C7QM00353F.

[52] S.A. Freunberger, Y. Chen, N.E. Drewett, L.J. Hardwick, F. Bardé, P.G. Bruce, The Lithium–Oxygen Battery with Ether-Based Electrolytes, Angewandte Chemie International Edition 50 (2011) 8609–8613. https://doi.org/10.1002/ANIE.201102357.

[53] N. Mahne, O. Fontaine, M.O. Thotiyl, M. Wilkening, S.A. Freunberger, Mechanism and performance of lithium–oxygen batteries – a perspective, Chem Sci 8 (2017) 6716–6729. https://doi.org/10.1039/C7SC02519J.

[54] J. Li, L. Hou, M. Yu, Q. Li, T. Zhang, H. Sun, Review and Recent Advances of Oxygen Transfer in Li-air Batteries, ChemElectroChem 8 (2021) 3588–3603. https://doi.org/10.1002/CELC.202100560.

[55] J.B. Park, S.H. Lee, H.G. Jung, D. Aurbach, Y.K. Sun, Redox Mediators for Li–O2 Batteries: Status and Perspectives, Advanced Materials 30 (2018) 1704162. https://doi.org/10.1002/ADMA.201704162.

[56] B. Huang, W. Zhang, J. Chen, Y. Cui, C. Zhu, S. Yan, Review—Research Progress and Prospects of Li-Air Battery in Wearable Devices, J Electrochem Soc 170 (2023) 020506. https://doi.org/10.1149/1945-7111/ACB66C.

[57] T. Liu, J.P. Vivek, E.W. Zhao, J. Lei, N. Garcia-Araez, C.P. Grey, Current Challenges and Routes Forward for Nonaqueous Lithium-Air Batteries, Chem Rev 120 (2020) 6558–6625. https://doi.org/10.1021/ACS.CHEMREV.9B00545/ASSET/IMAGES/MEDIUM/CR9B00545_0026.GIF.

[58] C. Allard, Li–air batteries hitting the road, Nature Reviews Materials 2023 8:3 8 (2023) 145–145. https://doi.org/10.1038/s41578-023-00546-0.

[59] O. Crowther, M. Salomon, Oxygen Selective Membranes for Li-Air (O2) Batteries, Membranes 2012, Vol. 2, Pages 216-227 2 (2012) 216–227. https://doi.org/10.3390/MEMBRANES2020216.

[60] L. Liu, H. Guo, L. Fu, S. Chou, S. Thiele, Y. Wu, J. Wang, L. Liu, H. Guo, S. Chou, J. Wang, S. Thiele, L. Fu, Y. Wu, Critical Advances in Ambient Air Operation of Nonaqueous Rechargeable Li–Air Batteries, Small 17 (2021) 1903854. https://doi.org/10.1002/SMLL.201903854.

[61] M.A. Rahman, X. Wang, C. Wen, A review of high energy density lithium-air battery technology, J Appl Electrochem 44 (2014) 5–22. https://doi.org/10.1007/S10800-013-0620-8/FIGURES/14.

[62] D. Wang, X. Mu, P. He, H. Zhou, Materials for advanced Li-O2 batteries: Explorations, challenges and prospects, Materials Today 26 (2019) 87–99. https://doi.org/10.1016/J.MATTOD.2019.01.016.

[63] Y. Wang, Y.C. Lu, Nonaqueous Lithium–Oxygen batteries: Reaction mechanism and critical open questions, Energy Storage Mater 28 (2020) 235–246. https://doi.org/10.1016/J.ENSM.2020.03.007.

[64] A. Kraytsberg, Y. Ein-Eli, Review on Li-air batteries - Opportunities, limitations and perspective, J Power Sources (2011). https://doi.org/10.1016/j.jpowsour.2010.09.031.

[65] H. Guo, W. Luo, J. Chen, S. Chou, H. Liu, J. Wang, Review of Electrolytes in Nonaqueous Lithium–Oxygen Batteries, Adv Sustain Syst 2 (2018) 1700183. https://doi.org/10.1002/ADSU.201700183.

[66] B.D. McCloskey, R. Scheffler, A. Speidel, D.S. Bethune, R.M. Shelby, A.C. Luntz, On the Efficacy of Electrocatalysis in Nonaqueous Li–O2 Batteries, J Am Chem Soc 133 (2011) 18038–18041. https://doi.org/10.1021/JA207229N.

[67] V.S. Bryantsev, V. Giordani, W. Walker, M. Blanco, S. Zecevic, K. Sasaki, J. Uddin, D. Addison, G. v. Chase, Predicting Solvent Stability in Aprotic Electrolyte Li–Air Batteries: Nucleophilic Substitution by the Superoxide Anion Radical (O2•–), Journal of Physical Chemistry A 115 (2011) 12399–12409. https://doi.org/10.1021/JP2073914.

[68] T. Liu, G. Kim, E. Jónsson, E. Castillo-Martinez, I. Temprano, Y. Shao, J. Carretero-González, R.N. Kerber, C.P. Grey, Understanding LiOH Formation in a Li-O2 Battery with LiI and H2O Additives, ACS Catal 9 (2019) 66–77. https://doi.org/10.1021/acscatal.8b02783.

[69] N. Meng, F. Lian, Y. Li, X. Zhao, L. Zhang, S. Lu, H. Li, Exploring PVFM-Based Janus Membrane-Supporting Gel Polymer Electrolyte for Highly Durable Li–O2 Batteries, ACS Appl Mater Interfaces 10 (2018) 22237–22247. https://doi.org/10.1021/acsami.8b05393.

[70] Y. Qiao, Q. Wang, X. Mu, H. Deng, P. He, J. Yu, H. Zhou, Advanced Hybrid Electrolyte Li-O2 Battery Realized by Dual Superlyophobic Membrane, Joule 3 (2019) 2986–3001. https://doi.org/10.1016/J.JOULE.2019.09.002.

[71] S. Song, D. Zhang, Y. Ruan, L. Yu, Y. Xu, J. Thokchom, D. Mei, Quasi-Solid-State Li–O2 Batteries Performance Enhancement Using an Integrated Composite Polymer-Based Architecture, ACS Appl Energy Mater 4 (2021) 6221–6232. https://doi.org/10.1021/acsaem.1c00989.

[72] Z. Gu, X. Xin, J. Yang, D. Guo, S. Yang, J. Wu, Y. Sun, X. Yao, Bilayer NASICON/Polymer Hybrid Electrolyte for Stable Solid-State Li–O2 Batteries, ACS Appl Energy Mater 5 (2022) 9149–9157. https://doi.org/10.1021/acsaem.2c01717.

[73] K.M. Abraham, Z. Jiang, A Polymer Electrolyte-Based Rechargeable Lithium/Oxygen Battery, J Electrochem Soc 143 (1996) 1–5. https://doi.org/10.1149/1.1836378/XML.

[74] T. Ogasawara, A. Débart, M. Holzapfel, P. Novák, P.G. Bruce, Rechargeable Li2O2 Electrode for Lithium Batteries, J Am Chem Soc 128 (2006) 1390–1393. https://doi.org/10.1021/ja056811q.

[75] J. Read, Characterization of the Lithium/Oxygen Organic Electrolyte Battery, J Electrochem Soc 149 (2002) A1190. https://doi.org/10.1149/1.1498256/XML.

[76] J. Xiao, J. Hu, D. Wang, D. Hu, W. Xu, G.L. Graff, Z. Nie, J. Liu, J.G. Zhang, Investigation of the rechargeability of Li–O2 batteries in non-aqueous electrolyte, J

Power Sources 196 (2011) 5674–5678. https://doi.org/10.1016/J.JPOWSOUR.2011.02.060.

[77] F. MIZUNO, S. NAKANISHI, Y. KOTANI, S. YOKOISHI, H. IBA, Rechargeable Li-Air Batteries with Carbonate-Based Liquid Electrolytes, Electrochemistry 78 (2010) 403–405. https://doi.org/10.5796/ELECTROCHEMISTRY.78.403.

[78] J. Lai, Y. Xing, N. Chen, L. Li, F. Wu, R. Chen, Electrolytes for Rechargeable Lithium–Air Batteries, Angewandte Chemie International Edition 59 (2020) 2974–2997. https://doi.org/10.1002/ANIE.201903459.

[79] M. Balaish, A. Kraytsberg, Y. Ein-Eli, A critical review on lithium–air battery electrolytes, Physical Chemistry Chemical Physics 16 (2014) 2801–2822. https://doi.org/10.1039/C3CP54165G.

[80] G. Horwitz, E.J. Calvo, L.P. Méndez De Leo, E. de la Llave, Electrochemical stability of glyme-based electrolytes for Li–O2 batteries studied by in situ infrared spectroscopy, Physical Chemistry Chemical Physics 22 (2020) 16615–16623. https://doi.org/10.1039/D0CP02568B.

[81] H.M. Kwon, M.L. Thomas, R. Tatara, Y. Oda, Y. Kobayashi, A. Nakanishi, K. Ueno, K. Dokko, M. Watanabe, Stability of Glyme Solvate Ionic Liquid as an Electrolyte for Rechargeable Li-O2 Batteries, ACS Appl Mater Interfaces 9 (2017) 6014–6021. https://doi.org/10.1021/ACSAMI.6B14449/ASSET/IMAGES/LARGE/AM-2016-14449D_0005.JPEG.

[82] J. Zhang, B. Sun, Y. Zhao, A. Tkacheva, Z. Liu, K. Yan, X. Guo, A.M. McDonagh, D. Shanmukaraj, C. Wang, T. Rojo, M. Armand, Z. Peng, G. Wang, A versatile functionalized ionic liquid to boost the solution-mediated performances of lithium-oxygen batteries, Nature Communications 2019 10:1 10 (2019) 1–10. https://doi.org/10.1038/s41467-019-08422-8.

[83] V. Giordani, D. Tozier, H. Tan, C.M. Burke, B.M. Gallant, J. Uddin, J.R. Greer, B.D. McCloskey, G. V. Chase, D. Addison, A Molten Salt Lithium-Oxygen Battery, J Am Chem Soc 138 (2016) 2656–2663. https://doi.org/10.1021/JACS.5B11744/SUPPL_FILE/JA5B11744_SI_001.PDF.

[84] J. Jang, J. Oh, H. Jeong, W. Kang, C. Jo, A review of functional separators for lithium metal battery applications, Materials 13 (2020) 1–37. https://doi.org/10.3390/MA13204625.

[85] P. Wang, Y. Ren, R. Wang, P. Zhang, M. Ding, C. Li, D. Zhao, Z. Qian, Z. Zhang, L. Zhang, L. Yin, Atomically dispersed cobalt catalyst anchored on nitrogen-doped carbon nanosheets for lithium-oxygen batteries, Nature Communications 2020 11:1 11 (2020) 1–11. https://doi.org/10.1038/s41467-020-15416-4.

[86] Y. Cui, Z. Wen, Y. Liu, A free-standing-type design for cathodes of rechargeable Li-O 2 batteries, Energy Environ Sci 4 (2011) 4727–4734. https://doi.org/10.1039/c1ee02365a.

[87] W. Y, W. T, Z. Y, X. S, H. X, Z. D, S. J, Electrocatalytic performances of g-C3N4-LaNiO3 composite as bi-functional catalysts for lithium-oxygen batteries, Sci Rep 6 (2016). https://doi.org/10.1038/SREP24314.

[88] Y. Li, K. Guo, J. Li, X. Dong, T. Yuan, X. Li, H. Yang, Controllable synthesis of ordered mesoporous NiFe2O4 with tunable pore structure as a bifunctional catalyst for Li-O2 batteries, ACS Appl Mater Interfaces 6 (2014). https://doi.org/10.1021/am505718k.

[89] S. Hemavathi, S. Srirama, A.S. Prakash, Present and Future Generation of Secondary Batteries: A Review, ChemBioEng Reviews 10 (2023) 1123–1145. https://doi.org/10.1002/CBEN.202200040.

[90] Y. Wu, H. Li, T. Liu, M. Xu, Versatile Protein and Its Subunit Biomolecules for Advanced Rechargeable Batteries, Advanced Materials 35 (2023) 2305063. https://doi.org/10.1002/ADMA.202305063.

[91] C. Wang, Z. Xie, Z. Zhou, Lithium-air batteries: Challenges coexist with opportunities, APL Mater (2019). https://doi.org/10.1063/1.5091444.

[92] T. Liu, J.P. Vivek, E.W. Zhao, J. Lei, N. Garcia-Araez, C.P. Grey, Current Challenges and Routes Forward for Nonaqueous Lithium-Air Batteries, Chem Rev (2020). https://doi.org/10.1021/acs.chemrev.9b00545.

[93] J. Uddin, V.S. Bryantsev, V. Giordani, W. Walker, G. v Chase, D. Addison, Lithium Nitrate As Regenerable SEI Stabilizing Agent for Rechargeable Li/O2 Batteries, J Phys Chem Lett 4 (2013) 3760–3765. https://doi.org/10.1021/jz402025n.

[94] T. Zhang, J. Yang, J. Zhu, J. Zhou, Z. Xu, J. Wang, F. Qiu, P. He, A lithium-ion oxygen battery with a Si anode lithiated in situ by a Li3N-containing cathode, Chemical Communications 54 (2018) 1069–1072. https://doi.org/10.1039/C7CC09024B.

[95] H. Song, H. Deng, C. Li, N. Feng, P. He, H. Zhou, Advances in Lithium-Containing Anodes of Aprotic Li–O2 Batteries: Challenges and Strategies for Improvements, Small Methods 1 (2017) 1700135. https://doi.org/https://doi.org/10.1002/smtd.201700135.

[96] R. Younesi, M. Hahlin, M. Roberts, K. Edström, The SEI layer formed on lithium metal in the presence of oxygen: A seldom considered component in the development of the Li-O2 battery, J Power Sources (2013). https://doi.org/10.1016/j.jpowsour.2012.10.011.

[97] S.M. Choi, I.S. Kang, Y.K. Sun, J.H. Song, S.M. Chung, D.W. Kim, Cycling characteristics of lithium metal batteries assembled with a surface modified lithium electrode, J Power Sources (2013). https://doi.org/10.1016/j.jpowsour.2012.12.106.

[98] P. Bai, J. Li, F.R. Brushett, M.Z. Bazant, Transition of lithium growth mechanisms in liquid electrolytes, Energy Environ Sci (2016). https://doi.org/10.1039/c6ee01674j.

[99] K. Chen, D.Y. Yang, G. Huang, X.B. Zhang, Lithium-Air Batteries: Air-Electrochemistry and Anode Stabilization, Acc Chem Res 54 (2021) 632–641. https://doi.org/10.1021/ACS.ACCOUNTS.0C00772/ASSET/IMAGES/MEDIUM/AR0C00772_0007.GIF.

[100] Q. Wang, B. Liu, Y. Shen, J. Wu, Z. Zhao, C. Zhong, W. Hu, Confronting the Challenges in Lithium Anodes for Lithium Metal Batteries, Advanced Science 8 (2021) 2101111. https://doi.org/10.1002/ADVS.202101111.

[101] X. Liu, D. Wang, S. Shi, Exploration on the possibility of Ni foam as current collector in rechargeable lithium-air batteries, Electrochim Acta (2013). https://doi.org/10.1016/j.electacta.2012.09.026.

[102] Y. An, H. Fei, G. Zeng, X. Xu, L. Ci, B. Xi, S. Xiong, J. Feng, Y. Qian, Vacuum distillation derived 3D porous current collector for stable lithium–metal batteries, Nano Energy (2018). https://doi.org/10.1016/j.nanoen.2018.03.036.

[103] P. López-Aranguren, X. Judez, M. Chakir, M. Armand, L. Buannic, High Voltage Solid State Batteries: Targeting High Energy Density with Polymer Composite Electrolytes, J Electrochem Soc 167 (2020) 20548. https://doi.org/10.1149/1945-7111/ab6dd7.

[104] Y.F. Deng, S.X. Zhao, Y.H. Xu, C.W. Nan, Electrochemical performance of layer-spinel composite cathode materials at elevated temperature and high rate, Appl Surf Sci 351 (2015) 209–215. https://doi.org/10.1016/j.apsusc.2015.05.132.

[105] S.K. Martha, N.J. Dudney, J.O. Kiggans, J. Nanda, Electrochemical Stability of Carbon Fibers Compared to Aluminum as Current Collectors for Lithium-Ion Batteries, J Electrochem Soc (2012). https://doi.org/10.1149/2.041210jes.

[106] B. De, A. Yadav, S. Khan, K.K. Kar, A Facile Methodology for the Development of a Printable and Flexible All-Solid-State Rechargeable Battery, ACS Appl Mater Interfaces (2017). https://doi.org/10.1021/acsami.7b04112.

[107] R. Zhang, S. Wen, N. Wang, K. Qin, E. Liu, C. Shi, N. Zhao, N-Doped Graphene Modified 3D Porous Cu Current Collector toward Microscale Homogeneous Li Deposition for Li Metal Anodes, Adv Energy Mater (2018). https://doi.org/10.1002/aenm.201800914.

[108] U. Sahapatsombut, H. Cheng, K. Scott, Modelling the micro-macro homogeneous cycling behaviour of a lithium-air battery, J Power Sources (2013). https://doi.org/10.1016/j.jpowsour.2012.11.053.

[109] P. Tan, W. Kong, Z. Shao, M. Liu, M. Ni, Advances in modeling and simulation of Li–air batteries, Prog Energy Combust Sci (2017). https://doi.org/10.1016/j.pecs.2017.06.001.

[110] X. Li, A. Faghri, Optimization of the Cathode Structure of Lithium-Air Batteries Based on a Two-Dimensional, Transient, Non-Isothermal Model, J Electrochem Soc (2012). https://doi.org/10.1149/2.043210jes.

[111] J. Li, F. Yan, Z. Su, T. Zhang, X. Zhang, H. Sun, Highly Efficient Li−Air Battery Using Linear Porosity Air Electrodes, J Electrochem Soc 167 (2020) 090529. https://doi.org/10.1149/1945-7111/ab8b98.

[112] C. Tran, X.Q. Yang, D. Qu, Investigation of the gas-diffusion-electrode used as lithium/air cathode in non-aqueous electrolyte and the importance of carbon material porosity, J Power Sources (2010). https://doi.org/10.1016/j.jpowsour.2009.10.012.

[113] C. Tran, J. Kafle, X.Q. Yang, D. Qu, Increased discharge capacity of a Li-air activated carbon cathode produced by preventing carbon surface passivation, Carbon N Y (2011). https://doi.org/10.1016/j.carbon.2010.11.045.

[114] Y. Gao, C. Wang, W. Pu, Z. Liu, C. Deng, P. Zhang, Z. Mao, Preparation of high-capacity air electrode for lithium-air batteries, Int J Hydrogen Energy 37 (2012) 12725–12730. https://doi.org/https://doi.org/10.1016/j.ijhydene.2012.03.127.

[115] P. Tan, W. Shyy, L. An, Z.H. Wei, T.S. Zhao, A gradient porous cathode for non-aqueous lithium-air batteries leading to a high capacity, Electrochem Commun (2014). https://doi.org/10.1016/j.elecom.2014.06.026.

[116] H. bin Yang, J. Miao, S.F. Hung, J. Chen, H.B. Tao, X. Wang, L. Zhang, R. Chen, J. Gao, H.M. Chen, L. Dai, B. Liu, Identification of catalytic sites for oxygen reduction and oxygen evolution in N-doped graphene materials: Development of highly efficient metal-free bifunctional electrocatalyst, Sci Adv 2 (2016) 1–12. https://doi.org/10.1126/sciadv.1501122.

[117] S. Shen, A. Wu, G. Xia, G. Wei, X. Yan, Y. Zhang, F. Zhu, J. Yin, J. Zhang, Facile preparation of unique three-dimensional (3D) α-MnO2/MWCNTs macroporous hybrid as the high-performance cathode of rechargeable Li-O2 batteries, Nano Research 2018 12:1 12 (2018) 69–75. https://doi.org/10.1007/S12274-018-2182-X.

[118] Z. Lyu, Y. Zhou, W. Dai, X. Cui, M. Lai, L. Wang, F. Huo, W. Huang, Z. Hu, W. Chen, Recent advances in understanding of the mechanism and control of Li2O2 formation in aprotic Li-O2 batteries, Chem Soc Rev 46 (2017). https://doi.org/10.1039/c7cs00255f.

[119] O.L. Li, T. Ishizaki, Development, Challenges, and Prospects of Carbon-Based Electrode for Lithium-Air Batteries, Emerging Materials for Energy Conversion and Storage (2018) 115–152. https://doi.org/10.1016/B978-0-12-813794-9.00004-1.

[120] H. Woo, J. Kang, J. Kim, C. Kim, S. Nam, B. Park, Development of carbon-based cathodes for Li-air batteries: Present and future, Electronic Materials Letters 2016 12:5 12 (2016) 551–567. https://doi.org/10.1007/S13391-016-6183-1.

[121] E. Yoo, H. Zhou, Li-air rechargeable battery based on metal-free graphene nanosheet catalysts, ACS Nano 5 (2011) 3020–3026. https://doi.org/10.1021/NN200084U/SUPPL_FILE/NN200084U_SI_001.PDF.

[122] Z. Ma, X. Yuan, L. Li, Z.F. Ma, D.P. Wilkinson, L. Zhang, J. Zhang, A review of cathode materials and structures for rechargeable lithium-air batteries, Energy Environ Sci (2015). https://doi.org/10.1039/c5ee00838g.

[123] A. I. Belova, D. G. Kwabi, L. V. Yashina, Y. Shao-Horn, D. M. Itkis, Mechanism of Oxygen Reduction in Aprotic Li–Air Batteries: The Role of Carbon Electrode Surface Structure, The Journal of Physical Chemistry C 121 (2017) 1569–1577. https://doi.org/10.1021/acs.jpcc.6b12221.

[124] V.S. Dilimon, C. Hwang, Y.-G. Cho, J. Yang, H.-D. Lim, K. Kang, S.J. Kang, H.-K. Song, Superoxide stability for reversible Na-O 2 electrochemistry, (n.d.). https://doi.org/10.1038/s41598-017-17745-9.

[125] L. Qin, L. Schkeryantz, J. Zheng, N. Xiao, Y. Wu, Superoxide-Based K–O2 Batteries: Highly Reversible Oxygen Redox Solves Challenges in Air Electrodes, J Am Chem Soc 142 (2020) 11629–11640. https://doi.org/10.1021/jacs.0c05141.

[126] C. Cao, Z. Lan, Y. Yan, H. Cheng, B. Pan, J. Xie, Y. Lu, H. Zhang, S. Zhang, G. Cao, X. Zhao, Mechanistic insight into the synergetic catalytic effect of Pd and MnO2 for high-performance Li–O2 cells, Energy Storage Mater 12 (2018) 8–16. https://doi.org/10.1016/J.ENSM.2017.11.009.

[127] X. Gao, Y. Chen, L. Johnson, P.G. Bruce, Promoting solution phase discharge in Li–O2 batteries containing weakly solvating electrolyte solutions, Nature Materials 2016 15:8 15 (2016) 882–888. https://doi.org/10.1038/nmat4629.

[128] S. Guo, L. Zou, Z. Wang, M. Sun, Y. Chen, B. Chi, J. Pu, J. Li, Wrinkled Perovskite La0.9Mn0.6Ni0.4O3−δ Nanofibers as Highly Efficient Electrocatalyst for Rechargeable Li−O2 Batteries, ChemElectroChem 6 (2019). https://doi.org/10.1002/celc.201901671.

[129] H. Liu, L. Zhao, Y. Xing, J. Lai, L. Li, F. Wu, N. Chen, R. Chen, Enhancing the Long Cycle Performance of Li–O2 Batteries at High Temperatures Using Metal–Organic Framework-Based Electrolytes, ACS Appl Energy Mater 5 (2022) 7185–7191. https://doi.org/10.1021/acsaem.2c00735.

[130] N.B. Aetukuri, B.D. McCloskey, J.M. Garciá, L.E. Krupp, V. Viswanathan, A.C. Luntz, Solvating additives drive solution-mediated electrochemistry and enhance toroid growth in non-aqueous Li–O2 batteries, Nature Chemistry 2014 7:1 7 (2014) 50–56. https://doi.org/10.1038/nchem.2132.

[131] J. Lu, S. Dey, I. Temprano, Y. Jin, C. Xu, Y. Shao, C. P. Grey, Co3O4-Catalyzed LiOH Chemistry in Li–O2 Batteries, ACS Energy Lett 5 (2020) 3681–3691. https://doi.org/10.1021/acsenergylett.0c01940.

[132] I. Temprano, T. Liu, E. Petrucco, J.H.J. Ellison, G. Kim, C.P. Grey, Toward Reversible and Moisture-Tolerant Aprotic Lithium-Air Batteries, (n.d.). https://doi.org/10.1016/j.joule.2020.09.021.

[133] B.G. Kim, H.J. Kim, S. Back, K.W. Nam, Y. Jung, Y.K. Han, J.W. Choi, Improved reversibility in lithium-oxygen battery: Understanding elementary reactions and surface charge engineering of metal alloy catalyst, Scientific Reports 2014 4:1 4 (2014) 1–9. https://doi.org/10.1038/srep04225.

[134] D. Su, D.H. Seo, Y. Ju, Z. Han, K. Ostrikov, S. Dou, H.J. Ahn, Z. Peng, G. Wang, Ruthenium nanocrystal decorated vertical graphene nanosheets@Ni foam as highly efficient cathode catalysts for lithium-oxygen batteries, NPG Asia Materials 2016 8:7 8 (2016) e286–e286. https://doi.org/10.1038/am.2016.91.

[135] J. Huang, Z. Jin, Z.L. Xu, L. Qin, H. Huang, Z. Sadighi, S. Yao, J. Cui, B. Huang, J.K. Kim, Porous RuO2 nanosheet/CNT electrodes for DMSO-based Li-O2 and Li ion O2 batteries, Energy Storage Mater 8 (2017) 110–118. https://doi.org/10.1016/J.ENSM.2017.05.004.

[136] N.C. Lai, G. Cong, Z. Liang, Y.C. Lu, A Highly Active Oxygen Evolution Catalyst for Lithium-Oxygen Batteries Enabled by High-Surface-Energy Facets, Joule 2 (2018) 1511–1521. https://doi.org/10.1016/j.joule.2018.04.009.

[137] N. Mahne, B. Schafzahl, C. Leypold, M. Leypold, S. Grumm, A. Leitgeb, G.A. Strohmeier, M. Wilkening, O. Fontaine, D. Kramer, C. Slugovc, S.M. Borisov, S.A. Freunberger, Singlet oxygen generation as a major cause for parasitic reactions during cycling of aprotic lithium–oxygen batteries, Nat Energy 2 (2017) 17036. https://doi.org/10.1038/nenergy.2017.36.

[138] A. Pierini, S. Brutti, E. Bodo, Reactive pathways toward parasitic release of singlet oxygen in metal-air batteries, NPJ Comput Mater 7 (2021) 126. https://doi.org/10.1038/s41524-021-00597-3.

[139] S. Mondal, R.B. Jethwa, B. Pant, R. Hauschild, S.A. Freunberger, Singlet oxygen formation in non-aqueous oxygen redox chemistry: direct spectroscopic evidence for formation pathways and reliability of chemical probes, Faraday Discuss (2024). https://doi.org/10.1039/D3FD00088E.

[140] D. Córdoba, L.N. Benavides, D.H. Murgida, H.B. Rodríguez, E.J. Calvo, Operando detection and suppression of spurious singlet oxygen in Li–O2 batteries, Faraday Discuss (2024). https://doi.org/10.1039/D3FD00081H.

[141] V. S. Bryantsev, F. Faglioni, Predicting Autoxidation Stability of Ether- and Amide-Based Electrolyte Solvents for Li–Air Batteries, J Phys Chem A 116 (2012) 7128–7138. https://doi.org/10.1021/jp301537w.

[142] V. S. Bryantsev, V. Giordani, W. Walker, M. Blanco, S. Zecevic, K. Sasaki, J. Uddin, D. Addison, G. V. Chase, Predicting Solvent Stability in Aprotic Electrolyte Li–Air Batteries: Nucleophilic Substitution by the Superoxide Anion Radical (O2•–), J Phys Chem A 115 (2011) 12399–12409. https://doi.org/10.1021/jp2073914.

[143] N. Zheng, X. He, R. Hu, R. Wang, Q. Zhou, Y. Lian, Z. Hu, In-situ production of singlet oxygen by dioxygen activation on iron phosphide for advanced oxidation processes, Appl Catal B 307 (2022) 121157. https://doi.org/10.1016/J.APCATB.2022.121157.

[144] A. Jain, Y. Shin, K.A. Persson, Computational predictions of energy materials using density functional theory, Nature Reviews Materials 2016 1:1 1 (2016) 1–13. https://doi.org/10.1038/natrevmats.2015.4.

[145] Z. Xia, S. Guo, Strain engineering of metal-based nanomaterials for energy electrocatalysis, Chem Soc Rev 48 (2019) 3265–3278. https://doi.org/10.1039/C8CS00846A.

[146] Z. Zhou, L. Zhao, J. Wang, Y. Zhang, Y. Li, S. Shoukat, X. Han, Y. Long, Y. Liu, Optimizing Eg Orbital Occupancy of Transition Metal Sulfides by Building Internal Electric Fields to Adjust the Adsorption of Oxygenated Intermediates for Li-O2 Batteries, Small 19 (2023) 2302598. https://doi.org/10.1002/SMLL.202302598.

[147] L. Ren, R. Zheng, D. Du, Y. Yan, M. He, Z. Ran, M. Li, C. Shu, Optimized orbital occupancy of transition metal in spinel Ni-Co oxides with heteroatom doping for Aprotic Li-O2 battery, Chemical Engineering Journal 430 (2022) 132977. https://doi.org/10.1016/J.CEJ.2021.132977.

[148] A.M. Abdelkader, Electrochemical synthesis of highly corrugated graphene sheets for high performance supercapacitors, J Mater Chem A Mater 3 (2015) 8519–8525. https://doi.org/10.1039/C5TA00545K.

[149] A.R. Kamali, Scalable fabrication of highly conductive 3D graphene by electrochemical exfoliation of graphite in molten NaCl under Ar/H2 atmosphere, Journal of Industrial and Engineering Chemistry 52 (2017) 18–27. https://doi.org/10.1016/J.JIEC.2017.03.013.

[150] M. M. Ottakam Thotiyl, S. A. Freunberger, Z. Peng, P. G. Bruce, The Carbon Electrode in Nonaqueous Li–O2 Cells, J Am Chem Soc 135 (2012) 494–500. https://doi.org/10.1021/ja310258x.

[151] Y. Li, J. Wang, X. Li, D. Geng, R. Li, X. Sun, Superior energy capacity of graphene nanosheets for a nonaqueous lithium-oxygen battery, Chemical Communications 47 (2011) 9438–9440. https://doi.org/10.1039/C1CC13464G.

[152] J.L. Gómezurbano, An Overview of Engineered Graphene-Based Cathodes: Boosting Oxygen Reduction and Evolution Reactions in Lithium-and Sodium-Oxygen Batteries, (n.d.). https://doi.org/10.1002/cssc.201902972.

[153] D.Y. Kim, M. Kim, D.W. Kim, J. Suk, J.J. Park, O.O. Park, Y. Kang, Graphene paper with controlled pore structure for high-performance cathodes in Li–O2 batteries, Carbon N Y 100 (2016) 265–272. https://doi.org/10.1016/J.CARBON.2016.01.013.

[154] X. Xin, K. Ito, Y. Kubo, Graphene/activated carbon composite material for oxygen electrodes in lithium–oxygen rechargeable batteries, Carbon N Y 99 (2016) 167–173. https://doi.org/10.1016/J.CARBON.2015.12.015.

[155] K.A. Novčić, A.S. Dobrota, M. Petković, B. Johansson, N. V. Skorodumova, S. V. Mentus, I.A. Pašti, Theoretical analysis of doped graphene as cathode catalyst in Li-O2 and Na-O2 batteries – the impact of the computational scheme, Electrochim Acta 354 (2020) 136735. https://doi.org/10.1016/J.ELECTACTA.2020.136735.

[156] J. Zhu, A. Abdelkader, D. Demko, L. Deng, P. Zhang, T. He, Y. Wang, L. Huang, Electrocatalytic Assisted Performance Enhancement for the Na-S Battery in Nitrogen-

Doped Carbon Nanospheres Loaded with Fe, Molecules 25 (2020). https://doi.org/10.3390/molecules25071585.

[157] F. Xiao, Y. Meng, Z. Lin, Y. Lei, X. Chen, J. Zhang, H. Lu, Y. Tong, G. Liu, J. Xu, Highly boron-doped holey graphene for lithium oxygen batteries with enhanced electrochemical performance, Carbon N Y 189 (2022) 404–412. https://doi.org/10.1016/J.CARBON.2021.12.061.

[158] X. Ren, J. Zhu, F. Du, J. Liu, W. Zhang, B-doped graphene as catalyst to improve charge rate of lithium-air battery, Journal of Physical Chemistry C 118 (2014) 22412–22418. https://doi.org/10.1021/JP505876Z/SUPPL_FILE/JP505876Z_SI_001.PDF.

[159] S. Hyun, B. Son, H. Kim, J. Sanetuntikul, S. Shanmugam, The synergistic effect of nickel cobalt sulfide nanoflakes and sulfur-doped porous carboneous nanostructure as bifunctional electrocatalyst for enhanced rechargeable Li-O2 batteries, Appl Catal B 263 (2020) 118283. https://doi.org/10.1016/J.APCATB.2019.118283.

[160] J. Wu, Z. Pan, Y. Zhang, B. Wang, H. Peng, The recent progress of nitrogen-doped carbon nanomaterials for electrochemical batteries, J Mater Chem A Mater 6 (2018). https://doi.org/10.1039/c8ta03968b.

[161] Y. Li, J. Wang, X. Li, J. Liu, D. Geng, J. Yang, R. Li, X. Sun, Nitrogen-doped carbon nanotubes as cathode for lithium-air batteries, Electrochem Commun 13 (2011) 668–672. https://doi.org/10.1016/j.elecom.2011.04.004.

[162] S. Chen, X. Min, Y. Zhao, X. Wu, D. Zhang, X. Hou, X. Wu, Y. Liu, Z. Huang, Amr.M. Abdelkader, K. Xi, M. Fang, Nickel Quantum Dots Anchored in Biomass-Derived Nitrogen-Doped Carbon as Bifunctional Electrocatalysts for Overall Water Splitting, Adv Mater Interfaces 9 (2022) 2102014. https://doi.org/https://doi.org/10.1002/admi.202102014.

[163] A. Ejaz, S. Jeon, The individual role of pyrrolic, pyridinic and graphitic nitrogen in the growth kinetics of Pd NPs on N-rGO followed by a comprehensive study on ORR, Int J Hydrogen Energy 43 (2018) 5690–5702. https://doi.org/10.1016/j.ijhydene.2017.12.184.

[164] W.H. Shin, H.M. Jeong, B.G. Kim, J.K. Kang, J.W. Choi, Nitrogen-doped multiwall carbon nanotubes for lithium storage with extremely high capacity, Nano Lett 12 (2012). https://doi.org/10.1021/nl3000908.

[165] A. Shen, Y. Zou, Q. Wang, R.A.W. Dryfe, X. Huang, S. Dou, L. Dai, S. Wang, Oxygen reduction reaction in a droplet on graphite: Direct evidence that the edge is more active than the basal plane, Angewandte Chemie - International Edition 53 (2014). https://doi.org/10.1002/anie.201406695.

[166] T.S.E.F. Karunarathne, C. Sandaruwan, W.P.S.L. Wijesinghe, A. Karalasignham, A.M. Abdelkader, G.A.J. Amaratunga, S.G.M. de Silva, Development of universal fabric dyeing and adhesion through RF glow discharge plasma treatment, Vacuum 204 (2022) 111394. https://doi.org/10.1016/J.VACUUM.2022.111394.

[167] Y. Li, Z. Zhang, D. Duan, Y. Han, K. Wang, X. Hao, J. Wang, S. Liu, F. Wu, An integrated structural air electrode based on parallel porous nitrogen-doped carbon nanotube arrays for rechargeable li–air batteries, Nanomaterials 9 (2019). https://doi.org/10.3390/nano9101412.

[168] G. Wu, N. H. Mack, W. Gao, S. Ma, R. Zhong, J. Han, J. K. Baldwin, P. Zelenay, Nitrogen-Doped Graphene-Rich Catalysts Derived from Heteroatom Polymers for Oxygen Reduction in Nonaqueous Lithium–O2 Battery Cathodes, ACS Nano 6 (2012) 9764–9776. https://doi.org/10.1021/nn303275d.

[169] Y. Li, J. Wang, X. Li, D. Geng, M.N. Banis, R. Li, X. Sun, Nitrogen-doped graphene nanosheets as cathode materials with excellent electrocatalytic activity for high capacity lithium-oxygen batteries, Electrochem Commun 18 (2012) 12–15. https://doi.org/10.1016/J.ELECOM.2012.01.023.

[170] T. Zheng, Y. Ren, X. Han, J. Zhang, Design principles of nitrogen-doped graphene nanoribbons as highly effective bifunctional catalysts for Li–O2 batteries, Physical Chemistry Chemical Physics 24 (2022) 22589–22598. https://doi.org/10.1039/D2CP03001B.

[171] Y. Li, J. Wang, X. Li, D. Geng, M.N. Banis, R. Li, X. Sun, Nitrogen-doped graphene nanosheets as cathode materials with excellent electrocatalytic activity for high capacity lithium-oxygen batteries, Electrochem Commun 18 (2012). https://doi.org/10.1016/j.elecom.2012.01.023.

[172] C. Shu, Y. Lin, D. Su, N-doped onion-like carbon as an efficient oxygen electrode for long-life Li-O2 battery, J Mater Chem A Mater 4 (2016). https://doi.org/10.1039/c5ta09539e.

[173] C. Lei, F. Han, D. Li, W.C. Li, Q. Sun, X.Q. Zhang, A.H. Lu, Dopamine as the coating agent and carbon precursor for the fabrication of N-doped carbon coated Fe3O4 composites as superior lithium ion anodes, Nanoscale 5 (2013) 1168–1175. https://doi.org/10.1039/C2NR33043A.

[174] K.H. Lim, H. Kweon, H. Kim, Polydopamine-Derived Nitrogen-Doped Graphitic Carbon for a Bifunctional Oxygen Electrode in a Non-Aqueous Li-O2Battery, J Electrochem Soc 164 (2017) A1595–A1600. https://doi.org/10.1149/2.1321707jes.

[175] K.H. Lim, H. Kweon, H. Kim, Three-Dimensional Nitrogen-Doped Hollow Carbon Fiber with a Micro-Scale Diameter as a Binder-Free Oxygen Electrode for Li-O 2 Batteries , J Electrochem Soc 166 (2019). https://doi.org/10.1149/2.1101914jes.

[176] H. Bin Yang, J. Miao, S.F. Hung, J. Chen, H.B. Tao, X. Wang, L. Zhang, R. Chen, J. Gao, H.M. Chen, L. Dai, B. Liu, Identification of catalytic sites for oxygen reduction and oxygen evolution in N-doped graphene materials: Development of highly efficient metal-free bifunctional electrocatalyst, Sci Adv 2 (2016) 1–12. https://doi.org/10.1126/sciadv.1501122.

[177] A. Ejaz, S. Jeon, The individual role of pyrrolic, pyridinic and graphitic nitrogen in the growth kinetics of Pd NPs on N-rGO followed by a comprehensive study on ORR, Int

J Hydrogen Energy 43 (2018) 5690–5702. https://doi.org/10.1016/j.ijhydene.2017.12.184.

[178] X. Yi, X. Liu, J. Fang, H. Huo, R. Dou, Z. Wen, W. Zhou, An atomic/molecular-level strategy for the design of a preferred nitrogen-doped carbon nanotube cathode for Li-O2 batteries, Appl Surf Sci 615 (2023) 156367. https://doi.org/10.1016/J.APSUSC.2023.156367.

[179] X. Yi, X. Liu, R. Dou, Z. Wen, W. Zhou, Understanding the Catalytic Activity of the Preferred Nitrogen Configuration on the Carbon Nanotube Surface and Its Implications for Li–O2 Batteries, The Journal of Physical Chemistry C 125 (2021) 22570–22580. https://doi.org/10.1021/acs.jpcc.1c07024.

[180] K.H. Lim, H. Kweon, H. Kim, Three-Dimensional Nitrogen-Doped Hollow Carbon Fiber with a Micro-Scale Diameter as a Binder-Free Oxygen Electrode for Li-O2 Batteries, J Electrochem Soc 166 (2019) A3425. https://doi.org/10.1149/2.1101914jes.

[181] W. Meng, L. Wen, Z. Song, N. Cao, X. Qin, Metal-free boron-doped carbon microspheres as excellent cathode catalyst for rechargeable Li–O2 battery, Journal of Solid State Electrochemistry 21 (2017) 665–671. https://doi.org/10.1007/S10008-016-3412-3/METRICS.

[182] F. Wu, Y. Xing, L. Li, J. Qian, W. Qu, J. Wen, D. Miller, Y. Ye, R. Chen, K. Amine, J. Lu, Facile Synthesis of Boron-Doped rGO as Cathode Material for High Energy Li–O2 Batteries, ACS Applied Materials & Interfaces 8 (2016) 23635–23645. https://doi.org/10.1021/acsami.6b05403.

[183] F. Xiao, Y. Meng, Z. Lin, Y. Lei, X. Chen, J. Zhang, H. Lu, Y. Tong, G. Liu, J. Xu, Highly boron-doped holey graphene for lithium oxygen batteries with enhanced electrochemical performance, Carbon N Y 189 (2022) 404–412. https://doi.org/10.1016/J.CARBON.2021.12.061.

[184] L. Deng, H. Fang, P. Zhang, A. Abdelkader, X. Ren, Y. Li, N. Xie, Nitrogen and Sulfur Dual-Doped Carbon Microtubes with Enhanced Performances for Oxygen Reduction Reaction, J Electrochem Soc 163 (2016) H343. https://doi.org/10.1149/2.1131605jes.

[185] X. Ma, G. Ning, C. Qi, C. Xu, J. Gao, Phosphorus and nitrogen dual-doped few-layered porous graphene: A high-performance anode material for lithium-ion batteries, ACS Appl Mater Interfaces 6 (2014). https://doi.org/10.1021/am503692g.

[186] A. Wu, G. Wei, F. Yang, G. Xia, X. Yan, S. Shen, F. Zhu, C. Ke, J. Zhang, Nitrogen and iodine dual-doped 3D porous graphene as a bi-functional cathode catalyst for Li-O2 batteries, Electrochim Acta 318 (2019) 354–361. https://doi.org/10.1016/j.electacta.2019.05.099.

[187] S. Wang, L. Zhang, Z. Xia, A. Roy, D.W. Chang, J.B. Baek, L. Dai, BCN graphene as efficient metal-free electrocatalyst for the oxygen reduction reaction, Angewandte Chemie - International Edition 51 (2012) 4209–4212. https://doi.org/10.1002/anie.201109257.

[188] Y.-J. Wang, B. Fang, D. Zhang, A. Li, D.P. Wilkinson, A. Ignaszak, L. Zhang, J. Zhang, A Review of Carbon-Composited Materials as Air-Electrode Bifunctional Electrocatalysts for Metal–Air Batteries, Electrochemical Energy Reviews 1 (2018). https://doi.org/10.1007/s41918-018-0002-3.

[189] T. Akhter, M.M. Islam, S.N. Faisal, E. Haque, A.I. Minett, H.K. Liu, K. Konstantinov, S.X. Dou, Self-Assembled N/S Codoped Flexible Graphene Paper for High Performance Energy Storage and Oxygen Reduction Reaction, ACS Appl Mater Interfaces 8 (2016). https://doi.org/10.1021/acsami.5b10545.

[190] Z. Lei, W. Feng, C. Feng, W. Zhou, C. Wei, X. Wang, Nitrified coke wastewater sludge flocs: an attractive precursor for N,S dual-doped graphene-like carbon with ultrahigh capacitance and oxygen reduction performance, J Mater Chem A Mater 5 (2017). https://doi.org/10.1039/C6TA09887H.

[191] J.H. Kim, A.G. Kannan, H.S. Woo, D.G. Jin, W. Kim, K. Ryu, D.W. Kim, A bi-functional metal-free catalyst composed of dual-doped graphene and mesoporous carbon for rechargeable lithium-oxygen batteries, J Mater Chem A Mater 3 (2015) 18456–18465. https://doi.org/10.1039/c5ta05334j.

[192] S. Jang, J. Kim, E. Na, M. Song, J. Choi, K. Song, S. Hyeon, Facile synthesis of mesoporous and highly nitrogen / sulfur dual - doped graphene and its ultrahigh discharge capacity in non - aqueous lithium oxygen batteries, Carbon Letters (2019). https://doi.org/10.1007/s42823-019-00026-y.

[193] V.A. Online, X. Wang, J. Wang, D. Wang, S. Dou, J. Wu, L. Tao, A. Shen, C. Ouyang, Q. Liu, S. Wang, co-doped graphene as efficient metal-free, (2014) 4839–4842. https://doi.org/10.1039/c4cc00440j.

[194] J.H. Kim, A.G. Kannan, H.S. Woo, D.G. Jin, W. Kim, K. Ryu, D.W. Kim, A bi-functional metal-free catalyst composed of dual-doped graphene and mesoporous carbon for rechargeable lithium-oxygen batteries, J Mater Chem A Mater 3 (2015) 18456–18465. https://doi.org/10.1039/c5ta05334j.

[195] S. Jang, J. Kim, E. Na, M. Song, J. Choi, K. Song, S. Hyeon, Facile synthesis of mesoporous and highly nitrogen / sulfur dual - doped graphene and its ultrahigh discharge capacity in non - aqueous lithium oxygen batteries, Carbon Letters (2019). https://doi.org/10.1007/s42823-019-00026-y.

[196] V.A. Online, X. Wang, J. Wang, D. Wang, S. Dou, J. Wu, L. Tao, A. Shen, C. Ouyang, Q. Liu, S. Wang, co-doped graphene as efficient metal-free, (2014) 4839–4842. https://doi.org/10.1039/c4cc00440j.

[197] Z.L. Wu, P. Zhang, M.X. Gao, C.F. Liu, W. Wang, F. Leng, C.Z. Huang, One-pot hydrothermal synthesis of highly luminescent nitrogen-doped amphoteric carbon dots for bioimaging from Bombyx mori silk-natural proteins, J Mater Chem B 1 (2013). https://doi.org/10.1039/c3tb20418a.

[198] Z. Chen, Z. Chen, D. Higgins, Nitrogen doped carbon nanotubes and their impact on the oxygen reduction reaction in fuel cells, Carbon N Y 48 (2010) 3057–3065. https://doi.org/10.1016/j.carbon.2010.04.038.

[199] L. Zhang, Z. Xia, Mechanisms of oxygen reduction reaction on nitrogen-doped graphene for fuel cells, Journal of Physical Chemistry C 115 (2011). https://doi.org/10.1021/jp201991j.

[200] J.I. Aihara, Reduced HOMO-LUMO Gap as an Index of Kinetic Stability for Polycyclic Aromatic Hydrocarbons, Journal of Physical Chemistry A 103 (1999). https://doi.org/10.1021/jp990092i.

[201] L. Li, A. Manthiram, O- and N-doped carbon nanowebs as metal-free catalysts for hybrid Li-air batteries, Adv Energy Mater 4 (2014). https://doi.org/10.1002/aenm.201301795.

[202] A. Wu, G. Wei, F. Yang, G. Xia, X. Yan, S. Shen, F. Zhu, C. Ke, J. Zhang, Nitrogen and iodine dual-doped 3D porous graphene as a bi-functional cathode catalyst for Li-O2 batteries, Electrochim Acta 318 (2019) 354–361. https://doi.org/10.1016/j.electacta.2019.05.099.

[203] B. M. Gallant, R. R. Mitchell, D. G. Kwabi, J. Zhou, L. Zuin, C. V. Thompson, Y. Shao-Horn, Chemical and Morphological Changes of Li–O2 Battery Electrodes upon Cycling, The Journal of Physical Chemistry C 116 (2012) 20800–20805. https://doi.org/10.1021/jp308093b.

[204] P. Kichambare, S. Rodrigues, Graphene Nanosheets Based Cathodes for Lithium-Oxygen Batteries, C (Basel) 1 (2015) 27–42. https://doi.org/10.3390/c1010027.

[205] Y.S. Jeong, J.-B. Park, H.-G. Jung, J. Kim, X. Luo, J. Lu, L. Curtiss, K. Amine, Y.-K. Sun, B. Scrosati, Y.J. Lee, Study on the Catalytic Activity of Noble Metal Nanoparticles on Reduced Graphene Oxide for Oxygen Evolution Reactions in Lithium–Air Batteries, Nano Lett 15 (2015) 4261–4268. https://doi.org/10.1021/NL504425H.

[206] B. Sun, P. Munroe, G. Wang, Ruthenium nanocrystals as cathode catalysts for lithium-oxygen batteries with a superior performance, Scientific Reports 2013 3:1 3 (2013) 1–7. https://doi.org/10.1038/srep02247.

[207] Donggang Li, Tianlong Shan, Chongguo Liu, Can Zhao, Andrew Doherty, A. Reza Kamali, Qiang Wang, Homogenizing of Pt on NiCu films for enhanced HER activity by two-step magneto-electrodeposition, New Journal of Chemistry 47 (2023) 13098–13105. https://doi.org/10.1039/D3NJ01397A.

[208] C.R. Ratwani, S. Karunarathne, A.R. Kamali, A.M. Abdelkader, Transforming Nature's Bath Sponge into Stacking Faults-Enhanced Ag Nanorings-Decorated Catalyst for Hydrogen Evolution Reaction, ACS Appl Mater Interfaces (2023). https://doi.org/10.1021/ACSAMI.3C16115/SUPPL_FILE/AM3C16115_SI_001.PDF.

[209] M. Winter, R.J. Brodd*, What Are Batteries, Fuel Cells, and Supercapacitors?, Chem Rev 104 (2004) 4245–4269. https://doi.org/10.1021/CR020730K.

[210] I. V. Zenyuk, P.K. Das, A.Z. Weber, Understanding Impacts of Catalyst-Layer Thickness on Fuel-Cell Performance via Mathematical Modeling, J Electrochem Soc 163 (2016) F691. https://doi.org/10.1149/2.1161607JES.

[211] F. Wu, Y. Xing, X. Zeng, Y. Yuan, X. Zhang, R. Shahbazian-Yassar, J. Wen, D.J. Miller, L. Li, R. Chen, J. Lu, K. Amine, Platinum-Coated Hollow Graphene Nanocages as Cathode Used in Lithium-Oxygen Batteries, Adv Funct Mater 26 (2016) 7626–7633. https://doi.org/10.1002/ADFM.201602246.

[212] K. Song, J. Jung, M. Park, H. Park, H.-J. Kim, S.-I. Choi, J. Yang, K. Kang, Y.-K. Han, Y.-M. Kang, Anisotropic Surface Modulation of Pt Catalysts for Highly Reversible Li–O2 Batteries: High Index Facet as a Critical Descriptor, ACS Catal 8 (2018) 9006–9015. https://doi.org/10.1021/acscatal.8b02172.

[213] D. Su, D.H. Seo, Y. Ju, Z. Han, K. Ostrikov, S. Dou, H.J. Ahn, Z. Peng, G. Wang, Ruthenium nanocrystal decorated vertical graphene nanosheets@ni foam as highly efficient cathode catalysts for lithium-oxygen batteries, NPG Asia Mater 8 (2016) 1–10. https://doi.org/10.1038/AM.2016.91.

[214] G. Wang, F. Tu, J. Xie, G. Du, S. Zhang, G. Cao, X. Zhao, High-Performance Li–O2 Batteries with Controlled Li2O2 Growth in Graphene/Au-Nanoparticles/Au-Nanosheets Sandwich, Advanced Science 3 (2016) 1500339. https://doi.org/10.1002/ADVS.201500339.

[215] B. D. McCloskey, R. Scheffler, A. Speidel, D. S. Bethune, R. M. Shelby, A. C. Luntz, On the Efficacy of Electrocatalysis in Nonaqueous Li–O2 Batteries, J Am Chem Soc 133 (2011) 18038–18041. https://doi.org/10.1021/ja207229n.

[216] A. Samojlov, D. Schuster, J. Kahr, S.A. Freunberger, Surface and catalyst driven singlet oxygen formation in Li-O2 cells, Electrochim Acta 362 (2020) 137175. https://doi.org/10.1016/J.ELECTACTA.2020.137175.

[217] Y.-C. Lu, H. A. Gasteiger, Y. Shao-Horn, Catalytic Activity Trends of Oxygen Reduction Reaction for Nonaqueous Li-Air Batteries, J Am Chem Soc 133 (2011) 19048–19051. https://doi.org/10.1021/ja208608s.

[218] C.C. Li, W. Zhang, H. Ang, H. Yu, B.Y. Xia, X. Wang, Y.H. Yang, Y. Zhao, H.H. Hng, Q. Yan, Compressed hydrogen gas-induced synthesis of Au–Pt core–shell nanoparticle chains towards high-performance catalysts for Li–O2 batteries, J Mater Chem A Mater 2 (2014) 10676–10681. https://doi.org/10.1039/C4TA01475H.

[219] B. Sun, P. Munroe, G. Wang, Ruthenium nanocrystals as cathode catalysts for lithium-oxygen batteries with a superior performance, Scientific Reports 2013 3:1 3 (2013) 1–7. https://doi.org/10.1038/srep02247.

[220] Y. Liu, B. Li, Z. Cheng, C. Li, X. Zhang, S. Guo, P. He, H. Zhou, Intensive investigation on all-solid-state Li-air batteries with cathode catalysts of single-walled carbon nanotube/RuO2, J Power Sources 395 (2018) 439–443. https://doi.org/10.1016/J.JPOWSOUR.2018.05.080.

[221] S. Bie, M. Du, W. He, H. Zhang, Z. Yu, J. Liu, M. Liu, W. Yan, L. Zhou, Z. Zou, Carbon Nanotube@RuO 2 as a High Performance Catalyst for Li-CO 2 Batteries, ACS Appl Mater Interfaces 11 (2019) 5146–5151. https://doi.org/10.1021/ACSAMI.8B20573/ASSET/IMAGES/LARGE/AM-2018-20573B_0003.JPEG.

[222] M. Hayashi, M. Nohara, H. Minowa, K. Asakura, K. Hayashi, H. Kitabayashi, Electrochemical Properties of RuO 2 Catalyst for Air Electrode of Lithium Air Battery , ECS Trans 64 (2015) 1–15. https://doi.org/10.1149/06419.0001ECST/XML.

[223] L. Zhao, Y. Xing, N. Chen, J. Lai, L. Li, F. Wu, R. Chen, A robust cathode of RuO2 nH2O clusters anchored on the carbon nanofibers for ultralong-life lithium-oxygen batteries, J Power Sources 463 (2020) 228161. https://doi.org/10.1016/J.JPOWSOUR.2020.228161.

[224] Y. Zhu, T. Zhang, Q. Li, Z. Xue, M. Yu, J. Li, X. Wang, H. Sun, MOFs-derived 3D nanoporous Co-N-C coupled with RuO2 composite as enhanced catalysts for Li-O2 batteries, J Alloys Compd 983 (2024) 173877. https://doi.org/10.1016/J.JALLCOM.2024.173877.

[225] P. Zhang, X. Hui, Y. Nie, R. Wang, C. Wang, Z. Zhang, L. Yin, New Conceptual Catalyst on Spatial High-Entropy Alloy Heterostructures for High-Performance Li-O2 Batteries, Small 19 (2023) 2206742. https://doi.org/10.1002/SMLL.202206742.

[226] Y. Zhang, S. Zhang, J. Ma, A. Huang, M. Yuan, Y. Li, G. Sun, C. Chen, C. Nan, Oxygen Vacancy-Rich RuO2-Co3O4Nanohybrids as Improved Electrocatalysts for Li-O2Batteries, ACS Appl Mater Interfaces 13 (2021) 39239–39247. https://doi.org/10.1021/ACSAMI.1C08720/SUPPL_FILE/AM1C08720_SI_001.PDF.

[227] Z. Lian, Y. Lu, S. Zhao, Z. Li, Q. Liu, Engineering the Electronic Interaction between Atomically Dispersed Fe and RuO2 Attaining High Catalytic Activity and Durability Catalyst for Li-O2 Battery, Advanced Science 10 (2023) 2205975. https://doi.org/10.1002/ADVS.202205975.

[228] B. Sun, S. Chen, H. Liu, G. Wang, Mesoporous Carbon Nanocube Architecture for High-Performance Lithium–Oxygen Batteries, Adv Funct Mater 25 (2015) 4436–4444. https://doi.org/10.1002/ADFM.201500863.

[229] W. Yang, Z. Qian, C. Du, C. Hua, P. Zuo, X. Cheng, Y. Ma, G. Yin, Hierarchical ordered macroporous/ultrathin mesoporous carbon architecture: A promising cathode scaffold with excellent rate performance for rechargeable Li-O2 batteries, Carbon N Y 118 (2017) 139–147. https://doi.org/10.1016/J.CARBON.2017.03.037.

[230] M. Zheng, J. Jiang, Z. Lin, P. He, Y. Shi, H. Zhou, Stable Voltage Cutoff Cycle Cathode with Tunable and Ordered Porous Structure for Li-O2 Batteries, Small 14 (2018) 1803607. https://doi.org/10.1002/SMLL.201803607.

[231] A.R. Kamali, D. Qiao, Z. Shi, D. Wang, Green molten salt modification of cobalt oxide for lithium ion battery anode application, Mater Chem Phys 267 (2021) 124585. https://doi.org/https://doi.org/10.1016/j.matchemphys.2021.124585.

[232] M.S. Yilmaz, M. Coşkun, T. Şener, Ö. Metin, Silica Coated ZnFe2O4 Nanoparticles as Cathode Catalysts for Rechargeable Lithium-Air Batteries, Batter Supercaps 2 (2019) 380–386. https://doi.org/https://doi.org/10.1002/batt.201800095.

[233] P. Moni, S. Hyun, A. Vignesh, S. Shanmugam, Chrysanthemum flower-like NiCo2O4–nitrogen doped graphene oxide composite: an efficient electrocatalyst for

lithium–oxygen and zinc–air batteries, Chemical Communications 53 (2017) 7836–7839. https://doi.org/10.1039/C7CC03826G.

[234] D. Ma, Y. Li, P. Zhang, A.J. Cooper, A.M. Abdelkader, X. Ren, L. Deng, Mesoporous Li1.2Mn0.54Ni0.13Co0.13O2 nanotubes for high-performance cathodes in Li-ion batteries, J Power Sources 311 (2016) 35–41. https://doi.org/https://doi.org/10.1016/j.jpowsour.2016.01.031.

[235] Y. Yu, B. Zhang, Y.B. He, Z.D. Huang, S.W. Oh, J.K. Kim, Mechanisms of capacity degradation in reduced graphene oxide/α- MnO2 nanorod composite cathodes of Li-air batteries, J Mater Chem A Mater 1 (2013). https://doi.org/10.1039/c2ta00426g.

[236] Z. Dai, X. Du, X. Zhang, Controlled synthesis of NiCo2O4@Ni-MOF on Ni foam as efficient electrocatalyst for urea oxidation reaction and oxygen evolution reaction, Int J Hydrogen Energy 47 (2022) 17252–17262. https://doi.org/https://doi.org/10.1016/j.ijhydene.2022.03.217.

[237] Y.Y. Kannangara, S. Karunarathne, W.P.S.L. Wijesinghe, C. Sandaruwan, C.R. Ratwani, A.R. Kamali, A.M. Abdelkader, The electrochemical performance of various NiCo2O4 nanostructures in hybrid supercapacitors: Investigating the impact of crystalline defects, J Energy Storage 84 (2024) 110717. https://doi.org/10.1016/J.EST.2024.110717.

[238] S.A.L. Sameera, N.P. Edirisinghe, Y.Y. Kannangara, S. Karunarathne, K.R. Koswattage, H.C.S. Perera, G. Das, M.M.M.G.P.G. Mantilaka, W.P.S.L. Wijesinghe, Enhanced Wide Spectrum Photocatalytic Activity by in-Situ Magnetite-Graphite Nanoplatelets Heterostructure, IEEE Access 11 (2023) 68912–68924. https://doi.org/10.1109/ACCESS.2023.3290029.

[239] C.K. Lee, Y.J. Park, Carbon and Binder-Free Air Electrodes Composed of Co3O4 Nanofibers for Li-Air Batteries with Enhanced Cyclic Performance, Nanoscale Res Lett 10 (2015). https://doi.org/10.1186/s11671-015-1027-8.

[240] R.S. Kalubarme, H.S. Jadhav, D.T. Ngo, G.E. Park, J.G. Fisher, Y. Il Choi, W.H. Ryu, C.J. Park, Simple synthesis of highly catalytic carbon-free MnCo2O4@Ni as an oxygen electrode for rechargeable Li-O2 batteries with long-term stability, Sci Rep 5 (2015). https://doi.org/10.1038/srep13266.

[241] G.E. Park, H.T.T. Le, H.S. Kim, P.N. Didwal, C.J. Park, Mn/Co oxide on Ni foam as a bifunctional catalyst for Li–air cells, Ceram Int 46 (2020). https://doi.org/10.1016/j.ceramint.2020.05.122.

[242] S. Karunarathne, Y.Y. Kannangara, C.R. Ratwani, C. Sandaruwan, W.P.S.L. Wijesinghe, A.R. Kamali, A.M. Abdelkader, Stoichiometrically optimized eg orbital occupancy of Ni–Co oxide catalysts for Li–air batteries, Nanoscale (2024). https://doi.org/10.1039/D4NR00518J.

[243] Y. Wu, T. Wang, Y. Zhang, S. Xin, X. He, D. Zhang, J. Shui, Electrocatalytic performances of g-C3N4-LaNiO3 composite as bi-functional catalysts for lithium-oxygen batteries, Sci Rep 6 (2016) 24314. https://doi.org/10.1038/srep24314.

[244] M. S. Burke, M. G. Kast, L. Trotochaud, A. M. Smith, S. W. Boettcher, Cobalt–Iron (Oxy)hydroxide Oxygen Evolution Electrocatalysts: The Role of Structure and Composition on Activity, Stability, and Mechanism, J Am Chem Soc 137 (2015) 3638–3648. https://doi.org/10.1021/jacs.5b00281.

[245] T. Şener, E. Kayhan, M. Sevim, Ö. Metin, Monodisperse CoFe2O4 nanoparticles supported on Vulcan XC-72: High performance electrode materials for lithium-air and lithium-ion batteries, J Power Sources 288 (2015). https://doi.org/10.1016/j.jpowsour.2015.04.120.

[246] Y. Liu, Y. Ying, L. Fei, Y. Liu, Q. Hu, G. Zhang, S.Y. Pang, W. Lu, C.L. Mak, X. Luo, L. Zhou, M. Wei, H. Huang, Valence engineering via selective atomic substitution on tetrahedral sites in spinel oxide for highly enhanced oxygen evolution catalysis, J Am Chem Soc 141 (2020) 8136–8145. https://doi.org/10.1021/JACS.8B13701/SUPPL_FILE/JA8B13701_SI_001.PDF.

[247] J. Suntivich, K.J. May, H.A. Gasteiger, J.B. Goodenough, Y. Shao-Horn, A perovskite oxide optimized for oxygen evolution catalysis from molecular orbital principles, Science (1979) 334 (2011) 1383–1385. https://doi.org/10.1126/SCIENCE.1212858/SUPPL_FILE/SUNTIVICH.SOM.PDF.

[248] D.A. Agyeman, M. Park, Y.M. Kang, Pd-Impregnated NiCo2O4 nanosheets/porous carbon composites as a free-standing and binder-free catalyst for a high energy lithium–oxygen battery, J Mater Chem A Mater 5 (2017) 22234–22241. https://doi.org/10.1039/C7TA05391F.

[249] S.-T. Myung, K. Izumi, S. Komaba, Y.-K. Sun, H. Yashiro, N. Kumagai, Role of Alumina Coating on Li−Ni−Co−Mn−O Particles as Positive Electrode Material for Lithium-Ion Batteries, Chemistry of Materials 17 (2005) 3695–3704. https://doi.org/10.1021/cm050566s.

[250] Y. Fan, J. Wang, Z. Tang, W. He, J. Zhang, Effects of the nanostructured SiO2 coating on the performance of LiNi0.5Mn1.5O4 cathode materials for high-voltage Li-ion batteries, Electrochim Acta 52 (2007) 3870–3875. https://doi.org/10.1016/J.ELECTACTA.2006.10.063.

[251] P. Tan, M. Liu, Z. Shao, M. Ni, Recent Advances in Perovskite Oxides as Electrode Materials for Nonaqueous Lithium–Oxygen Batteries, Adv Energy Mater 7 (2017) 1602674. https://doi.org/https://doi.org/10.1002/aenm.201602674.

[252] P. Tan, W. Shyy, T.S. Zhao, Z.H. Wei, L. An, Discharge product morphology versus operating temperature in non-aqueous lithium-air batteries, J Power Sources 278 (2015). https://doi.org/10.1016/j.jpowsour.2014.12.049.

[253] X. Wang, X. Chen, A. Thomas, X. Fu, M. Antonietti, Metal-containing carbon nitride compounds: a new functional organic-metal hybrid material, Advanced Materials 21 (2009). https://doi.org/10.1002/adma.200802627.

[254] C. Shang, X. Zhang, L. Shui, Z. Chen, H. Liao, M. Li, X. Wang, G. Zhou, Fe3O4@CoO mesospheres with core-shell nanostructure as catalyst for Li-O2

batteries, Appl Surf Sci 457 (2018) 804–808. https://doi.org/10.1016/J.APSUSC.2018.07.026.

[255] J. Cheng, M. Zhang, Y. Jiang, L. Zou, Y. Gong, B. Chi, J. Pu, L. Jian, Perovskite La0.6Sr0.4Co0.2Fe0.8O3 as an effective electrocatalyst for non-aqueous lithium air batteries, Electrochim Acta 191 (2016) 106–115. https://doi.org/10.1016/j.electacta.2016.01.058.

[256] M. Sun, S. Guo, Z. Wang, L. Zou, B. Chi, J. Pu, J. Li, Novel and highly efficient catalyst for Li–O2 battery: Porous LaCo0.6Ni0.4O3 nanofibers decorated with ultrafine Co3O4 nanoparticles, Electrochim Acta 363 (2020) 137235. https://doi.org/10.1016/j.electacta.2020.137235.

[257] S. Lu, T. Zhu, H. Wu, Y. Wang, J. Li, A. Abdelkader, K. Xi, W. Wang, Y. Li, S. Ding, G. Gao, R.V. Kumar, Construction of ultrafine ZnSe nanoparticles on/in amorphous carbon hollow nanospheres with high-power-density sodium storage, Nano Energy 59 (2019) 762–772. https://doi.org/10.1016/J.NANOEN.2019.03.008.

[258] A. Molla, M. Sahu, S. Hussain, Synthesis of Tunable Band Gap Semiconductor Nickel Sulphide Nanoparticles: Rapid and Round the Clock Degradation of Organic Dyes, Sci Rep 6 (2016). https://doi.org/10.1038/srep26034.

[259] S. Ullah, A. Bouich, H. Ullah, B. Mari, M. Mollar, Comparative study of binary cadmium sulfide (CdS) and tin disulfide (SnS2) thin buffer layers, Solar Energy 208 (2020) 637–642. https://doi.org/10.1016/j.solener.2020.08.036.

[260] S. Lu, H. Wu, S. Xu, Y. Wang, J. Zhao, Y. Li, A.M. Abdelkader, J. Li, W. Wang, K. Xi, Y. Guo, S. Ding, G. Gao, R.V. Kumar, Iron Selenide Microcapsules as Universal Conversion-Typed Anodes for Alkali Metal-Ion Batteries, Small 17 (2021) 2005745. https://doi.org/10.1002/SMLL.202005745.

[261] M. Asadi, B. Kumar, C. Liu, P. Phillips, P. Yasaei, A. Behranginia, P. Zapol, R.F. Klie, L.A. Curtiss, A. Salehi-Khojin, Cathode Based on Molybdenum Disulfide Nanoflakes for Lithium-Oxygen Batteries, ACS Nano 10 (2016). https://doi.org/10.1021/acsnano.5b06672.

[262] Y. Xiao, L. Tang, High-Throughput Approach Exploitation: Two-Dimensional Double-Metal Sulfide (M2S2) of Efficient Electrocatalysts for Oxygen Reduction Reaction in Fuel Cells, Energy and Fuels 34 (2020). https://doi.org/10.1021/acs.energyfuels.0c00297.

[263] Y. Li, Q. Li, H. Wang, L. Zhang, D.P. Wilkinson, J. Zhang, Recent Progresses in Oxygen Reduction Reaction Electrocatalysts for Electrochemical Energy Applications, Electrochemical Energy Reviews 2 (2019). https://doi.org/10.1007/s41918-019-00052-4.

[264] S. Chandrasekaran, L. Yao, L. Deng, C. Bowen, Y. Zhang, S. Chen, Z. Lin, F. Peng, P. Zhang, Recent advances in metal sulfides: From controlled fabrication to electrocatalytic, photocatalytic and photoelectrochemical water splitting and beyond, Chem Soc Rev 48 (2019). https://doi.org/10.1039/c8cs00664d.

[265] Y.N. Zhou, Y.R. Zhu, X.Y. Chen, B. Dong, Q.Z. Li, Y.M. Chai, Carbon–based transition metal sulfides/selenides nanostructures for electrocatalytic water splitting, J Alloys Compd 852 (2021) 156810. https://doi.org/10.1016/j.jallcom.2020.156810.

[266] J. Joo, T. Kim, J. Lee, S. Il Choi, K. Lee, Morphology-Controlled Metal Sulfides and Phosphides for Electrochemical Water Splitting, Advanced Materials 31 (2019). https://doi.org/10.1002/adma.201806682.

[267] Z. Ma, X. Yuan, Z. Zhang, D. Mei, L. Li, Z.F. Ma, L. Zhang, J. Yang, J. Zhang, Novel flower-like nickel sulfide as an efficient electrocatalyst for non-aqueous lithium-air batteries, Sci Rep 5 (2015). https://doi.org/10.1038/srep18199.

[268] Q. Wang, X. Wang, H. He, Integrated 3D foam-like porous Ni3S2 as improved deposition support for high-performance Li–O2 battery, J Power Sources 448 (2020) 227397. https://doi.org/10.1016/j.jpowsour.2019.227397.

[269] P. Sennu, M. Christy, V. Aravindan, Y.G. Lee, K.S. Nahm, Y.S. Lee, Two-Dimensional Mesoporous Cobalt Sulfide Nanosheets as a Superior Anode for a Li-Ion Battery and a Bifunctional Electrocatalyst for the Li-O2 System, Chemistry of Materials 27 (2015). https://doi.org/10.1021/acs.chemmater.5b02364.

[270] X. Lin, T. Zhang, C. Chu, Z. Li, R. Liu, P. Li, Y. Li, Z. Huang, Y. Ma, Synthesis of ZIF-Derived CoS2Nanocages Interconnected by CNTs for Rechargeable Li-O2Batteries, ACS Sustain Chem Eng 8 (2020). https://doi.org/10.1021/acssuschemeng.9b07714.

[271] X. Lin, R. Yuan, S. Cai, Y. Jiang, J. Lei, S.G. Liu, Q.H. Wu, H.G. Liao, M. Zheng, Q. Dong, An Open-Structured Matrix as Oxygen Cathode with High Catalytic Activity and Large Li2O2 Accommodations for Lithium–Oxygen Batteries, Adv Energy Mater 8 (2018). https://doi.org/10.1002/aenm.201800089.

[272] M. Samadi, N. Sarikhani, M. Zirak, H. Zhang, H.L. Zhang, A.Z. Moshfegh, Group 6 transition metal dichalcogenide nanomaterials: Synthesis, applications and future perspectives, Nanoscale Horiz 3 (2018). https://doi.org/10.1039/c7nh00137a.

[273] Jakob Kibsgaard, Zhebo Chen, Benjamin N.Reinecke, Thomas F.Jaramillo, Engineering the surface structure of MoS2 to preferentially expose active edge sites for electrocatalysis, Nat Mater 11 (2012).

[274] T.F. Jaramillo, K.P. Jørgensen, J. Bonde, J.H. Nielsen, S. Horch, I. Chorkendorff, Identification of active edge sites for electrochemical H2 evolution from MoS2 nanocatalysts, Science (1979) 317 (2007). https://doi.org/10.1126/science.1141483.

[275] M. Chhowalla, H.S. Shin, G. Eda, L.J. Li, K.P. Loh, H. Zhang, The chemistry of two-dimensional layered transition metal dichalcogenide nanosheets, Nat Chem 5 (2013). https://doi.org/10.1038/nchem.1589.

[276] Y. Cheng, Y. Wang, C. Jia, F. Bao, MnS hierarchical hollow spheres with novel shell structure, Journal of Physical Chemistry B 110 (2006). https://doi.org/10.1021/jp063698x.

[277] S. Li, Z. Jiang, X. Hou, J. Xu, M. Xu, X. Yu, Z.-F. Ma, J. Yang, X. Yuan, High Performance Li-O2 Batteries Enabled with Manganese Sulfide as Cathode Catalyst, J Electrochem Soc 167 (2020) 20520. https://doi.org/10.1149/1945-7111/ab68c6.

[278] M. Xu, X. Hou, X. Yu, Z.-F. Ma, J. Yang, X. Yuan, Spinel NiCo 2 S 4 as Excellent Bi-Functional Cathode Catalysts for Rechargeable Li-O 2 Batteries , J Electrochem Soc 166 (2019). https://doi.org/10.1149/2.1151906jes.

[279] A. Hu, J. Long, C. Shu, C. Xu, T. Yang, R. Liang, J. Li, Three-dimensional CoNi 2 S 4 nanorod arrays anchored on carbon textiles as an integrated cathode for high-rate and long-life Lithium−Oxygen battery, Electrochim Acta 301 (2019) 69–79. https://doi.org/10.1016/j.electacta.2019.01.163.

[280] P. Zhang, X. Hui, H. Wang, X. Gao, L. Yin, Porous hollow ZnCo2S4 nanosheet arrays derived from metal-organic framework as efficient cathode for lithium oxygen batteries, J Alloys Compd 860 (2021). https://doi.org/10.1016/j.jallcom.2020.157656.

[281] Z. Sadighi, J. Liu, F. Ciucci, J.K. Kim, Mesoporous MnCo2S4 nanosheet arrays as an efficient catalyst for Li-O2 batteries, Nanoscale 10 (2018). https://doi.org/10.1039/c8nr03942a.

[282] P. Kulkarni, S.K. Nataraj, R.G. Balakrishna, D.H. Nagaraju, M. V. Reddy, Nanostructured binary and ternary metal sulfides: Synthesis methods and their application in energy conversion and storage devices, J Mater Chem A Mater 5 (2017). https://doi.org/10.1039/c7ta07329a.

[283] P. Ramakrishnan, S. Shanmugam, J.H. Kim, Dual Heteroatom-Doped Carbon Nanofoam-Wrapped Iron Monosulfide Nanoparticles: An Efficient Cathode Catalyst for Li–O2 Batteries, ChemSusChem 10 (2017) 1554–1562. https://doi.org/10.1002/CSSC.201601810.

[284] Y. Cao, H. Lu, B. Xu, W. Yang, Q. Hong, Nitrogen/sulfur dual-doped porous carbon nanofibers with Co9S8 nanoparticles encapsulated by graphitic shells: A highly active stable free-standing air electrode for rechargeable non-aqueous Li-O2 batteries and primary alkaline Al-air batteries, Chemical Engineering Journal 378 (2019) 122247. https://doi.org/10.1016/J.CEJ.2019.122247.

[285] S. Hyun, B. Son, H. Kim, J. Sanetuntikul, S. Shanmugam, The synergistic effect of nickel cobalt sulfide nanoflakes and sulfur-doped porous carboneous nanostructure as bifunctional electrocatalyst for enhanced rechargeable Li-O2 batteries, Appl Catal B 263 (2020) 118283. https://doi.org/https://doi.org/10.1016/j.apcatb.2019.118283.

[286] Y. Zhao, B. Jin, A. Vasileff, Y. Jiao, S.Z. Qiao, Interfacial nickel nitride/sulfide as a bifunctional electrode for highly efficient overall water/seawater electrolysis, J Mater Chem A Mater 7 (2019). https://doi.org/10.1039/c9ta01903k.

[287] Y. Zhang, B. Ouyang, J. Xu, G. Jia, S. Chen, R.S. Rawat, H.J. Fan, Rapid Synthesis of Cobalt Nitride Nanowires: Highly Efficient and Low-Cost Catalysts for Oxygen Evolution, Angewandte Chemie - International Edition 55 (2016). https://doi.org/10.1002/anie.201604372.

[288] Y. Du, L. Zhao, H. Chen, Z. Huang, X. He, W. Fang, W. Li, X. Zeng, F. Zhang, Synthesis of cobalt-doped tubular carbon nitride from organic–inorganic hybrid precursor for photocatalytic hydrogen generation, J Mater Sci 55 (2020). https://doi.org/10.1007/s10853-019-04071-w.

[289] S. Hyun, B. Son, H. Kim, J. Sanetuntikul, S. Shanmugam, The synergistic effect of nickel cobalt sulfide nanoflakes and sulfur-doped porous carboneous nanostructure as bifunctional electrocatalyst for enhanced rechargeable Li-O2 batteries, Appl Catal B 263 (2020) 118283. https://doi.org/10.1016/J.APCATB.2019.118283.

[290] M.F. Delley, Z. Wu, M.E. Mundy, D. Ung, B.M. Cossairt, H. Wang, J.M. Mayer, Hydrogen on Cobalt Phosphide, J Am Chem Soc 141 (2019). https://doi.org/10.1021/jacs.9b07986.

[291] M. Wei, Y. Luo, C. Jin, J. Sui, Z. Wang, C. Li, R. Yang, MoP Nanoflakes as Efficient Electrocatalysts for Rechargeable Li-O2 Batteries, ACS Appl Energy Mater 1 (2018). https://doi.org/10.1021/acsaem.7b00299.

[292] M. Wei, B. Li, C. Jin, Y. Ni, C. Li, X. Pan, J. Sun, C. Yang, R. Yang, A 3D free-standing thin film based on N, P-codoped hollow carbon fibers embedded with MoP quantum dots as high efficient oxygen electrode for Li-O2 batteries, Energy Storage Mater 17 (2019). https://doi.org/10.1016/j.ensm.2018.07.012.

[293] F. Zhang, M. Wei, J. Sui, C. Jin, Y. Luo, S. Bie, R. Yang, Cobalt phosphide microsphere as an efficient bifunctional oxygen catalyst for Li-air batteries, J Alloys Compd 750 (2018). https://doi.org/10.1016/j.jallcom.2018.04.070.

[294] A. Hu, C. Shu, X. Qiu, M. Li, R. Zheng, J. Long, Improved Cyclability of Lithium–Oxygen Batteries by Synergistic Catalytic Effects of Two-Dimensional MoS2 Nanosheets Anchored on Hollow Carbon Spheres, ACS Sustain Chem Eng 7 (2019) 6929–6938. https://doi.org/10.1021/acssuschemeng.8b06496.

[295] M. Ma, G. Zhu, F. Xie, F. Qu, Z. Liu, G. Du, A.M. Asiri, Y. Yao, X. Sun, Homologous Catalysts Based on Fe-Doped CoP Nanoarrays for High-Performance Full Water Splitting under Benign Conditions, ChemSusChem 10 (2017) 3188–3192. https://doi.org/10.1002/CSSC.201700693.

[296] T. Zhang, J. Du, P. Xi, C. Xu, Hybrids of Cobalt/Iron Phosphides Derived from Bimetal–Organic Frameworks as Highly Efficient Electrocatalysts for Oxygen Evolution Reaction, ACS Appl Mater Interfaces 9 (2016) 362–370. https://doi.org/10.1021/ACSAMI.6B12189.

[297] K. Sun, J. Li, L. Huang, S. Ji, P. Kannan, D. Li, L. Liu, S. Liao, Biomass-derived 3D hierarchical N-doped porous carbon anchoring cobalt-iron phosphide nanodots as bifunctional electrocatalysts for Li–O2 batteries, J Power Sources 412 (2019) 433–441. https://doi.org/10.1016/j.jpowsour.2018.11.079.

[298] H. Liang, X. Gong, L. Jia, F. Chen, Z. Rao, S. Jing, P. Tsiakaras, Highly efficient Li-O2 batteries based on self-standing NiFeP@NC/BC cathode derived from biochar supported Prussian blue analogues, Journal of Electroanalytical Chemistry 867 (2020) 114124. https://doi.org/10.1016/J.JELECHEM.2020.114124.

[299] H. Liang, Y. Zhang, F. Chen, S. Jing, S. Yin, P. Tsiakaras, A novel NiFe@NC-functionalized N-doped carbon microtubule network derived from biomass as a highly efficient 3D free-standing cathode for Li-CO2 batteries, Appl Catal B 244 (2019) 559–567. https://doi.org/10.1016/J.APCATB.2018.11.075.

[300] M. Shalom, D. Ressnig, X. Yang, G. Clavel, T.P. Fellinger, M. Antonietti, Nickel nitride as an efficient electrocatalyst for water splitting, J Mater Chem A Mater 3 (2015) 8171–8177. https://doi.org/10.1039/C5TA00078E.

[301] X. Zhong, L. Liu, Y. Jiang, X. Wang, L. Wang, G. Zhuang, X. Li, D. Mei, J. Wang, D.S. Su, Synergistic Effect of Nitrogen in Cobalt Nitride and Nitrogen-Doped Hollow Carbon Spheres for the Oxygen Reduction Reaction, ChemCatChem 7 (2015) 1826–1832. https://doi.org/10.1002/CCTC.201500195.

[302] B. Cao, G.M. Veith, J.C. Neuefeind, R.R. Adzic, P.G. Khalifah, Mixed Close-Packed Cobalt Molybdenum Nitrides as Non-noble Metal Electrocatalysts for the Hydrogen Evolution Reaction, J Am Chem Soc 135 (2013) 19186–19192. https://doi.org/10.1021/JA4081056.

[303] S. Dong, X. Chen, K. Zhang, L. Gu, L. Zhang, X. Zhou, L. Li, Z. Liu, P. Han, H. Xu, J. Yao, C. Zhang, X. Zhang, C. Shang, G. Cui, L. Chen, Molybdenum nitride based hybrid cathode for rechargeable lithium–O2 batteries, Chemical Communications 47 (2011) 11291–11293. https://doi.org/10.1039/C1CC14427H.

[304] K. Zhang, L. Zhang, X. Chen, X. He, X. Wang, S. Dong, L. Gu, Z. Liu, C. Huang, G. Cui, Molybdenum Nitride/N-Doped Carbon Nanospheres for Lithium-O2 Battery Cathode Electrocatalyst, ACS Appl Mater Interfaces 5 (2013) 3677–3682. https://doi.org/10.1021/AM400209U.

[305] L. F, O. R, Y. Y, K. J, D. K, Y. A, Z. H, Carbon supported TiN nanoparticles: an efficient bifunctional catalyst for non-aqueous Li-O2 batteries, Chem Commun (Camb) 49 (2013) 1175–1177. https://doi.org/10.1039/C2CC37042E.

[306] K. Zhang, L. Zhang, X. Chen, X. He, X. Wang, S. Dong, P. Han, C. Zhang, S. Wang, L. Gu, G. Cui, Mesoporous Cobalt Molybdenum Nitride: A Highly Active Bifunctional Electrocatalyst and Its Application in Lithium–O2 Batteries, Journal of Physical Chemistry C 117 (2013) 858–865. https://doi.org/10.1021/JP310571Y.

[307] J. Chen, K. Takanabe, R. Ohnishi, D. Lu, S. Okada, H. Hatasawa, H. Morioka, M. Antonietti, J. Kubota, K. Domen, Nano-sized TiN on carbon black as an efficient electrocatalyst for the oxygen reduction reaction prepared using an mpg-C3N4 template, Chemical Communications 46 (2010) 7492–7494. https://doi.org/10.1039/C0CC02048F.

[308] C. WF, S. K, M. C, F. AI, M. N, M. JT, Z. Y, A. RR, Hydrogen-evolution catalysts based on non-noble metal nickel-molybdenum nitride nanosheets, Angew Chem Int Ed Engl 51 (2012) 6131–6135. https://doi.org/10.1002/ANIE.201200699.

[309] D. Mckay, D.H. Gregory, J.S.J. Hargreaves, S.M. Hunter, X. Sun, Towards nitrogen transfer catalysis: reactive lattice nitrogen in cobalt molybdenum nitride, Chemical Communications (2007) 3051–3053. https://doi.org/10.1039/B707913C.

[310] L. Huang, K. Sun, M. Liu, J. Li, H. Song, X. Lu, S. Liao, Yucca-like CoO–CoN Nanoarray with Abundant Oxygen Vacancies as a High-Performance Cathode for Lithium–Oxygen Batteries, ACS Appl Energy Mater 3 (2020) 12000–12008. https://doi.org/10.1021/ACSAEM.0C02172.

[311] Z. Zhang, K. Tan, Y. Gong, H. Wang, R. Wang, L. Zhao, B. He, An integrated bifunctional catalyst of metal-sulfide/perovskite oxide for lithium-oxygen batteries, J Power Sources 437 (2019) 226908. https://doi.org/10.1016/J.JPOWSOUR.2019.226908.

[312] M. Yuasa, T. Matsuyoshi, T. Kida, K. Shimanoe, Discharge/charge characteristic of Li-air cells using carbon-supported LaMn0.6Fe0.4O3 as an electrocatalyst, J Power Sources 242 (2013) 216–221. https://doi.org/10.1016/J.JPOWSOUR.2013.05.076.

[313] P. Wang, C. Li, S. Dong, X. Ge, P. Zhang, X. Miao, Z. Zhang, C. Wang, L. Yin, One-Step Route Synthesized Co2P/Ru/N-Doped Carbon Nanotube Hybrids as Bifunctional Electrocatalysts for High-Performance Li–O2 Batteries, Small 15 (2019). https://doi.org/10.1002/SMLL.201900001.

[314] P. Wang, C. Li, S. Dong, X. Ge, P. Zhang, X. Miao, R. Wang, Z. Zhang, L. Yin, Hierarchical NiCo2S4@NiO Core–Shell Heterostructures as Catalytic Cathode for Long-Life Li-O2 Batteries, Adv Energy Mater 9 (2019) 1900788. https://doi.org/10.1002/AENM.201900788.

[315] P. Zhang, S. Zhang, M. He, J. Lang, A. Ren, S. Xu, X. Yan, Realizing the Embedded Growth of Large Li2O2 Aggregations by Matching Different Metal Oxides for High-Capacity and High-Rate Lithium Oxygen Batteries, Advanced Science 4 (2017) 1700172. https://doi.org/10.1002/ADVS.201700172.

[316] P. Tan, Z.H. Wei, W. Shyy, T.S. Zhao, X.B. Zhu, A nano-structured RuO2/NiO cathode enables the operation of non-aqueous lithium–air batteries in ambient air, Energy Environ Sci 9 (2016) 1783–1793. https://doi.org/10.1039/C6EE00550K.

[317] D. Du, R. Zheng, X. Chen, W. Xiang, C. Zhao, B. Zhou, R. Li, H. Xu, C. Shu, Adjusting the Covalency of Metal–Oxygen Bonds in LaCoO3 by Sr and Fe Cation Codoping to Achieve Highly Efficient Electrocatalysts for Aprotic Lithium–Oxygen Batteries, ACS Appl Mater Interfaces 13 (2021) 33133–33146. https://doi.org/10.1021/ACSAMI.1C08586.

[318] J. Greeley, T.F. Jaramillo, J. Bonde, I. Chorkendorff, J.K. Nørskov, Computational high-throughput screening of electrocatalytic materials for hydrogen evolution, Nature Materials 2006 5:11 5 (2006) 909–913. https://doi.org/10.1038/nmat1752.

[319] J. Tian, Y. Rao, W. Shi, J. Yang, W. Ning, H. Li, Y. Yao, H. Zhou, S. Guo, Sabatier Relations in Electrocatalysts Based on High-entropy Alloys with Wide-distributed d-band Centers for Li-O2 Batteries, Angewandte Chemie International Edition 62 (2023) e202310894. https://doi.org/10.1002/ANIE.202310894.

[320] J. Li, L. Chen, R. Ye, J. Gao, W. Huang, Y. Lin, Z. Huang, Improved lithium-O2 battery performance enabled by catalysts of yolk-shell Fe3O4@C mixed with Pt-Ru

nanoparticles, Appl Surf Sci 507 (2020) 145103. https://doi.org/10.1016/J.APSUSC.2019.145103.

[321] Y. Cao, H. Lu, Q. Hong, J. Bai, J. Wang, X. Li, Co decorated N-doped porous carbon nanofibers as a free-standing cathode for Li-O2 battery: Emphasis on seamlessly continuously hierarchical 3D nano-architecture networks, J Power Sources 368 (2017) 78–87. https://doi.org/10.1016/J.JPOWSOUR.2017.09.071.

[322] Z. Wang, S. Peng, Y. Hu, L. Li, T. Yan, G. Yang, D. Ji, M. Srinivasan, Z. Pan, S. Ramakrishna, Cobalt nanoparticles encapsulated in carbon nanotube-grafted nitrogen and sulfur co-doped multichannel carbon fibers as efficient bifunctional oxygen electrocatalysts, J Mater Chem A Mater 5 (2017) 4949–4961. https://doi.org/10.1039/C6TA10291C.

[323] Y. Chen, S.A. Freunberger, Z. Peng, O. Fontaine, P.G. Bruce, Charging a Li–O2 battery using a redox mediator, Nature Chemistry 2013 5:6 5 (2013) 489–494. https://doi.org/10.1038/nchem.1646.

[324] B. J. Bergner, A. Schürmann, K. Peppler, A. Garsuch, J. Janek, TEMPO: A Mobile Catalyst for Rechargeable Li-O2 Batteries, J Am Chem Soc 136 (2014) 15054–15064. https://doi.org/10.1021/ja508400m.

[325] X. Gao, Y. Chen, L. Johnson, P.G. Bruce, Promoting solution phase discharge in Li–O2 batteries containing weakly solvating electrolyte solutions, Nature Materials 2016 15:8 15 (2016) 882–888. https://doi.org/10.1038/nmat4629.

[326] X. Gao, Y. Chen, L.R. Johnson, Z.P. Jovanov, P.G. Bruce, A rechargeable lithium–oxygen battery with dual mediators stabilizing the carbon cathode, Nature Energy 2017 2:9 2 (2017) 1–7. https://doi.org/10.1038/nenergy.2017.118.

[327] X. Shen, S. Zhang, Y. Wu, Y. Chen, Promoting Li–O2 Batteries With Redox Mediators, ChemSusChem 12 (2019) 104–114. https://doi.org/10.1002/CSSC.201802007.

[328] A. Kondori, M. Esmaeilirad, A.M. Harzandi, R. Amine, M.T. Saray, L. Yu, T. Liu, J. Wen, N. Shan, H.H. Wang, A.T. Ngo, P.C. Redfern, C.S. Johnson, K. Amine, R. Shahbazian-Yassar, L.A. Curtiss, M. Asadi, A room temperature rechargeable Li2O-based lithium-air battery enabled by a solid electrolyte, Science (1979) 379 (2023) 499–505. https://doi.org/10.1126/SCIENCE.ABQ1347/SUPPL_FILE/SCIENCE.ABQ1347_SM.PDF.

1